The Concept of Nonlinear Modes Applied to Friction-Damped Systems

Von der Fakultät für Maschinenbau
der Gottfried Wilhelm Leibniz Universität Hannover
zur Erlangung des akademischen Grades
Doktor-Ingenieur
genehmigte

Dissertation

von
Dipl.-Ing. Malte Krack
geb. am 25. April 1986 in Rinteln

2014

1. Referent: Prof. Dr.-Ing. habil. Jörg Wallaschek
2. Referent: Prof. Dr.-Ing. Jörg Seume
3. Referent: Prof. Dr.-Ing. Annika Raatz

Tag der Promotion: 25. November 2014

Preface

The present thesis was completed during my time as a research assistant at the Institute of Dynamics and Vibration Research of the Leibniz Universität Hannover, Germany, between November 2010 and April 2014. Initially, I worked on an application-oriented project related to friction damping in turbomachinery bladed disks. In quest of more effective model reduction approaches, I stumbled over the concept of nonlinear modes, which turned out to be particularly useful in this regard. This thesis is only about the part of my scientific work dealing with the novel theoretical developments which were required for a successful application to friction-damped systems.
If I had traveled forward in time a couple of years ago to read my own thesis, I probably would have had difficulties understanding the terminology which I now regard as crucial for a correct and concise language. In order to help myself in this unlikely case, but also other prospective readers, I wrote a glossary which can be found at the end of this thesis. The first occurrence of a term listed in the glossary is underlined.

Acknowledgements

Above all, I thank Professor Jörg Wallaschek for facilitating the suitable environment for self-determined, scientifically independent research and the infrastructure to develop novel ideas and approaches. His interest in my work was exceedingly motivating for me. My thanks go also to him, Professor Jörg Seume and Professor Annika Raatz for accepting their role as the referees and the president of the Examining Board.
Special thanks go to Lars Panning-von Scheidt for his encouragingly positive character, for constantly backing me and for always being willing to listen to my concerns, no matter whether related to our work or not.
Moreover, I express my gratitude to Christian Siewert, Marcus Neubauer and Lars Panning-von Scheidt for exchanging ideas and for their comments on the present thesis. It is a pleasure to acknowledge the invaluable support of my present and former co-workers in the form of scientific and non-scientific discussions.
The present work would not have been possible without the financial support of the BMWi, the Siemens Energy Sector, and MTU Aero Engines. It is my firm belief that the challenging physical problems encountered in real-world engineering applications lead to novel ideas and trigger important fundamental research work.
Last but not least, I am particularly grateful to my family, in particular to my wife Gundula and my parents Susanne and Dieter, for being there for me.

Malte Krack Hannover, November 2014

Abstract

In the present work, a novel computational procedure for the efficient dynamic analysis of friction-damped mechanical structures is presented. From a given set of nonlinear differential equations governing the motion of a system, its energy-dependent vibrational features are extracted, represented by eigenfrequencies, damping ratios and vibrational deflection shapes. Based on these modal characteristics, a reduced order model is then constructed that facilitates the efficient vibration prediction in a wide range of operating conditions.
The capabilities and limitations of the proposed approach were investigated for several numerical examples. The novel procedure outperforms conventional methods in terms of computational efficiency, while retaining reasonable prediction quality. The approach is, however, currently limited to the dynamic regime of primary interest for friction-damped systems, namely to the regime of an isolated resonance. The application to state-of-the-art models of turbine blades with friction interfaces demonstrated that the proposed approach is capable of drastically reducing the computational effort of extensive parameter studies and thus facilitating the design of effective and more reliable friction-damped systems.

Keywords: nonlinear dynamics, mechanical vibrations, model order reduction, dry friction, design optimization, reliability, turbine blades

Kurzfassung

Titel: Anwendung des Konzepts der nichtlinearen Moden auf reibungsgedämpfte Systeme

In der vorliegenden Arbeit wird ein neues rechnergestütztes Verfahren für die effiziente dynamische Analyse reibungsgedämpfter mechanischer Strukturen vorgestellt. Ausgehend von einem gegebenen Satz nichtlinearer Differentialgleichungen, welche die Bewegung eines Systems bestimmen, werden seine Schwingungseigenschaften, dargestellt durch Eigenfrequenzen, Dämpfungsgrade und Schwingungsformen, extrahiert. Basierend auf diesen modalen Charakteristika wird dann ein Modell reduzierter Ordnung aufgebaut, welches die effiziente Schwingungsvorhersage in einem weiten Bereich von Betriebsbedingungen ermöglicht.
Die Möglichkeiten und Grenzen des vorgeschlagenen Vorgehens wurden für mehrere numerische Beispiele untersucht. Das neuartige Verfahren übertrifft gebräuchliche Methoden hinsichtlich Berechnungseffizienz, wobei es eine angemessene Vorhersagegüte beibehält. Die Anwendung auf zeitgemäße Modelle von Turbinenschaufeln mit Reibfugen zeigte, dass das vorgeschlagene Verfahren dazu in der Lage ist, den Berechnungsaufwand umfangreicher Parameterstudien drastisch zu reduzieren und damit die Auslegung wirksamer und zuverlässigerer reibungsgedämpfter Systeme zu ermöglichen.

Schlagwörter: Nichtlineare Dynamik, mechanische Schwingungen, Modellordnungsreduktion, Trockenreibung, Design-Optimierung, Zuverlässigkeit, Turbinenschaufeln

Contents

Abstract **IV**

Kurzfassung **V**

Introduction 1

1 Motivation **1**

2 State of knowledge **4**
2.1 Analysis of friction-damped systems 4
2.1.1 Modeling of mechanical structures 4
2.1.2 Contact modeling 7
2.1.3 Direct dynamic analysis methods 11
2.2 Design of friction-damped systems 16
2.2.1 Mechanisms of vibration reduction 16
2.2.2 Dynamic regimes of interest 17
2.2.3 Performance measures 17
2.2.4 Parameter dependencies 18
2.3 The concept of nonlinear modes 21
2.3.1 Definition of nonlinear modes 22
2.3.2 Calculation of nonlinear modes 23
2.3.3 Model reduction based on nonlinear modes 26

3 Purpose of the present thesis **28**

Methodology 31

4 A nonlinear modal analysis method for non-conservative systems **32**
4.1 Derivation of the general method 32
4.1.1 Dynamic regime of interest 32
4.1.2 A new definition of nonlinear modes 34
4.1.3 Computation of modal characteristics 36
4.1.4 Relation to generalized Fourier-Galerkin method 37
4.2 Computational improvements 40

4.2.1 Exploiting the sparsity of the nonlinear force vector 41
4.2.2 Solution using analytical gradients 43
4.2.3 Numerical path continuation 43
4.2.4 Evaluation of the proposed improvements 44

5 A model reduction approach based on nonlinear modes 47
5.1 Derivation of the general ROM 47
5.1.1 Reconstruction of the invariant manifold 47
5.1.2 Governing equations for the unsteady flow on the manifold 48
5.1.3 Governing equations for limit cycles on the manifold 50
5.1.4 Synthesis with off-resonant modes 50
5.2 Remarks on the ROM's attributes 51
5.3 Derivation of special cases for the design of friction-damped systems 53
5.3.1 Steady-state dynamics 53
5.3.2 Unsteady dynamics 55

Application 55

6 Application to simple models with contact interfaces 56
6.1 System with preloaded unilateral contact 57
6.1.1 Modal characteristics 57
6.1.2 Autonomous response 61
6.1.3 Forced response 62
6.2 System with dry friction contact 65
6.2.1 Modal characteristics 65
6.2.2 Autonomous response 67
6.2.3 Forced response 70
6.2.4 Computational benefit of the ROM for unsteady dynamics 75

7 Application to detailed models of friction-damped systems 76
7.1 Modal analysis and model reduction of a bladed disk with shroud joints . . 76
7.1.1 Description of the model 77
7.1.2 Modal characteristics 79
7.1.3 Steady-state forced response 81
7.1.4 Computational benefit of the ROM for steady-state predictions . . . 85
7.2 Robust design of a bladed disk with underplatform dampers 87
7.2.1 Description of the model 87
7.2.2 Modal characteristics 88
7.2.3 Sensitivity analysis of the resonant forced response 89
7.2.4 Reliability optimization 90

Evaluation **94**

8 Discussion of the results **95**

9 Conclusions and future work **101**

Appendices **104**

A Parseval's theorem **104**

B Modal properties in accordance with different conceptions **104**

C Derivation of the unsteady flow on the invariant manifold **105**

D Proof of scale invariance of a family of contact laws **109**

E Computational resources for the numerical study in Section 4.2.4 **110**

List of frequently used symbols **111**

Glossary **115**

Bibliography **118**

1 Motivation

Friction damping

Many machines undergo structural vibrations during operation. These vibrations may cause material fatigue and noise, and thus (a) lead to safety issues and discomfort, (b) result in costs, and (c) increase the environmental footprint. The mitigation of vibration-induced alternating stresses can enhance the structure's lifetime and increase its reliability. Moreover, it can extend the feasible design space and tolerable operating conditions, which in turn may improve the efficiency of the machine.
Friction damping is one means of accomplishing vibration reduction. The damping effect is achieved by the dissipative character of dry friction occurring in mechanical joints. For this purpose, friction interfaces may be either newly introduced to the system or existing ones are used e. g. in the form of bolted or riveted joints. Friction damping is particularly suited for the passive vibration reduction of lightly damped structures. Various applications can be found in the field of aerospace structures, combustion engines or turbomachinery blades.
Friction is a nonlinear phenomenon, i. e. the measures which describe the vibration behavior are energy-dependent in contrast to the linear case where these measures are con-

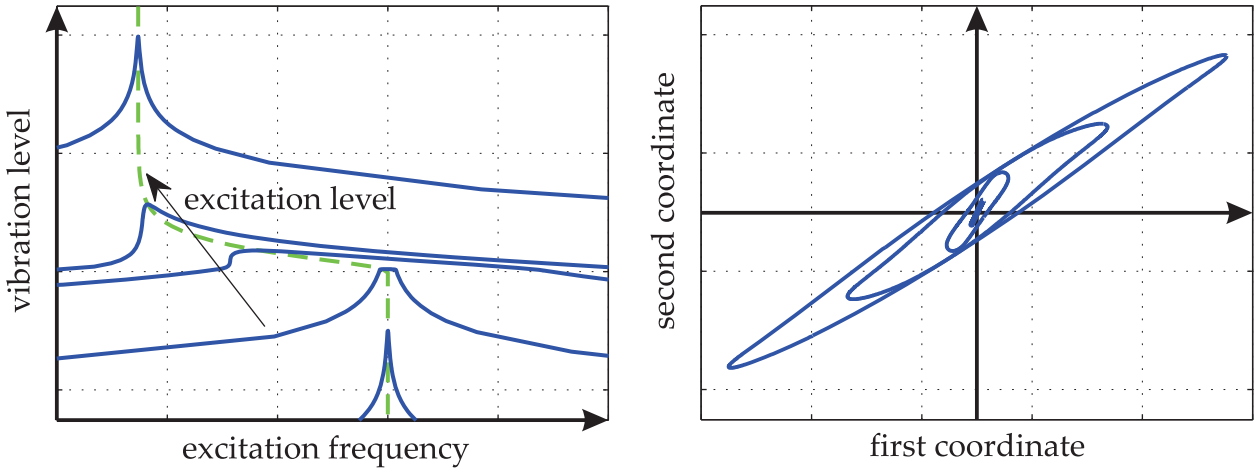

(a) (b)

Figure 1.1: Energy-dependent vibration behavior of friction-damped systems: (a) frequency-response curves for varying level of the harmonic forcing, (b) displacement space illustrations of resonant deflection shapes

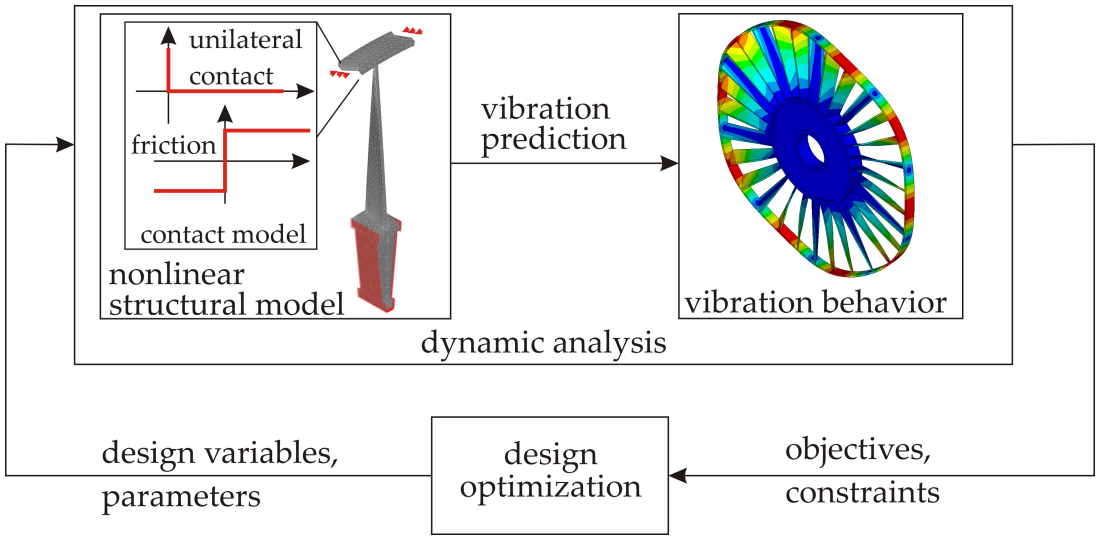

Figure 1.2: Conceptual diagram of the structural dynamic design process of friction-damped systems

stant. As can be seen in **Fig. 1.1**a, the resonance frequencies of a friction-damped system vary with the level of harmonic forcing. Likewise, the width of the resonance peak, which is a measure for effective damping, depends on the excitation level. Finally, the deflection shape obviously changes with the energy, which can be deduced from their illustrations in the displacement space, see **Fig. 1.1**b. In addition to this quantitative influence, nonlinearity may in general enrich the possible dynamics by phenomena not present in the linear regime, such as the change of stability, the so-called jump phenomenon, non-synchronous response and energy localization.

Complexity of the design process

The nonlinearity adds up to the overall complexity of the structural dynamic design process of friction-damped systems, cf. **Fig. 1.2**. This process commonly involves predictive models rather than experiments.
In order to predict the vibration behavior with sufficient accuracy, often detailed structural models have to be used. A fine level of spatial discretization is required in order to resolve the alternating stress distribution. In addition, a fine level of spatial discretization is required to resolve the possibly inhomogeneous contact interactions in extended friction interfaces. The strongly nonlinear character of the contact interactions necessitates a fine level of temporal disretization and generally the use of iterative computational schemes for the vibration prediction.
Typically, comprehensive parameter studies have to be carried out in order to find the optimum set of design variables that achieves the most effective vibration reduction and does not violate any design constraints. The design process is further hampered by the uncertainty associated with various system parameters. For instance, loading conditions are often only known in terms of their stochastic characteristics. The friction interfaces induce additional uncertainty, since contact parameters are typically not exactly known and may change during operation. It is thus necessary to assess the robustness of the de-

sign with respect to different parameters.
The overall complexity of the design process is hence caused by the combined demands of treating detailed nonlinear models and evaluating an extensive number of parameter variations. This complexity leads to considerable computational cost. In a competitive economy, this often results in compromises with respect to model fidelity or simplifications of the design problem. As a consequence, the design may exhibit inferior performance. Therefore, the performance of friction-damped systems could be increased, if the relevant dynamic characteristics were assessed more efficiently in the course of the design process.

Nonlinear modes

Linear modes of vibration are central to the analysis and the design of systems which behave linearly in the regime of interest. They are known to reflect the vibration signature in terms of eigenfrequencies, modal damping ratios and deflection shapes. They can be utilized for model reduction and therefore accelerate the vibration prediction in the course of the design process. There exists a unified concept and a profound theoretical basis for numerical and experimental approaches. Computational procedures for the modal analysis of quite generic linear mechanical structures are available in conventional software tools, and thus accessible to the common engineer.
The dynamic behavior of friction-damped systems cannot be regarded as linear within the regime of interest. The concept of nonlinear modes is far less established than its linear counterpart. Different approaches exist for the modal analysis, each having a limited scope of applicability. In particular, most approaches are only applicable to small-scale models involving smooth conservative forces [78]. This obviously limits their usefulness for the outlined problem class. Furthermore, computational procedures for the nonlinear modal analysis are currently not available in conventional software tools.

Contributions of this thesis

The present thesis contributes to making modal analysis efficient for friction-damped systems. Furthermore, a versatile model reduction approach based on the computed modal characteristics is developed which can be readily used in the design process. The performance of the method is assessed for a wide range of operating conditions and for detailed models of structures with extended contact interfaces.
This thesis is structured as follows: In Chapter 2, the state of knowledge regarding friction-damped systems and nonlinear modes is presented. The purpose of the present thesis is detailed in Chapter 3. A modal analysis method for nonlinear systems is derived in Chapter 4 and strategies for improving its efficiency are proposed. A model reduction approach is developed in Chapter 5. The range of validity of the framework is investigated in detail for comparatively simple models in Chapter 6. The applicability to detailed models and extensive parameter studies of state-of-the-art friction-damped systems is demonstrated in Chapter 7. The accomplished goals of this thesis are discussed in Chapter 8. Conclusions and possible directions of future work are presented in Chapter 9.

2 State of knowledge

An overview of basic notions, conventional approaches and common assumptions related to the analysis and to the design of friction-damped systems is provided in Section 2.1 and Section 2.2, respectively. This background is relevant for the synthesis of an appropriate solution strategy based on nonlinear modes. The state of knowledge regarding nonlinear modes is presented in Section 2.3.

2.1 Analysis of friction-damped systems

A friction-damped system represents (part of) a machine which is exposed to dynamic forces and undergoes vibrations during operation. The system consists of elastic bodies which are connected to themselves or to each other via mechanical joints which may feature nonlinear contact interactions. This section is further divided into the modeling of these bodies in Section 2.1.1, the description of the contact interactions in Section 2.1.2 and the computation of the nonlinear vibration behavior in Section 2.1.3.

2.1.1 Modeling of mechanical structures

Spatial discretization

The finite element (FE) method has established itself as the standard method for modeling the structural dynamics of friction-damped systems. As illustrated in **Fig. 2.1**, the spatially continuous displacement field ${}_{\mathcal{D}}\boldsymbol{u}(\boldsymbol{x},t)$ in a body $\mathcal{D}$ is approximated in the form ${}_{\mathcal{D}}\boldsymbol{u}(\boldsymbol{x},t) \approx \boldsymbol{N}(\boldsymbol{x})\,{}_{\mathrm{d}}\boldsymbol{u}(t)$ by a finite set of physical deformations ${}_{\mathrm{d}}\boldsymbol{u}(t)$ combined with a set of spatial shape functions $\boldsymbol{N}(\boldsymbol{x})$. By applying a Galerkin-type procedure, a set of second-order ordinary differential equations (ODEs) is obtained that govern the dynamic behavior,

$$ {}_{\mathrm{d}}\boldsymbol{M}\,{}_{\mathrm{d}}\ddot{\boldsymbol{u}}(t) + {}_{\mathrm{d}}\boldsymbol{C}\,{}_{\mathrm{d}}\dot{\boldsymbol{u}}(t) + {}_{\mathrm{d}}\boldsymbol{K}\,{}_{\mathrm{d}}\boldsymbol{u}(t) + {}_{\mathrm{d}}\boldsymbol{g}\left({}_{\mathrm{d}}\boldsymbol{u}\left(t\right), {}_{\mathrm{d}}\dot{\boldsymbol{u}}\left(t\right)\right) = {}_{\mathrm{d}}\boldsymbol{e}(t)\,. \tag{2.1} $$

Herein, ${}_{\mathrm{d}}\boldsymbol{M} = {}_{\mathrm{d}}\boldsymbol{M}^{\mathrm{T}} > \boldsymbol{0}$ and ${}_{\mathrm{d}}\boldsymbol{K} = {}_{\mathrm{d}}\boldsymbol{K}^{\mathrm{T}} > \boldsymbol{0}$ are the symmetric, positive mass and stiffness matrices. ${}_{\mathrm{d}}\boldsymbol{C} = {}_{\mathrm{d}}\boldsymbol{C}^{\mathrm{T}}$ is the symmetric viscous damping matrix. The vector ${}_{\mathrm{d}}\boldsymbol{e}(t)$ comprises external forces. Small vibrations around the equilibrium point ${}_{\mathrm{d}}\boldsymbol{u} = \boldsymbol{0}$ are considered. The

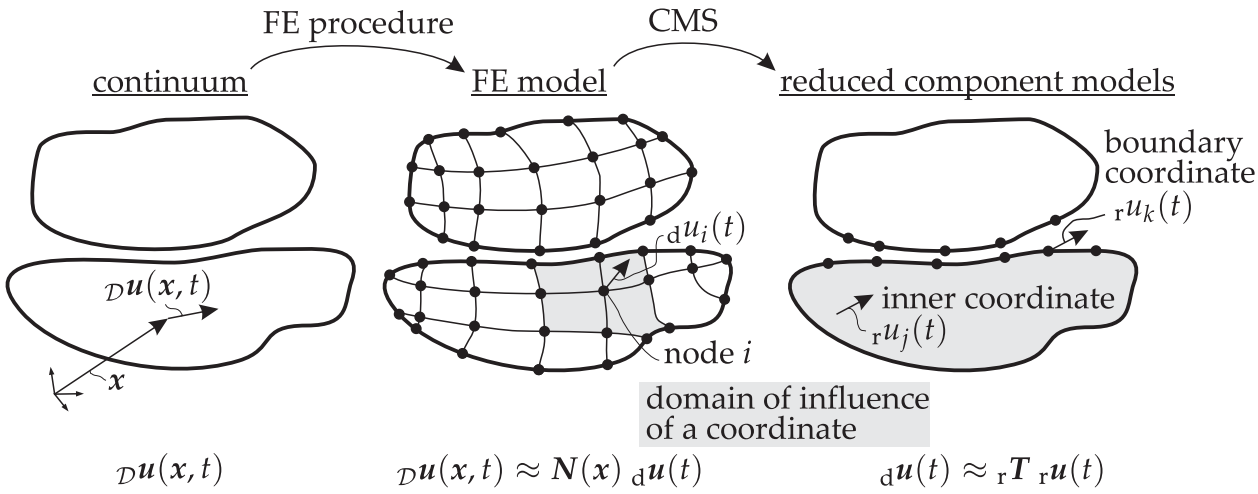

Figure 2.1: Spatial discretization and Component Mode Synthesis

nonlinear forces ${}_{\mathrm{d}}g\left({}_{\mathrm{d}}u\left(t\right), {}_{\mathrm{d}}\dot{u}\left(t\right)\right)$ are assumed to stem solely from the contact interactions and are addressed in Section 2.1.2. Linear non-symmetric terms, stemming e. g. from gyroscopic effects, are often not regarded, but could generally be incorporated in ${}_{\mathrm{d}}g$ to comply with the formalism in this thesis. Moreover, it is assumed throughout this thesis that the structural matrices and the nonlinear forces do not explicitly depend on time. The time variation of these properties, e. g. due to thermal effects or wear, is considered to happen on time scale much longer than the one on which the sought vibrations take place.
While the mass and the stiffness matrices directly follow from the FE procedure, it should be noted that it is not straightforward to determine the damping matrix. The damping matrix can be utilized to describe the dissipative character of the material behavior [97], the interaction with the surrounding fluid [16, 127, 131, 101] and the joints not explicitly taken into account in the term ${}_{\mathrm{d}}g$ [67]. The common assumption of weak damping is adopted throughout this thesis.

Component Mode Synthesis

As the domain of influence of each discrete physical coordinate ${}_{\mathrm{d}}u_i$ is bounded, cf. **Fig. 2.1**, the structural matrices ${}_{\mathrm{d}}M, {}_{\mathrm{d}}C, {}_{\mathrm{d}}K$ are sparse. It is common to condense the equations of motion and thus reduce the number of coordinates contained in the model by means of Component Mode Synthesis (CMS). A good overview of this topic can be found in [84, 34]. This introduces a further step of approximation, where the set of N_{d} physical coordinates ${}_{\mathrm{d}}u(t)$ is approximated as ${}_{\mathrm{d}}u(t) = {}_{\mathrm{r}}T\ {}_{\mathrm{r}}u(t)$ by a set of N_{r} generalized coordinates ${}_{\mathrm{r}}u(t)$ via a set of component mode vectors assembled as columns in the matrix ${}_{\mathrm{r}}T$, where typically $N_{\mathrm{r}} \ll N_{\mathrm{d}}$. The projection of the equations of motion (2.1) onto this reduced set of base vectors gives rise to a reduced set of equations of motion,

$$\begin{aligned} {}_{\mathrm{r}}M\ {}_{\mathrm{r}}\ddot{u}(t) + {}_{\mathrm{r}}C\ {}_{\mathrm{r}}\dot{u}(t) + {}_{\mathrm{r}}K\ {}_{\mathrm{r}}u(t) + {}_{\mathrm{r}}g\left({}_{\mathrm{d}}u, {}_{\mathrm{d}}\dot{u}\right) &= {}_{\mathrm{r}}e(t)\,, \\ \text{with} \quad {}_{\mathrm{r}}\{M,C,K\} = {}_{\mathrm{r}}T^{\mathrm{T}}\ {}_{\mathrm{d}}\{M,C,K\}\ {}_{\mathrm{r}}T\,,\ {}_{\mathrm{r}}\{g,e\} &= {}_{\mathrm{r}}T^{\mathrm{T}}\ {}_{\mathrm{d}}\{g,e\}\,. \end{aligned} \tag{2.2}$$

As a consequence of this condensation, the reduced structural matrices are in general no longer sparse and the domain of influence of the generalized coordinates may spread over the entire domain. The overall procedure of spatial discretization and CMS, as illustrated in **Fig. 2.1**, can significantly reduce the solution space and thus simplify the dynamic analysis of friction-damped systems. Upon solution in the reduced space, the approximate physical displacement field can be expanded using the reduction ansatz.

Appropriate choice of base vectors

The appropriate selection and number of the base vectors, i. e. the matrix ${}_{\mathrm{r}}\boldsymbol{T}$ determines the accuracy of the reduced order model (ROM) in the dynamic regime of interest. On the other hand, the number of base vectors should be as small as possible in order to achieve the best computational efficiency.

It is useful to distinguish between the *boundary coordinates* which describe the deformation at the contact interface and the remaining *inner coordinates*. It is beneficial to retain the boundary coordinates as generalized coordinates for the ease of formulating the coupling through contact forces. Otherwise, an expansion-projection procedure is required for the evaluation of the reduced coupling forces, and the sparsity of the contact force vector ${}_{\mathrm{r}}\boldsymbol{g}$ is generally destroyed [146].

The local relative displacement in the contact interface is typically small compared to the global displacement of the structure [126]. An accurate description of the local elasticity is thus essential for the modeling of contact interactions. The dry contact interactions can essentially be described by quasi-static relations [49]. Hence, it is important to retain an accurate representation of the static deformation behavior in the ROM.

In the conventional modal truncation approach, the base vectors are the modal deflection shapes corresponding to the lowest eigenfrequencies of the structure without contact constraints (free boundary). This formulation is very popular, but it is not directly suited for contact problems, as the first modal deflection shapes barely contain information about the elasticity of contact interfaces [118]. To overcome this, the modal base can be augmented by the so-called *static residual compliance* [126]. For the same purpose, the set of free-boundary normal modes can be supplemented by so-called *residual attachment modes* in the Craig-Chang-Martinez (CCM) method [34].

Probably the most popular CMS method is the Craig-Bampton (CB) method, because it is particularly known for its superior numerical stability and great modal convergence [4]. The reduction base is formed here by the normal modes for fixed boundary and so-called *constraint modes* which represent the static deformation shapes for unit displacement at each boundary coordinate. Batailly et al. [4] compared the CCM with the CB method for a dynamical contact problem and found that both methods lead to similar results for higher numbers of modes. It can generally be stated that the CB method is better suited to describe almost sticking contact situations, while the CCM method is beneficial for nearly open contact situations. For both methods, only the interface coordinates involved in the nonlinear force formulation should be defined as boundary coordinates, in order to improve the convergence of the reduction base [25].

2.1.2 Contact modeling

The objective of contact modeling in friction-damped systems is to describe the essential interactions between dry rough surfaces, i. e. dry sliding friction in the tangential plane and unilateral contact in the normal direction. It has to be stated that there is not yet a scientific consensus regarding the accurate modeling of contact interactions in mechanical joints, and this is still a lively field of research. Part of the apparent complexity is due to the fact that a realistic model must generally be an appropriate combination of the models for the contact interaction and the underlying structure, which cannot be regarded separately from each other. Overviews of this topic can be found in [180, 182, 76]. In the following, a focus is set on contact modeling in the context of friction damping.
For friction-damped systems, a description based on first principles seems infeasible due to the lack of knowledge of exact surface geometry and material characteristics on all relevant length scales in practice. Moreover, the consideration of mechanical, thermal and chemical interactions, usually happening on different time scales, appears prohibitive. Hence, 'smeared' i. e. time and length scale averaged phenomenological models for the mechanical contact interactions are typically formulated and applied to idealized, smooth surface geometries. Phenomenological models inherently introduce parameters which need to be properly identified, which can be a difficult problem in general. The different contact modeling approaches mainly differ with respect to kinematic description, discretization and contact laws. These aspects are described below.

Contact kinematics

The contact kinematics represent the relationship between the relative displacement field ${}_{\mathcal{C}}\boldsymbol{u}_{\mathrm{rel}}(\boldsymbol{x},t)$ of the contact interface and the coordinates describing the vibration behavior of the underlying structure,

$$\begin{aligned} {}_{\mathcal{C}}\boldsymbol{u}_{\mathrm{rel}}(\boldsymbol{x},t) &= {}_{\mathcal{C}}\begin{bmatrix} u_{\mathrm{n}} & u_{\mathrm{t}_1} & u_{\mathrm{t}_2} \end{bmatrix}^{\mathrm{T}}_{\mathrm{rel}}(\boldsymbol{x},t) = {}_{\mathcal{C}_2}\boldsymbol{u}(\boldsymbol{x},t) - {}_{\mathcal{C}_1}\boldsymbol{u}(\boldsymbol{x},t) \\ &\approx \left({}_{\mathcal{C}_2}\boldsymbol{B}(\boldsymbol{x},\,{}_{\mathrm{d}}\boldsymbol{u}(t)) - {}_{\mathcal{C}_1}\boldsymbol{B}(\boldsymbol{x},\,{}_{\mathrm{d}}\boldsymbol{u}(t))\right)\,{}_{\mathrm{d}}\boldsymbol{u}(t) = {}_{\mathcal{C}}\boldsymbol{B}(\boldsymbol{x},{}_{\mathrm{d}}\boldsymbol{u}(t))\,{}_{\mathrm{d}}\boldsymbol{u}(t)\,. \end{aligned} \tag{2.3}$$

${}_{\mathcal{C}}\boldsymbol{u}_{\mathrm{rel}}(\boldsymbol{x},t)$ is given in the contact coordinate system spanned by the locally defined normal vector $\boldsymbol{n}$ and the two tangential vectors $\boldsymbol{t}_1, \boldsymbol{t}_2$, cf. **Fig. 2.2**a. The displacement field is defined at the common contact surface $\mathcal{C} = \mathcal{C}_1 \cap \mathcal{C}_2$. The contact surface $\mathcal{C}$ is the entire surface which can undergo nonzero contact pressures during vibration. It therefore also includes all regions which are initially separated, but potentially get into contact due to dynamic deformation. Friction joints for the purpose of damping are typically designed to be localized and only undergo comparatively small relative deflections. Hence, the determination of the contact surface $\mathcal{C}$ is typically not a difficult task, and it will be assumed as known in the following. The interested reader is referred to [182] for contact search algorithms relevant in situations where an a priori knowledge of the potential contact area is not available.
The continuous relative displacement field is approximated in accordance with the FE

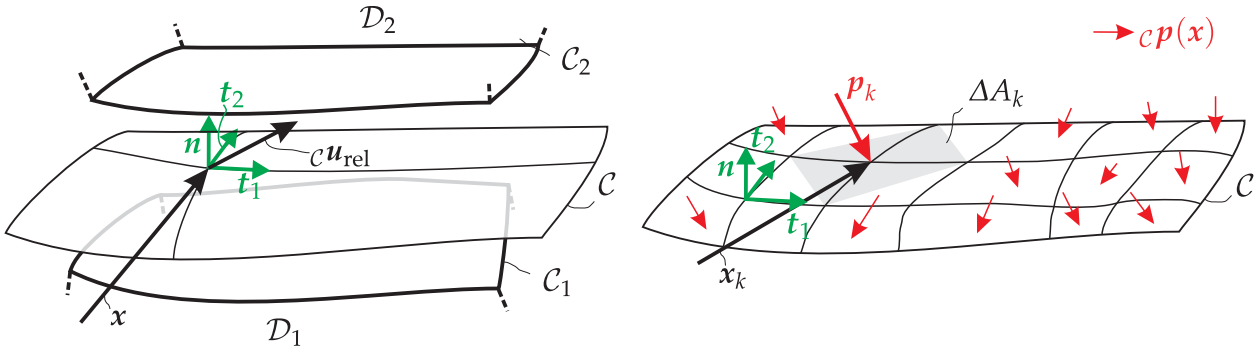

(a) (b)

Figure 2.2: Mechanics of a contact interface: (a) kinematics, (b) discretization and contact pressure field

procedure in terms of the coordinates ${}_{\mathrm{d}}\boldsymbol{u}$ and shape functions ${}_{\mathcal{C}}\boldsymbol{B}$ at the contact interface. The relationship ${}_{\mathcal{C}}\boldsymbol{B}(\boldsymbol{x}, {}_{\mathrm{d}}\boldsymbol{u})$ is geometrically nonlinear in general. It is a common simplification in the field of friction damping to linearize the kinematic relation for small relative deflections [25], resulting in a shape function ${}_{\mathcal{C}}\boldsymbol{B}(\boldsymbol{x})$ which is independent of the deformation ${}_{\mathrm{d}}\boldsymbol{u}$. Geometric linearity is assumed in the following.

Contact discretization

A contact pressure field ${}_{\mathcal{C}}\boldsymbol{p}\,(\boldsymbol{x}, {}_{\mathcal{C}}\boldsymbol{u}_{\mathrm{rel}})$ develops between adjacent interfaces in accordance with the contact law. ${}_{\mathcal{C}}\boldsymbol{p}\,(\boldsymbol{x}, {}_{\mathcal{C}}\boldsymbol{u}_{\mathrm{rel}})$ is generally inhomogeneous, i. e. it depends on the location $\boldsymbol{x}$. The contact law locally relates the pressure to the relative displacement as well as its time derivative and time history, as detailed in the next subsection. The contact pressure is taken into account in the weak form of the dynamic equilibrium (2.1) in terms of the nonlinear force vector ${}_{\mathrm{d}}\boldsymbol{g}$, which is obtained by integration over the contact surface $\mathcal{C}$,

$$ {}_{\mathrm{d}}\boldsymbol{g} = \int_{\mathcal{C}} {}_{\mathcal{C}}\boldsymbol{B}^{\mathrm{T}}(\boldsymbol{x})\ {}_{\mathcal{C}}\boldsymbol{p}\,(\boldsymbol{x}, {}_{\mathcal{C}}\boldsymbol{u}_{\mathrm{rel}})\,\mathrm{d}A \approx \sum_k \boldsymbol{B}_k^{\mathrm{T}} \boldsymbol{p}_k\,(\boldsymbol{u}_{\mathrm{rel},k})\,\Delta A_k\,. \tag{2.4} $$

In practice, the continuous integral is approximated by a weighted sum over a finite set of so-called contact points, as indicated in Eq. (2.4). For this purpose, the shape functions and the contact pressures are evaluated at the locations $\boldsymbol{x}_k$. The weights ΔA_k involved in the sum can be interpreted as the area associated with each contact point k, cf. **Fig. 2.2**b. It is important to note that the notion of general contact points is preferred here to embrace various discretization methods ranging from lumped formulations to so-called mortar methods [182] for the coupling of subdomains with non-matching FE meshes.
The appropriate density and type of distribution of the contact points has a crucial influence on the accuracy of the contact modeling. In the most sophisticated but also most computationally involved approaches, the contact points coincide with the integration points of the finite surface elements which in turn are defined depending on the underlying solid elements [130, 53]. Another common approach is to define a new grid of contact points independent of the underlying elements [113, 24]. However, if the number of con-

tact points exceeds the number of coordinates involved in the interface description by far, an over-stiffening effect known as locking phenomenon may occur and result in poor accuracy [43, 3, 64]. Finally, the limit case of a single contact point is frequently applied in practice [164, 65]. In this *lumped* formulation, the rotational motion may be considered in addition to the translation in order to account for the torque transmission across the contact interface. In this case, $\boldsymbol{u}_{\mathrm{rel}}$, $\boldsymbol{p}$ represent generalized relative displacement and generalized pressure. This formulation cannot resolve the inhomogeneous character of the contact interactions. This is particularly relevant for friction damping, where the optimum performance is typically achieved in the microslip regime, where inhomogeneous interface deformations are expected [145]. While providing the lowest computational effort, the lumped formulation may thus lead to less accurate results, and the associated contact parameters are only valid in a limited range of operating conditions [52].
In order to assess the discretization quality, it is generally advisable to investigate the convergence behavior of the sought results with respect to an increasing number of contact points and underlying finite elements. The mesh density should be as small as possible to avoid spurious computational burden and as large as necessary to achieve sufficient convergence among the quantities of interest. In the case of friction damping, the measures of interest are typically resonance frequencies or the (global) dynamic response of the structure. These measures tend to converge faster with respect to the contact discretization than the local stress field in the contact interface [5, 8]. For the analysis of turbomachinery blades with dovetail joints in [25, 24], a number of 75 contact points at the root interface was regarded as sufficient for the prediction of the resonance amplitude of the blade tip. For a similar application, 21 contact points were found to achieve convergence of a particular resonance frequency for a sticking contact situation [130]. It can, however, be stated that such convergence studies are seldom conducted, and the appropriate contact discretization remains a delicate issue in the modeling of friction-damped systems.

Contact laws

The contact law defines the relationship between local contact pressure and local relative displacement. Depending on the law, this relationship can be expressed either in explicit form or as a differential equation, i. e. the pressure at a specific time instant may also depend on the relative velocity and the time history of the displacement. It is convenient to distinguish between the laws for the normal direction and those for the tangential plane, $\boldsymbol{p}^{\mathrm{T}} = \left[p_{\mathrm{n}}\ \boldsymbol{p}_{\mathrm{t}}^{\mathrm{T}}\right]$. Common laws for the unilateral contact and the dry friction law are illustrated in **Fig. 2.3**. This relation can be either considered as a constraint or a regular constitutive law. The former notion gives rise to set-valued relations and to velocities which are non-smooth in time due to possible impacts [180, 182]. For this purpose, special mathematical treatment is required to directly enforce the constraints, see e. g. [56]. Alternatively, a *regularization* technique can be utilized to enforce the constraints in a weak sense. In this context, the augmented Lagrangian approach [135] should be mentioned along with its frequency domain counterpart, the Dynamic Lagrangian approach [103] which is well-suited in conjunction with the harmonic balance method.

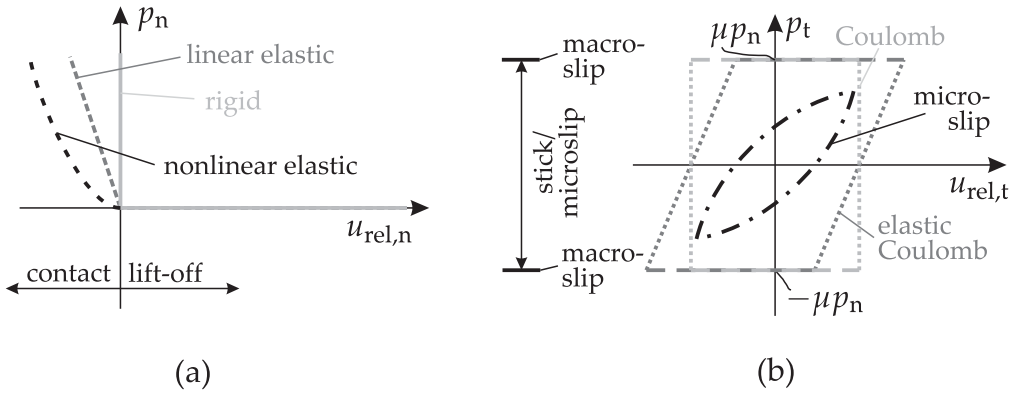

(a) (b)

Figure 2.3: Contact laws for dry interfaces: (a) unilateral contact, (b) dry friction

The so-called penalty regularization is mathematically equivalent to the elastic reformulation of the contact constraints and can thus be expressed as a regular constitutive law, see **Fig. 2.3**. Such a regular law gives rise to time-continuous pressures and continuously differentiable velocities.

Normal direction

The normal contact law restricts the interpenetration of interacting surfaces. Unilateral contact is typically assumed where the normal pressure is compressive in the case of contact and zero otherwise. The normal pressure is generally a variable quantity which depends on the initial normal pressure (i. e. in the absence of vibrations) and the contact normal dynamics, see e. g. [186, 184]. If the contact is initially open, the initial normal pressure is zero. As a consequence of vibrations, the contact may close, resulting in a generally nonzero, oscillating normal pressure. The reverse situation is also possible: If the contact is initially closed, the normal pressure level oscillates as well, and the contact point may lift off when this oscillation exceeds the initial pressure.

Different normal contact laws are depicted in **Fig. 2.3**a. Apart from the non-regular rigid formulation, the linear elastic penetration law is widely used. Moreover, nonlinear relations may be employed [147, 162] that aim at modeling the Hertzian contact of the entire contact surface or local surface asperities [58, 180, 182]. The normal contact interaction is typically considered conservative, although few approaches can be found that model the dissipative character of normal impacts in terms of a coefficient of restitution or viscous damping elements.

Tangential plane

The dissipative character of dry sliding friction essentially stems from the deformation behavior of surface asperities on different length scales. This behavior is of hysteretic type and is taken into account in the tangential contact laws. Different friction laws are illustrated in **Fig. 2.3**b for the case of steady alternating one-dimensional translational relative motion $u_{rel,t}$ subject to constant normal pressure p_n. It should be noted that p_n does not have to be constant, as explained in the previous paragraph.

The (elastic) Coulomb friction law describes the friction pressure for spatially homogeneous relative displacement. Assuming that the local geometric and elastic properties are

accurately described in an interface model with fine discretization, the local application of this law seems appropriate. However, such a fine discretization is often infeasible and local surface characteristics are not precisely known in practice. It is thus common to account for the inhomogeneous character of the interface behavior implicitly in so-called microslip models, cf. **Fig. 2.3**b. Common examples are the Dahl [37], the LuGre [181], the Bouc-Wen [175] and the Preisach [173] differential models. While the microslip laws are frequently applied to contact problems with time-constant normal load, numerical difficulties typically arise in conjunction with lift-off phases [129]. Microslip effects may have a significant influence on the friction damping performance. They are particularly relevant for large rough interfaces of compliant bodies subject to high normal loads [61].
The dry friction law is commonly assumed to be frequency-independent. In particular, the friction properties are regarded as independent of the magnitude of the relative velocity. Moreover, the static friction coefficient in the (elastic) Coulomb law is typically specified to be identical to the dynamic one. An important reason for this simplification is apparently the difficulty of parameter identification.
In contrast to the simplified illustration in **Fig. 2.3**b, the geometric coupling between the two cartesian coordinates spanning the tangential contact plane needs to be considered. However, it is common practice to account for each direction in a decoupled manner, see e. g. [128, 155, 188]. This can significantly decrease the computational burden in the dynamic analysis [30]. However, substantial quantitative differences between the coupled and the uncoupled approach are generally possible [129]. A qualitative difference is the possibility of a continuous sliding state which can only be described by the coupled approach.

2.1.3 Direct dynamic analysis methods

The dynamic analysis refers to the determination of the temporal evolution ${}_{\mathrm{r}}\boldsymbol{u}(t)$ of the generalized coordinates from the equations of motion (2.2). For the sake of brevity, the subscript will be omitted now, i. e. $\boldsymbol{u} \equiv {}_{\mathrm{r}}\boldsymbol{u}$. Direct analysis approaches are presented below, where the term *direct* is used to express that no further model (order) reduction is carried out, in contrast to the approaches based on nonlinear modes addressed later.
An exact solution can be established only for simplified special cases of friction-damped problems [39]. Analytical approximations obtained by asymptotic techniques are typically not capable of treating the non-smooth forces and are thus not well-suited for contact problems [48, 67]. Hence, numerical methods have established themselves for the dynamic analysis of friction-damped systems.
The most versatile class of dynamical analysis approaches is the family of numerical time integration methods. For contact problems, time integration methods can be classified into event-driven and time stepping algorithms. Event-driven algorithms aim at directly resolving the transitions between different situations (stick, slip, lift-off). This can be a computationally exhaustive endeavor, in particular if numerous events occur [44, 132]. In contrast, time stepping algorithms tend to perform well, even in the case of numerous

events. However, they inherently feature discretization errors which may lead to inferior accuracy. An important computational property of differential equations (2.2) is their *numerical stiffness*. This stiffness is caused by the strong deviation of the orders of magnitude of the relatively small global structural stiffness on one hand and the large local contact stiffness on the other hand. For numerically stiff problems, all time integration methods share the drawback that they require comparatively small time steps which results in considerable computational effort [135]. Time integration methods are therefore seldom applied in the context of extensive parameter studies. Owing to their high accuracy, time integration methods are widely used as reference for other approximate methods. Moreover, they are employed in situations where no alternative approaches are applicable.
For friction-damped systems, the family of periodic solutions of the equations of motion is often of primary interest in practice. For their efficient computation, special methods have been developed. Among these methods, the shooting method and the harmonic balance method are probably the most popular ones.

Shooting method

Starting from arbitrary initial values, the time integration often requires a long time span until reaching steady-state conditions because of the typically weak damping [47]. This computational burden can be decreased by directly enforcing periodicity of the state vector $\begin{bmatrix} \boldsymbol{u}^{\mathrm{T}} & \dot{\boldsymbol{u}}^{\mathrm{T}} \end{bmatrix}^{\mathrm{T}}$ after the minimal vibration period T,

$$\begin{bmatrix} \boldsymbol{u}(T) - \boldsymbol{u}(0) \\ \dot{\boldsymbol{u}}(T) - \dot{\boldsymbol{u}}(0) \end{bmatrix} = \boldsymbol{0}\,. \tag{2.5}$$

The initial value problem is thus reformulated as a boundary value problem, for which the initial state vector at time $t = 0$ is sought to satisfy Eq. (2.5). Eq. (2.5) represents a set of nonlinear algebraic equations which can be solved using e. g. Newton-like methods. In an iterative solution procedure, the state vector at time $t = T$ is still computed by means of time integration from the current estimate of the initial state vector. The shooting method has also been applied to friction-damped systems, see e. g. [44].

Harmonic balance

Another method for the computation of periodic solutions of ODEs is the harmonic balance method[1] [169, 22, 108]. To this end, the dynamic variables are expanded in a Fourier series truncated to harmonic order H and featuring the base frequency Ω, e. g.

$$\boldsymbol{u}(t) \approx \Re\{\sum_{n=0}^{H} \hat{\boldsymbol{u}}_n \mathrm{e}^{\mathrm{i}n\Omega t}\}\,. \tag{2.6}$$

[1] In the literature, other widely used names for the method described here are the Describing Function method and the method of Krylov-Bogoliubov-Mitropolsky. Moreover, the prefix 'multi' or 'high-order' are often used for the harmonic balance method in order to clarify the difference to the single-term variant which only considers the fundamental harmonic.

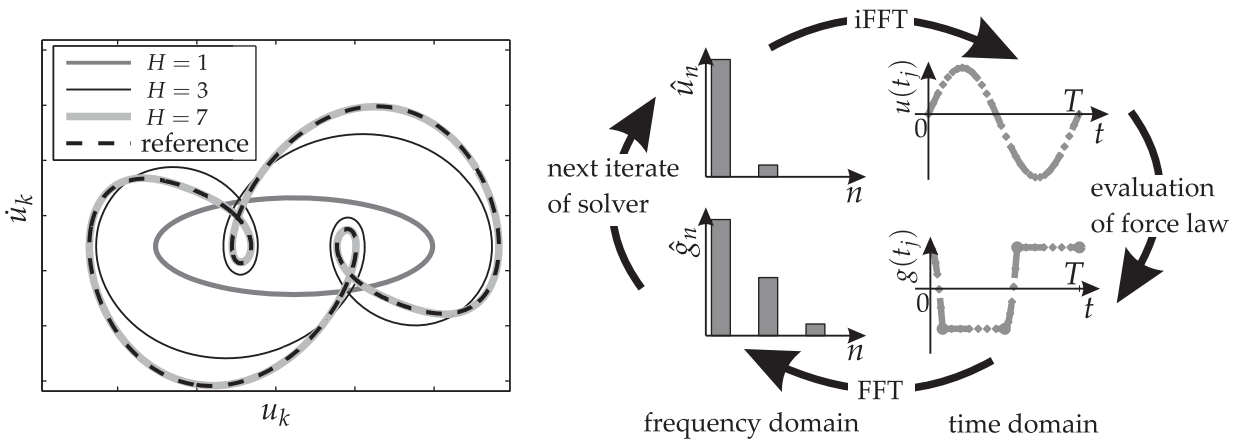

(a) (b)

Figure 2.4: Basic notions of the harmonic balance method: (a) convergence with respect to harmonic order H, (b) alternating-frequency-time scheme

Due to this particular choice of base functions, periodicity of the sought motion is automatically met.
The substitution of Eq. (2.6) into the equations of motion (2.2) and subsequent Fourier-Galerkin projection gives rise to a set of nonlinear algebraic equations in the unknown Fourier coefficients $\hat{\boldsymbol{u}}_n$ of the generalized coordinates,

$$\left[-(n\Omega)^2\boldsymbol{M} + \mathrm{i}n\Omega\boldsymbol{C} + \boldsymbol{K}\right]\hat{\boldsymbol{u}}_n + \hat{\boldsymbol{g}}_n\left(\hat{\boldsymbol{u}}_0, \ldots, \hat{\boldsymbol{u}}_H\right) = \hat{\boldsymbol{e}}_n \;\forall\, n = 0, \ldots, H\,. \tag{2.7}$$

Herein, the harmonic coefficients $\hat{\boldsymbol{g}}_n, \hat{\boldsymbol{e}}_n$ are related to their respective time-domain counterpart by the Fourier transform, e. g. $\hat{\boldsymbol{g}}_n = \frac{1}{2\pi}\int_{(2\pi)} \boldsymbol{g}\mathrm{e}^{-\mathrm{i}n\Omega t}\mathrm{d}\Omega t$ for $n \geq 1$.
For friction-damped systems with localized contact interfaces, the nonlinear forces are typically associated with only a small subset of the generalized coordinates. In this case, an exact condensation procedure to only these coordinates can be applied. This can significantly reduce the computational effort required for the iterative solution process [82, 60, 10, 26].
It should be noted that the approximation in Eq. (2.6) is infinitely smooth. This is in contrast to the exact solution which has a limited degree of smoothness owing to the non-smooth character of the contact forces. The approximation typically exhibits oscillatory behavior in the vicinity of these discontinuities, which is known as the Gibbs phenomenon. The harmonic balance method may therefore suffer from weak convergence behavior and lead to poor predictions, in particular for higher-order time derivatives of the generalized coordinates [80].

Influence of the harmonic order
It is assumed that for sufficiently large values of the harmonic order H, the approximation agrees with the exact solution to sufficient accuracy, as illustrated in **Fig. 2.4**a. In order to avoid spurious computational effort, the harmonic order should be selected as small as possible considering the required accuracy [95, 70].
Experiments and simulations of friction-damped systems often suggest that the funda-

mental harmonic component of the response is predominant within the dynamic regime of interest [72]. Hence, the single-term variant, where only the harmonic $n = 1$ is retained in the balance (2.7), is very popular [142, 27, 111, 15]. It is often reported that this variant provides good approximations when the normal pressure is almost constant [69]. However, the consideration of higher harmonics can significantly influence the fundamental harmonic component of the response [33]. The higher-order contributions are important for the accurate resolution of the stick, slip, and lift-off behavior at the contact interface [27]. Furthermore, it is crucial to consider the static balance, i. e. the zeroth harmonic in Eq. (2.7) for contact problems. Otherwise, the effects of settling and realignment of the contact interface [50, 51, 188, 141] or the static deflection induced by impact-type interactions cannot be taken into account. Hence, the single-term variant can suffer from poor accuracy for strongly nonlinear contact interactions [47, 186].
Particularly for the case of small clearances or low normal pressures [186], so-called sub- or superharmonic resonances are reported for numerical as well as for experimental investigations [177, 10, 27, 26, 85]. In these dynamic regimes, the response is no longer dominated by its fundamental harmonic component, and it cannot be predicted with the single-term harmonic balance method.

Computation of nonlinear forces

The harmonic components $\hat{\boldsymbol{g}}_n$ of the nonlinear forces depend on the harmonics $\hat{\boldsymbol{u}}_n$ of the sought coordinates. This functional relationship can in general not be expressed in closed form, and numerical procedures have to be utilized for the computation instead. This crucial task often becomes the bottleneck within the iterative solution process.
In analogy to time integration, event-driven schemes can be utilized to detect the transitions between different contact states directly [128, 15, 87]. Once the transition time instants are determined, the harmonic components $\hat{\boldsymbol{g}}_n$ are computed by piecewise integration. This step can be carried out analytically for piecewise polynomial systems [87]. Note that this class of systems includes systems with unilateral springs and elastic Coulomb friction, which are piecewise linear.
The alternating-frequency-time scheme is a widely used alternative to event-driven schemes and it is illustrated in **Fig. 2.4**b. The contact laws are directly applied in the time domain to force $g(t_j)$ and displacement $u(t_j)$ values at equally spaced time instants t_j. The conversion between time and frequency domain is efficiently performed through the (inverse) Fast Fourier Transform ((i)FFT) [18, 20].

Solution, continuation and bifurcation analysis

Both the shooting method and the harmonic balance method give rise to a set of nonlinear algebraic equations. In general, iterative procedures have to be used for the solution of these equations. A commonly used procedure is the Newton method. An iteration of the Newton method basically involves the solution of the following set of linear equations,

$$\left.\frac{\partial \boldsymbol{R}}{\partial \boldsymbol{Z}^{\mathrm{T}}}\right|_{\boldsymbol{Z}^{-}} \Delta \boldsymbol{Z}^{+} = -\boldsymbol{R}(\boldsymbol{Z}^{-})\,. \tag{2.8}$$

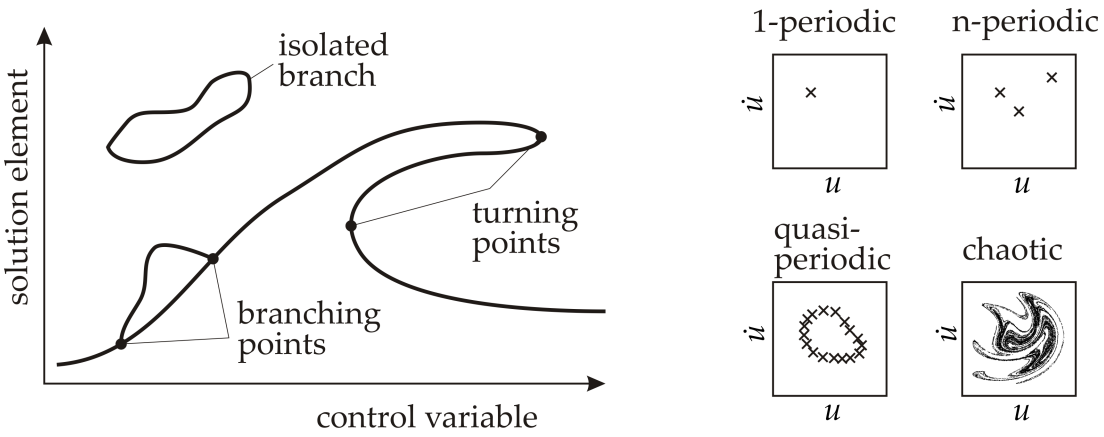

Figure 2.5: Important phenomena of a nonlinear dynamical system: (a) conceptual bifurcation diagram, (b) Poincaré sections of possible attractors

Herein, $\boldsymbol{R}$ and $\boldsymbol{Z}$ are the residual vector and the vector of unknowns, respectively, and $\frac{\partial \boldsymbol{R}}{\partial \boldsymbol{Z}^{\mathrm{T}}}$ is the gradient of the residual with respect to the unknowns. In each iteration, the residual and its gradient have to be determined at the current estimate $\boldsymbol{Z}^{-}$. Then Eq. (2.8) is solved in order to find the next correction step $\Delta\boldsymbol{Z}^{+}$ and the new estimate $\boldsymbol{Z}^{+} = \boldsymbol{Z}^{-} + \Delta\boldsymbol{Z}^{+}$. Starting from an initial guess, successive iterations are computed until the norm of the residual is smaller than a specified tolerance.

The Newton method is a gradient-based method. For such methods, the solution process can be significantly accelerated by providing the required gradients $\frac{\partial \boldsymbol{R}}{\partial \boldsymbol{Z}^{\mathrm{T}}}$ analytically [10]. Gradient-based methods are known for their superior convergence behavior in the vicinity of a good initial guess. Hence, so-called (path) continuation methods are applied that facilitate the iterative computation of solutions with respect to a control variable by accounting for the already known solutions [148]. A typical control variable is the excitation frequency when frequency-response curves are of interest. Possible difficulties, that may arise with the continuation of solutions, are illustrated in **Fig. 2.5**a. Groups of solutions are connected via so-called branches in the bifurcation diagram. The singularities at turning points can be easily overcome by means of continuation. In contrast, the detection of branching points and the switching to another branch require special treatment. In addition, isolated branches may be present which cannot be directly found by continuation. A good review of suitable methods for continuation and bifurcation analysis and related computational aspects is given in [148].

Both the shooting and the harmonic balance method only facilitate the computation of periodic motions. A nonlinear system may, however, also exhibit quasi-periodic or even chaotic steady-state vibration behavior [81, 144, 63]. The different possible attractors are illustrated in the form of Poincaré sections in **Fig. 2.5**b. For friction-damped systems, such non-periodic regimes are reported for the case of high-energy impacts and rubbing phenomena [105].

The Floquet theorem can be used to assess whether a found periodic motion is asymptotically stable, i. e. whether all trajectories starting in the vicinity will converge towards

this orbit. A change in stability indicates a bifurcation of the solution. In case of unstable periodic motion, one or more new stable attractors may be present instead, each being either periodic or non-periodic. In general, a sophisticated stability and bifurcation analysis may be appropriate, if such non-regular behavior is expected. The interested reader is referred to [159, 60, 115] for examples of such studies with applications to dynamical contact problems. It can generally be stated that the aspect of local stability, non-periodic attractors and the branching behavior or even the occurrence of isolated branches is only seldomly addressed in the field of friction damping.

2.2 Design of friction-damped systems

In this section, an overview of the design considerations of friction-damped systems is provided. In particular, it is described how the vibration reduction is achieved and under which conditions friction damping is typically applied. It is further detailed which dynamic characteristics are typically assessed in the course of the design process and which essential parameter dependencies exist.
Several aspects of the design of friction-damped systems are considered beyond the scope of this section. These aspects include (semi-)active vibration reduction strategies and the application-specific forms of coupling elements and interfaces. For these aspects, the interested reader is referred to [45, 134].

2.2.1 Mechanisms of vibration reduction

The essential vibration reduction mechanism of friction-damped systems is obviously the dissipation due to dry sliding friction. Moreover, the dissipative character of impacts can contribute to the effective damping. In addition to dissipative effects, dispersive effects may be induced by the strongly nonlinear contact interactions, in particular with regard to the normal contact dynamics. Dispersion causes a (re-)distribution of the kinetic energy in time and space. A special case of this mechanism is the so-called energy pumping[2] [96], where the kinetic energy of a base structure is passively (and irreversibly) transferred to a strongly nonlinear absorber. Because of the strong nonlinearity, this mechanism is effective in a wide frequency range [170]. The resulting dispersed vibration behavior may be acceptable from a design point of view, even without significant amount of dissipation [116]. Finally, contact joints can be utilized to shift the eigenfrequencies at such a rate that they do not coincide with the load spectrum, and to influence the vibrational deflection shape in order to reduce its coherence with the excitation field.

[2] Another widely used name for this mechanism is 'targeted energy transfer', and the corresponding absorber is often referred to as 'nonlinear energy sink'.

2.2.2 Dynamic regimes of interest

In order to design friction-damped systems, it has to be distinguished between the sources of vibration which the system is exposed to during operation. It can generally be stated that friction damping has been mainly applied to systems either exposed to essentially periodic external forcing or negative damping. In contrast, it can be observed from the literature that conceivable cases of parametric excitation, shock-type [96] or broad-band excitation [93] are only seldomly addressed. On one hand, friction damping is apparently well-suited for the mainly considered sources of excitation. On the other hand, it has to be remarked that a considerable amount of research related to friction damping has been carried out in the field turbomachinery bladed disks. Here two important scenarios are the forced response due to rotation within an inhomogeneous fluid pressure field or the self-excited response in the presence of aero-elastic instabilities [158]. These scenarios can be characterized by essentially periodic external forcing or negative damping, respectively.
Among periodically forced scenarios, the most important case is certainly harmonic forcing near a particular resonance. In general, the steady-state vibration behavior is of primary interest, since persisting oscillatory stresses are an important cause of material fatigue. Unsteady forcing as in the case of resonance passages, i. e. a coincidence of an eigenfrequency and a time-varying external forcing frequency, is also a relevant scenario [68, 67]. In the field of power plants, resonance passages are attested an increasingly important role in the design of gas and steam turbines [14].

2.2.3 Performance measures

For the purpose of fatigue investigations, an important measure is obviously the dynamic magnitude of displacement or stress at certain locations of the structure [163]. In externally forced scenarios, the resonance frequency shift is crucial for the detection and avoidance of possible resonances [41]. In self-excited scenarios, the limitation of the response with respect to negative damping is often of interest [156, 178].
The effective damping ratio represents another quantity which is frequently assessed experimentally or numerically [46]. Different approaches exist for its definition and computation. Several authors propose determining the effective damping ratio from the width of the resonance peak of the frequency-response curve using the so-called half-power method [177, 41, 77]. Another approach is to determine the effective damping ratio from the temporal evolution of the vibration envelope for the free decay response (typically from a near-resonant situation). An advantage of these two approaches is that they do not require system model. In contrast, a model is required for the energy-based determination of the loss factor [165, 176, 9, 153]. The loss factor is related to the energy ΔE_{diss} dissipated per vibration cycle and the maximum reversible potential energy $E_{\mathrm{pot,max}}$ attained during oscillation [110],

$$\eta_{\mathrm{loss}} = \frac{\Delta E_{\mathrm{diss}}}{2\pi E_{\mathrm{pot,max}}} \,. \tag{2.9}$$

All these approaches can be classified as a posteriori strategies, since they rely on vibration data to be measured or predicted. In the case of the loss factor, it is also common to assume a harmonic vibration with the linear deflection shape. The variation of the vibrational deflection shape and the influence of higher-harmonic vibration content are commonly neglected, which can lead to poor accuracy [187].
Most design studies address the performance optimization with respect to a given set of design variables by considering all parameters as fixed. This can lead to inferior performance, if the parameters are uncertain, i. e. if the parameters of the actual system deviate from those in the model. It is therefore relevant to investigate the influence of specific parameters on the performance, i. e. to carry out so-called sensitivity analyses. If the stochastic characteristics of the parameters are known, probabilistic methods can be employed in order to determine the stochastic characteristics of the resulting design performance [124]. Based on this approach, a measure of robustness can be defined [123]. It can generally be stated that parameter uncertainties are acknowledged as apparent difficulty in the design of friction-damped systems. However, appropriate robust design strategies are comparatively rare. This is most certainly because of the prohibitive computational cost associated with such approaches.

2.2.4 Parameter dependencies

Some of the most significant system parameters and their qualitative influences are listed below. In general, the parameters can influence the contact interactions arising in a specific contact interface. The contact interactions can be classified in three different regimes. In the sticking regime, there is no (or comparatively small) relative motion in the contact interface. As a consequence, (almost) no energy is dissipated, and the contact interface fully contributes to the overall stiffness of the structure. In the regime of moderate relative motion in the contact interface, stick-slip and possibly first lift-off transitions occur. As a consequence, energy is dissipated during the sliding friction phases, and the contact interface only contributes by a decreased amount to the overall stiffness of the structure. In the regime of large relative motion, less sticking friction occurs and the contact primarily undergoes sliding or lift-off. The effective stiffness typically tends to a constant value, and the effective damping ratio often tends to zero.

External forcing parameters

Level
The characteristic curve relating the resonant vibration level to the excitation level is termed *damper performance curve* [19], and a typical example is illustrated in **Fig. 2.6**a for the case of harmonic forcing. An increasing excitation level can induce larger relative motion in the contact interface, resulting in the different regimes as described above. It is often found that there exists a range where the damping mechanism is effective and the

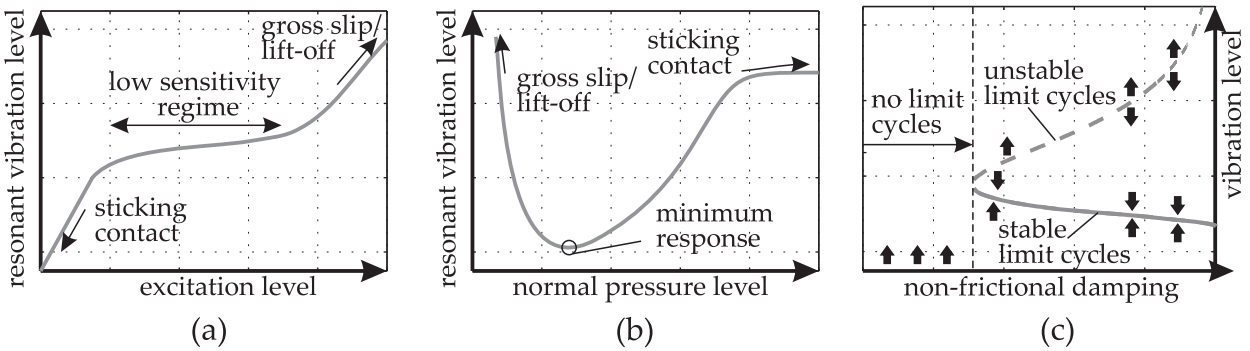

Figure 2.6: Frequently sought characteristics of friction-damped systems: (a) damper performance curve for harmonic forcing, (b) optimization curve for harmonic forcing, (c) stability map for negative damping

vibration level is almost constant under variation of the excitation level [36, 62, 23]. This range of low sensitivity is particularly valuable when the excitation level is uncertain.

Frequency spectrum
The frequency spectrum can generally be continuous or discrete. A particularly critical situation is the case of external resonance, i. e. when an excitation frequency coincides with an eigenfrequency of the system. Frequency-response curves are commonly analyzed to assess the vibration behavior near resonance. The excitation frequency is often directly linked to an operating condition such as the rotational speed in rotating machinery. The frequency spectrum depends on various influences and is often considered uncertain to some extent [146].

Spatial distribution
The spatial coherence of forcing and vibrational mode shape determines the excitability and the intensity of the vibration. Thus, it can have a similar effect as the excitation level. The spatial distribution plays a predominant role in rotationally periodic structures such as turbomachinery bladed disks [166]. If the forcing exhibits a particular order of symmetry (often termed engine order), the steady-state response typically features a corresponding symmetry as well.

Contact parameters

Level of normal pressure
A typical example for the relationship between resonant vibration level subject to harmonic forcing and the normal pressure level is illustrated in **Fig. 2.6**b. Since the normal pressure represents an important design variable, this characteristic is commonly denoted the *optimization curve*. An increasing normal pressure level tends to reduce the relative motion within the contact interface, resulting in the different regimes as described above. The vibration level typically reaches a minimum for a specific value of the normal pres-

sure level. It should be remarked that the pressure level can often not be regarded separately, since it depends on different system parameters and operating conditions [36].

Distribution of normal pressure and clearances
Depending on the initial pressure distributions, certain portions of the contact interface may undergo larger relative motion during vibration than others. This can have a significant influence on the damping performance, particularly for larger normal pressure levels. Inhomogeneous initial clearance distributions have a similar effect. During vibration, the effective contact area may vary when initially open portions of the interface come into contact or initially closed portions lift off [130, 86]. The effective contact area, in turn, influences effective stiffness of the interface.

Geometry of contact interface
For homogeneous normal pressure distribution, the area of the contact interface typically plays only a minor role for the damping behavior compared to the overall interlock load [77]. The area may, however, significantly affect the effective stiffness of the interface. The shape of the contact interface has a significant influence on the normal pressure distribution. The correlation between the orientation of the contact interface and the vibrational deflection shape determines whether the contact dynamics are dominated by tangential or normal relative motion. Greater damping performance is typically achieved for dominant tangential motion [75, 104].

Friction characteristic
Similar to the orientation of the contact interface, the friction characteristic has an effect on the preferential contact dynamics: If the friction forces are comparatively small, large relative motions in the tangential plane of the interface are possible [69, 121]. It can generally be stated that the friction characteristic is considered uncertain, since it is temperature-dependent and may change during operation e. g. due to wear-induced variation of surface properties [180, 121].

Parameters of the underlying system

Geometric and material properties of the underlying structure
These parameters influence the elastic and inertial forces within the structure and thus have an effect on the resulting vibrational deflection shape. This is particularly relevant in the case of rotationally periodic structures such as bladed disks. In this case, even slight deviation among the properties of individual segments may cause qualitatively different vibrational deflection shapes of the assembly and induce localization effects [28, 21]. In rotating machines, the centrifugal forces can cause large deflections and lead to geometric stiffening [32].

Non-frictional damping
The magnitude of a positive damping can strongly influence the relative reduction of the ratio between the resonant vibration level with and without friction damping. If the system is exposed to fluid flow, fluid-structure interaction can have a significant influence on the resulting vibration behavior. In particular, aero-elastic instabilities may result in negative damping, i. e. self-excitation [156, 62]. The positive damping contributed by the dissipative contact interactions in friction interfaces or contact-induced variations of the vibrational deflection shape can give rise to stabilized limit cycles. The resulting vibration level depends on the amount of negative damping. The relationship between amount of negative damping and resulting vibration level is termed *stability map*, and a typical example is illustrated in **Fig. 2.6**c. In the figure, the arrows indicate whether sufficiently small perturbations around the limit cycles are increased or decreased, i. e. whether the limit cycle is stable or unstable. If the negative damping is too intensive or the initial kinetic energy is too large, no limit cycle is reached and the vibration level increases unboundedly. It should be noted that non-frictional damping is also subject to uncertainties in many applications.

2.3 The concept of nonlinear modes

The concept of nonlinear modes is an attempt to extend the ideas of modal analysis to nonlinear systems. Unfortunately, several mathematical properties are lost when nonlinear effects become important. For instance, the superposition principle is not valid in nonlinear systems, and the modal deflection shapes are no longer orthogonal to each other. As a consequence, only some ideas can be generalized to nonlinear systems. In particular, the property of nonlinear modes to reproduce resonant vibration behavior subject to harmonic excitation can be adopted (*deformation-at-resonance* property). Moreover, the *invariance* property also applies in the nonlinear case, i. e. once an autonomous system vibrates in a particular nonlinear mode, this mode will persist and no other mode will be excited. As in the linear case, these properties can be utilized for the purpose of model (order) reduction.
Nonlinear modal analysis is concerned with the identification of the energy-dependent vibration signature in terms of eigenfrequencies, modal damping ratios and vibrational deflection shapes. A conservative, autonomous two-degree-of-freedom (DOF) oscillator with cubic spring as illustrated in **Fig. 2.7**a serves as illustrative example [78]. Its eigenfrequencies are depicted with respect to the kinetic energy in **Fig. 2.7**b. Due to the stiffening effect of the cubic spring, the eigenfrequencies essentially increase with energy. Moreover, the vibrational deflection shape varies, as it can be inferred from the phase projections illustrated in the subfigures in **Fig. 2.7**b.
The concept of nonlinear modes facilitates the qualitative understanding of nonlinear phenomena [172]. These phenomena include the localization of kinetic energy, the change of stability of modes and modal interactions. It can be deduced from the modal deflection

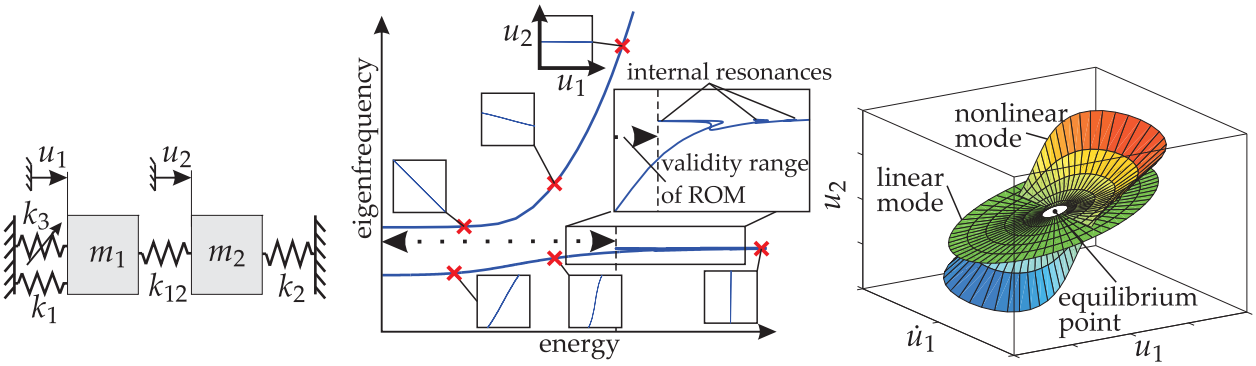

(a) (b) (c)

Figure 2.7: Nonlinear modes of a two-DOF oscillator with cubic spring $k_3 = 0.5$, $k_1 = k_2 = k_{12} = 1$, $m_1 = m_2 = 1$, similar to [78]: (a) model definition, (b) frequency-energy plot with phase projections of the vibration behavior, (c) two-dimensional invariant manifold of the first mode

shapes illustrated in **Fig. 2.7**b that for both modes the vibration localizes in a particular DOF for large energies. Owing to the energy dependence, initially distinct eigenfrequencies may become commensurable in the nonlinear regime. In such a situation, energy is exchanged between the modes, i. e. so-called nonlinear modal interactions occur [106]. This behavior is typically accompanied by folds in the frequency-energy plot (and also in phase space), which can also be observed for the example model, cf. **Fig. 2.7**b. The folds form 'tongues' in the frequency-energy plot. At the tip of the tongues, the eigenfrequencies are commensurable and a so-called internal resonance is present.
This section is structured as follows: First, the different definitions of nonlinear modes are introduced in Section 2.3.1. Conventional methods for the computation of nonlinear modes are presented in Section 2.3.2. Finally, the existing model reduction approaches based on nonlinear modes are addressed in Section 2.3.3. Based on this, the current shortcomings are identified in Chapter 3 upon which the purpose of this thesis is defined.

2.3.1 Definition of nonlinear modes

Definition as periodic motions

Rosenberg [140] first defined nonlinear modes for autonomous symmetric conservative systems as periodic motions *in unison*. Unison refers to motions for which all material points cross their equilibrium point and their extremum points simultaneously. For this type of vibration, the motions take place on so-called modal lines in the generalized displacement space which are normal to the surface of maximum potential energy [172][3]. This rather restrictive definition of Rosenberg was later generalized to non-trivial peri-

[3] In the literature, the term Nonlinear Normal Mode (NNM) is thus quite common. However, the term 'normal' may mislead to the wrong conclusion that nonlinear modes are orthogonal to each other. Moreover, orthogonal intersection with equipotential curves is a property which is only valid for symmetric conservative systems in general. Hence the term 'normal' in this context is avoided throughout this thesis.

odic motions of autonomous conservative systems [136]. The unison restriction was thus relaxed in order to include the case of internal resonance, where different parts of a system may oscillate with individual, but commensurable frequencies. Moreover, the orthogonal intersection of equipotential curves was eased, so that there may exist a phase lag between the oscillations of different coordinates.
It is important to note that the possible number of periodic motions for a given energy may exceed the number of coordinates [174]. In fact, a countable infinity of nonlinear modes may exist following this definition. These periodic motions are not necessarily continuations of the linear modes of vibration. An important feature of the periodic motion definition is that vibratory properties are directly associated with the modes: For instance, their eigenfrequency is part of their definition. The resonant vibration behavior for harmonic forcing, i. e. the backbone curve is also a by-product of their calculation. Furthermore, the local stability of the periodic motions can be analyzed in a straightforward manner. The extension of the periodic motion definition of nonlinear modes to non-conservative systems is impossible without further assumptions due to the lack of periodicity of the flow, i. e. the temporal evolution of the coordinates in this case.

Definition as invariant manifolds in the phase space

Shaw and Pierre [149, 150, 151] define a nonlinear mode as the invariant relationship between the states of an autonomous dynamical system in the form of a two-dimensional manifold in phase space which is tangent to the eigenspace of the linear mode at the equilibrium point, cf. **Fig. 2.7**c. On this subspace, all the flow of the nonlinear mode takes place and the system behaves like a single-DOF oscillator [149]. This definition has also been extended to the case of internal resonances. In this case, the flow of the nonlinear mode takes place on a higher-dimensional manifold and behaves like a multi-DOF oscillator. In order to account for external harmonic forcing, the state space can be artificially augmented by the phase of excitation, thus making the system autonomous [74].
In contrast to the periodic motion definition, the application to non-conservative systems is straightforward. It should be noted that the invariant manifold concept primarily defines the geometry of the nonlinear mode. Unlike the periodic motion definition, the notion of vibratory properties is therefore not preserved. Characteristic features of the nonlinear mode such as eigenfrequency, modal damping ratio and local stability have to be derived from the flow on the manifold [13, 2]. Furthermore, the definition of Shaw and Pierre is restrictive in the sense that the invariant manifold must be connected to the linear modes via the equilibrium point, which is in contrast to the periodic motion definition.

2.3.2 Calculation of nonlinear modes

Following the periodic motion and the invariant manifold definitions, several researchers developed techniques for the construction of nonlinear modes. In the following, the most important classes of methods are detailed.

Periodic motion based methods

The notion of periodic motions permits the utilization of the methods presented in Section 2.1.3 in general. In contrast to the externally forced case, the fundamental oscillation frequency is an additional unknown, and instead of a single solution, a family of solutions exists for the same parameters. For this purpose, the set of equations is augmented by additional normalization conditions. Once a periodic motion has been found, a continuation with respect to the modal amplitude can be performed in order to determine the energy-dependent modal properties.
Kerschen et al. [114] employed the *shooting method* for the analysis of nonlinear modes in the time domain. They used a predictor-corrector continuation technique for a successive computation of the modes. This facilitated the detection of internal resonances which are often accompanied by turning points in the frequency-energy plot. Moreover, a stability analysis was carried out using the Floquet theorem. Several strategies for the reduction of the computational burden were proposed such as to provide analytical gradients for the iterative solution procedure. Unfortunately, it is not clear whether the method can be extended to non-conservative systems.
The harmonic balance method has been widely used for the computation of nonlinear modes following their definition as periodic motions of autonomous, conservative systems [138, 139, 31]. As in the non-autonomous case, frequency domain methods are typically attested a greater computational efficiency than time domain methods, particularly in the case of numerically stiff contact problems [135].
A modification of the conventional harmonic balance method, particularly relevant for the present thesis, is the generalized Fourier-Galerkin method (gFGM) proposed by Laxalde and Thouverez [94]. Inspired by the eigensolution for linear damped systems, the authors introduced a complex eigenvalue λ in their generalized Fourier ansatz,

$$\boldsymbol{u}(t) \approx \Re\{\sum_{n=0}^{H} \hat{\boldsymbol{u}}_n \mathrm{e}^{n\lambda t}\}\,. \tag{2.10}$$

This eigenvalue λ is related to the undamped eigenfrequency ω_0 and the modal damping ratio D by $\lambda = -D\omega_0 + \mathrm{i}\omega_0\sqrt{1-D^2}$. Compared to the conventional harmonic balance ansatz in Eq. (2.6), a possible real part of λ accounts for the decay of the motion in addition to the imaginary part which describes the oscillation, which is the key feature for treating dissipative systems. The same decay rate is used for all harmonics in Eq. (2.10), implying the assumption of a frequency-independent source of dissipation which is not necessarily the case for arbitrary damping sources. Allowing complex-valued coefficients $\hat{\boldsymbol{u}}$ takes into account possible phase lags between the generalized coordinates.
In analogy to the conventional harmonic balance method, the following set of algebraic equations is derived:

$$\left((n\lambda)^2\,\boldsymbol{M} + n\lambda\boldsymbol{C} + \boldsymbol{K}\right)\hat{\boldsymbol{u}} + \hat{\boldsymbol{g}}_n\left(\lambda, \hat{\boldsymbol{u}}_0, \ldots, \hat{\boldsymbol{u}}_H\right) = \boldsymbol{0}\ \forall\, n = 0, \ldots, H\,. \tag{2.11}$$

Since the ansatz (2.10) is not periodic, the numerical computation of the generalized Fourier coefficients $\hat{\boldsymbol{g}}_n$ of the nonlinear forces would involve an integral over infinity.

It was proposed in [94] to approximate these quantities by their periodic counterpart assuming that the amplitude decay takes place on a time scale much longer than the one of the oscillations. To this end, all time dependent variables are regarded as periodic with the damped eigenfrequency $\omega_0\sqrt{1-D^2}$ in contrast to the pseudo-periodic ansatz (2.10). Hence, standard procedures can be used for the evaluation of the generalized Fourier coefficients. The gFGM was applied to systems featuring dry friction contact with constant normal load [94]. The authors did not take into account the occurrence of internal resonances, so that a sequential continuation technique was sufficient for the computation of the energy-dependent modal properties.

Invariant manifold based methods

For the invariant manifold approach, the equations of motion are first recast into state space form with the state variables $\boldsymbol{u}$, $\boldsymbol{v} = \dot{\boldsymbol{u}}$. The nonlinear mode is established as invariant relation between the state variables and a (smaller) set of so-called manifold coordinates $\boldsymbol{\zeta}$ [150, 106, 74, 133, 168, 11],

$$\boldsymbol{u}(t) = \boldsymbol{U}\left(\boldsymbol{\zeta}(t)\right) \ , \quad \boldsymbol{v}(t) = \boldsymbol{V}\left(\boldsymbol{\zeta}(t)\right) \ . \tag{2.12}$$

Herein, the functions $\boldsymbol{U}, \boldsymbol{V}$ represent the manifold in state space. The dimension of the manifold corresponds to the dimension of $\boldsymbol{\zeta}$, which is equal to two in the absence of internal resonances.
The manifold coordinates uniquely characterize a location on the manifold. While the choice of the coordinate system may affect the solution process, the resulting geometry of the manifold in state space is of course invariant. In the case of the *master-slave parametrization*, a specific set of generalized coordinates and associated velocities is directly used as manifold coordinates, i. e. $\boldsymbol{\zeta} \in \boldsymbol{u} \cup \boldsymbol{v}$. However, it was found that it is more beneficial from a numerical point of view to choose a coordinate system which is more in line with the expected flow on the manifold [11]. This idea was followed in [6, 2, 7, 109] by defining an amplitude-phase parametrization of the invariant manifold. This choice of the coordinate system is known to lead to a better conditioning and to some degree of decoupling of the equations governing the manifold.
In order to determine the flow on the manifold, a set of ODEs in the manifold coordinates,

$$\dot{\boldsymbol{\zeta}} = \boldsymbol{f}\left(\boldsymbol{\zeta}\right) \ , \tag{2.13}$$

is required. This flow equation is typically obtained by substituting Eq. (2.12) into the system's equations of motion. The substitution of the manifold relation (2.12) and the flow equation (2.13) into the equations of motion in state space form gives rise to a set of partial differential equations in $\boldsymbol{\zeta}$,

$$\frac{\partial \boldsymbol{U}}{\partial \boldsymbol{\zeta}^{\mathrm{T}}}\boldsymbol{f} = \boldsymbol{V} \ , \tag{2.14}$$

$$\boldsymbol{M}\frac{\partial \boldsymbol{V}}{\partial \boldsymbol{\zeta}^{\mathrm{T}}}\boldsymbol{f} = -\boldsymbol{C}\boldsymbol{V} - \boldsymbol{K}\boldsymbol{U} - \boldsymbol{g}\left(\boldsymbol{U}, \boldsymbol{V}\right) \ . \tag{2.15}$$

Herein, the dependence (ζ) of the sought quantities $\boldsymbol{U}, \boldsymbol{V}$ and of $\boldsymbol{f}$ is not explicitly denoted. It should be noted that these equations are time-independent and thus only govern the geometry of the underlying dynamics.
A variety of techniques has been developed for the solution of Eqs. (2.14)-(2.15). While asymptotic techniques give rise to analytical solutions [150, 168], they are not generally applicable to arbitrary nonlinearities and are only valid up to comparatively small amplitudes [120]. A numerical, Galerkin-type procedure was proposed in [120, 74, 133], which provides high accuracy even for strongly nonlinear regimes. Although this approach is applicable to a broad problem class, the attention of most researchers was clearly focused on conservative systems with low-order polynomial type nonlinearities. Dissipative nonlinearities of the van-der-Pol type have been addressed recently in [109, 137]. The work in [73] overcomes the typical limitation to polynomial nonlinearities by considering a two-DOF oscillator with an elastic unilateral contact.

2.3.3 Model reduction based on nonlinear modes

The framework of nonlinear modes can be employed for the purpose of model (order) reduction. The dimension of the reduced order model (ROM) depends on the number of interacting nonlinear modes, i. e. it equals two in the absence of internal resonances. This facilitates a drastic reduction potential, if the dynamics of the original system are described by a large number of coordinates. This model reduction is actually the second step after an optional prior Component Mode Synthesis (CMS) step within the model reduction cascade depicted in **Fig. 2.8**a.
The actual model reduction approach depends on the concept which has been followed for the calculation of nonlinear modes. For invariant manifold based methods, the idea is to constrain the system dynamics to the so-called in-manifold dynamics, i. e. the flow inside the invariant manifold in phase space [117, 119]. This idea is illustrated in **Fig. 2.8**b. The flow inside the manifold is governed by Eq. (2.13). Upon solution in the reduced space, the response in the original state space can be recovered by Eq. (2.12).
For the periodic motion concept, model reduction approaches are generally limited to those dynamic regimes which are dominated by an isolated nonlinear mode. Thus, the presence of internal resonances represents a natural limitation of their range of validity, as illustrated in **Fig. 2.7**b [11]. Only under this assumption, the system behavior can be approximated by a single modal oscillator in accordance with the single nonlinear mode theory [160, 161]. The properties of this single modal oscillator correspond to the energy-dependent modal properties obtained during the preceding modal analysis step. It has also been proposed by several authors [29, 55] to take into account the off-resonant modes in their linear form in an approximate synthesis procedure.

Approximate superposition of linear damping and harmonic forcing
Although the superposition principle does not hold in the case of nonlinear systems, it has been widely used in the course of model reduction [71, 29, 55]. For this purpose, lin-

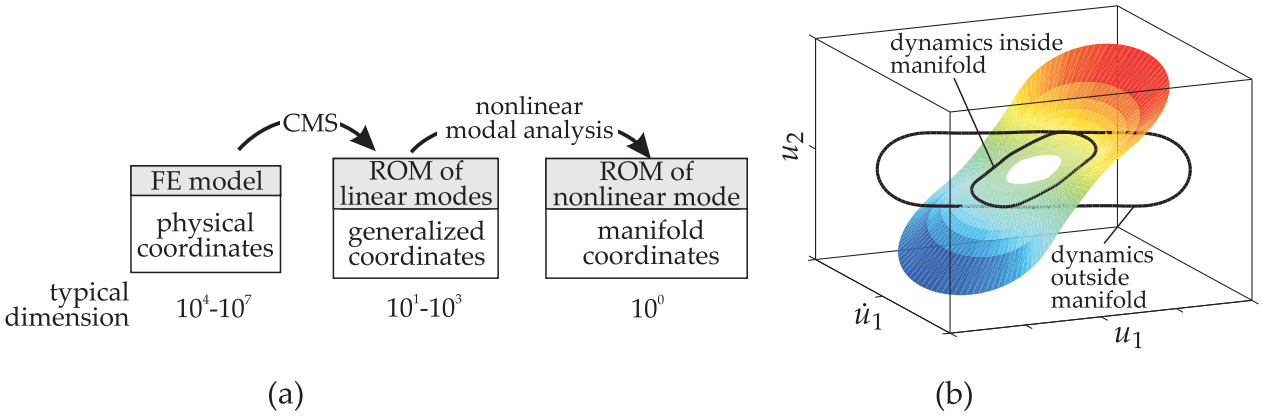

Figure 2.8: Model reduction based on nonlinear modes: (a) cascade of model reduction steps in structural dynamics, (b) dynamics inside and outside of the invariant manifold

ear damping and harmonic forcing terms are superimposed in the governing equations of the ROM. This enhances the parameter space by the according damping and forcing parameters.

The superposition approach generally compromises the integrity of the ROM [117]. It was found in [168] that the modal coupling induced by comparatively strong and inhomogeneous damping may lead to poor predictions based on superposition. For the considered case of geometrically nonlinear systems, it was noticed that damping can change the frequency-energy dependence from a stiffening to a softening type of relationship.

3 Purpose of the present thesis

Shortcomings in the analysis and design of friction-damped systems

Inaccuracy
The design process of friction-damped systems is hampered by

- the sensitivity of the vibration behavior with respect to numerous parameters,
- the uncertainty of parameters, particularly those associated with damping and external forcing, and
- the need to assess the different dynamic regimes of externally forced and self-excited steady-state as well as unsteady vibrations.

Therefore, the vibration behavior has to be determined for various parameter sets and operating conditions in the course of design optimization and uncertainty analysis. Since computational resources are strictly limited in practice, a design process of such complexity is often infeasible in conjunction with high-fidelity analysis. Hence, simplifications are applied to the design process and/or the analysis.
It is thus a common approach to neglect uncertainty and to perform optimization for a fixed set of actually uncertain parameters. Simplified modeling approaches are employed for the description of the contact interactions and the underlying structures, and approximate methods are used for the vibration predictions. The simplified analyses can help understanding the underlying basic vibration phenomena in many situations. However, it is typically difficult to ensure an acceptable quantitative agreement with high-fidelity analysis.
The simplifications of the design problem and/or the dynamic analysis lead to inferior performance and reliability, and may in the worst case result in failure of the designed machine. Therefore, more computational efficiency in the vibration prediction is required in order to bridge the gap between accurate models and sophisticated design approaches.

Indirectness
For the design of most friction-damped systems the dynamic regime around specific external resonances is of primary interest. The assessed characteristics include in particular

the resonance frequency, the effective damping ratio and the vibrational deflection shape at resonance. Despite the fact that these are obviously modal characteristics, these quantities are typically estimated from crude forced response computations. Moreover, damping measures are frequently employed that are not well-defined, if the vibrations feature multi-harmonic content and the vibrational deflection shape varies with energy.

Shortcomings in the field of nonlinear modes

The concept of nonlinear modes certainly has potential for enhancing the analysis and the design of friction-damped systems: Firstly, it facilitates the computation of the often sought modal characteristics. And secondly, it permits the model reduction down to a considerably small dimension near a particular resonance without significantly compromising the model accuracy.

Inefficiency of modal analysis approaches
Depending on the modal analysis approach, the vibratory properties of interest such as the eigenfrequency and the modal damping ratio may not be directly obtained. For invariant manifold based methods, these properties typically have to be determined indirectly from simulation of the associated ROM. In contrast, they are directly obtained from periodic motion based methods.
The potential benefit of using ROMs can be easily diminished by the computational overhead required for the preceding modal analysis. For the direct analysis of periodic motions of the original model, only a (one-dimensional) limit cycle in phase space is sought at the same time. In contrast, a two-dimensional surface in phase space is sought during modal analysis in general. The effort for modal analysis is particularly large, if a two-dimensional annular region or even the entire two-dimensional surface has to be computed simultaneously, as in the case of the invariant manifold based Galerkin method [120]. Compared with direct analysis, this ROM approach seems only to be useful, if a large number of limit cycles on the manifold is of interest.

Limitations regarding dissipative and strong nonlinearities
For an application to friction-damped systems, modal analysis approaches must obviously allow the treatment of non-smooth and dissipative forces arising in contact interfaces. Even though the invariant manifold concept generally appears not to be limited in this regard, existing numerical methods have not yet proven their applicability to such problems. Non-smooth unilateral contact and hysteretic-type friction forces are expected to be more challenging from a numerical point of view than the usually considered low-order polynomial-type forces. Periodic motion based methods can be easily applied to strong nonlinearities because of the use of time integration or harmonic balance method. Yet, the gFGM is the only numerical method which has been successfully applied to strongly nonlinear and, at the same time, dissipative systems. Thus, the gFGM served as an important inspiration for the method developed in the present thesis.

Unknown range of validity of the generalized Fourier-Galerkin approach
Due to the simplifications adopted in the gFGM, the range of validity of the overall approach is difficult to estimate. It was not clearly discussed by Laxalde and Thouverez [94], within what dynamic regime the modal characteristics actually reflect the essential vibration behavior of the nonlinear system. In particular, no comment was given regarding the treatment of internal resonances or the performance of the method in this case. The proposed ROM is further limited to steady-state harmonically forced vibrations. In the ROM, only a single harmonic and a single mode were considered. This might clearly lead to inaccurate predictions, if the contact interactions induce significant multi-harmonic vibration content or if other modes become relevant. Finally, the authors limited their investigations to dry friction-damped systems subject to constant normal load. The applicability of the overall approach to systems featuring strongly nonlinear three-dimensional contact interactions with possible lift-off, variable normal load and variation of the contact area remains an open question.

Specification of the goals of the present thesis

How can modal characteristics of friction-damped systems be assessed efficiently?
The modal analysis approach needs to provide the following qualifying features:

- *direct assessment* of eigenfrequency, modal damping ratio and vibrational deflection shape which characterize the vibration behavior of the nonlinear system in the dynamic regime of primary interest, i. e. in the presence of an isolated resonance
- *consistency* with linear modal analysis
- take advantage of the *localized character* of contact nonlinearities
- applicability to generic contact laws involving *strongly nonlinear and dissipative forces*
- resolution of *internal resonances*, which are known to limit the range of validity of associated ROMs

How can the dynamic analysis effort be reduced in the context of the complex design process?
The model reduction approach needs to comply with the following requirements:

- *validity* in the dynamic regime of primary interest
- *applicability* to detailed models typically employed for the description of state-of-the-art friction-damped systems
- *reduction of the problem dimension* down to only two (invariant manifold) coordinates
- ensure the *parametric character* of the ROM to avoid a possibly expensive recomputation of modal characteristics, which is essential for making the approach attractive for extensive parameter studies required during the design process

- predictability of both *externally forced and autonomous* vibrations
- predictability of both *steady-state and unsteady* dynamics

It is essential for understanding the purpose of the present thesis not to confuse strongly nonlinear forces with strongly nonlinear dynamics. Contact interactions involve strongly nonlinear forces and must be accounted for in the present thesis in order to describe friction-damped systems. Strongly nonlinear dynamic regimes, on the other hand, may exhibit internal resonances, bifurcations of periodic motions and non-periodic steady-state behavior. In the present thesis, only the weakly nonlinear dynamic regime is addressed, where the assumption of an isolated nonlinear mode is justified. It will, however, turn out to be crucial to resolve internal resonances in order to determine up to which limits the assumption of an isolated nonlinear mode holds. Such a restriction is an unavoidable compromise between superiority and range of validity of a useful ROM.

Brief description of approach and outline

The approach for the computation of nonlinear modes followed in this thesis is presented in Chapter 4. It was inspired by the gFGM and is thus readily capable of computing the desired modal characteristics of strongly nonlinear and dissipative mechanical systems. Special attention is paid to the computational efficiency of the numerical approach. Moreover, a path continuation strategy is utilized to overcome turning points in the frequency-energy characteristic, which is an important feature to detect internal resonances.
A novel ROM is developed in Chapter 5 assuming that the kinetic energy is confined to an isolated nonlinear mode. The parametric character is retained by superposition of linear damping and forcing terms as well as a scale invariance. Averaging is employed in order to derive a model for slow unsteady dynamics.
The computational procedure was implemented in a program code developed within the Matlab software environment. Several numerical examples have been considered in order to investigate the capabilities and limitations of the approach. Comparatively simple models are studied in Chapter 6 to systematically assess the approach in the presence of isolated unilateral or dry friction contact for a wide range of operating conditions. The applicability to detailed, state-of-the-art models of turbomachinery bladed disks with friction interfaces is shown in Chapter 7. These test cases are particularly well-suited to assess the approach in the presence of three-dimensional contact interactions in extended friction joints. A focus is set on the efficient derivation of characteristics often sought during the design process of such structures as well as on a probabilistic approach for reliability optimization.

4 A nonlinear modal analysis method for non-conservative systems

In this chapter, a nonlinear modal analysis technique is presented, which will be applied to the numerical examples given throughout this thesis. In Section 4.1, the general method is derived. In Section 4.2, several improvements are proposed aiming at the enhancement of its numerical efficiency and its ability to overcome turning points in the frequency-energy characteristic. Parts of the theoretical developments have already been published in Krack et al. [88, 89].

4.1 Derivation of the general method

Akin to their linear counterpart, nonlinear modes are basically a mathematical concept. Their usefulness resides in their ability to reflect the vibration behavior of nonlinear systems in certain dynamic regimes. The sequence of derivations in this section does justice to this fact: First, the relevant dynamic regime is defined. Then, an appropriate novel definition of nonlinear modes is proposed, in such a way that the nonlinear modes are capable of characterizing this dynamic regime in terms of eigenfrequency, modal damping ratio and vibrational deflection shape. Then a method for their numerical computation is proposed. Despite the fact that the proposed original method is based on a novel definition of nonlinear modes, the governing equations will turn out to share similarities with an existing method, namely the gFGM. Similarities and differences between these approaches are highlighted in Section 4.1.4.

4.1.1 Dynamic regime of interest

The motions of the nonlinear systems considered in this study are governed by differential equations of the form

$$\boldsymbol{M}\ddot{\boldsymbol{u}}(t) + \boldsymbol{C}\dot{\boldsymbol{u}}(t) + \boldsymbol{K}\boldsymbol{u}(t) + \boldsymbol{g}\left(\boldsymbol{u}(t), \dot{\boldsymbol{u}}(t)\right) = \boldsymbol{e}(t)\,. \tag{4.1}$$

Any set of generalized coordinates $\boldsymbol{u}$ can be used in these equations. Hence, the prior application of Component Mode Synthesis does not pose any difficulties and Eq. (4.1) may represent the Eqs. (2.1) or (2.2). Without loss of generality, $\boldsymbol{K}$ and $\boldsymbol{C}$ are related to all linear terms in $\boldsymbol{u}$ and $\dot{\boldsymbol{u}}$, respectively. The nonlinear force $\boldsymbol{g}$ is thus essentially nonlinear in

$\boldsymbol{u}$ and $\dot{\boldsymbol{u}}$.
The motions of this system can be erratic in general. Its flow may be steady or unsteady and exhibit sub-, super- or combination resonances as well as chaotic behavior. As stated in Chapter 3, however, only the regime of a particular, isolated resonance is of interest in the present thesis. In the context of this thesis, an isolated resonance is defined as follows:

Definition 1 (isolated resonance)**.** *A system is considered to be in (or near) an isolated resonance, if and only if its flow is essentially periodic with fundamental frequency identical to (or near) its energy-dependent eigenfrequency and the flow features a dominant fundamental harmonic component.*

The term *essentially* in this definition means that the properties of the periodic motion are allowed to vary slowly with time. It should be noted that the resonant case is particularly relevant for the design of vibrating structures, since comparatively large vibration amplitudes are typical for this regime.
Such a resonance situation can occur in the externally forced or in the autonomous configuration. The particular situations considered in this study are:

1. *externally forced* with essentially harmonic excitation $\boldsymbol{e}(t)$ featuring a frequency near a particular eigenfrequency;
2. *autonomous*, i. e. without external forcing $\boldsymbol{e}(t) = \boldsymbol{0}$
   (a) in the presence of *self-excitation* the system might respond with a particular mode and oscillate in its eigenfrequency or
   (b) in the presence of weak *positive damping*, the flow may be dominated by an isolated resonance, particularly if the motion was initiated at resonance.

The harmonic forcing case (1) occurs for example, if the system consists of a machine which features recurrent behavior, as in rotating machinery. It is important to note that (1) only covers external forces with a peak-like frequency spectrum. An external forcing with multiple discrete frequencies or even a continuous spectrum generally leads to a significant response of multiple modes. Hence, the dynamic behavior is no longer dominated by an isolated resonance in accordance with the above definition. Such a situation is, by definition, beyond the regime of interest. Self-excitation (2a) can be induced for instance by aero-elastic instabilities. Analogous to the restriction of the external forcing type, the self-excitation must lead to a response in only one mode to comply with the regime of interest. If the (self- or external) excitation source suddenly disappears, a free decay from resonance may be initiated, which corresponds to case (2b).
In the linear regime, a particular linear mode will dominate the vibration behavior in the vicinity of an isolated resonance. This mode can be identified by comparing the eigenfrequencies with the excitation frequency range (1), by finding the mode with negative modal damping ratio (2a), or by relating the initial conditions of the free decay to a particular mode (2b). If the excitation source drives the system beyond the linear regime, the system behavior becomes nonlinear. Consequently, the resonant vibration behavior is not

described by the particular linear mode anymore. The nonlinear onset is termed nonlinear mode and is regarded as direct extension of the corresponding linear mode in this study. The isolation of the resonance implies that this resonance is stable. Hence, there occurs no bifurcation, i. e. folding or branching of the nonlinear mode in the considered energy regime.
Instead of deriving the modal characteristics directly from Eq. (4.1), it is proposed in this study to neglect external forcing and linear damping terms during the modal analysis step, and to re-introduce i. e. *superimpose* them in the model reduction step. The benefit of this procedure is that it increases the parameter space of the associated ROM and simplifies the modal analysis step. This benefit might, however, come at the cost of lower accuracy. Treating harmonic forcing in this manner is in accordance with the so-called *deformation-at-resonance* property which indicates that the external forcing magnitude and distribution only determine the response level, but the underlying resonance amplitude and frequency characteristic only depends on the frequency-energy dependence of the corresponding nonlinear mode, see Section 2.3. A reasonable approximation can be accomplished only, if the superimposed linear damping terms remain sufficiently weak in the sense that they do not induce any significant modal interactions. To this end, the linear damping matrix $\boldsymbol{C}$ is divided into a (modal-like) part $\boldsymbol{C}_{\mathrm{mod}}$ for which this superposition is accurate and a remaining part $\boldsymbol{C}_{\mathrm{g}}$ which is subsequently treated like the nonlinear terms,

$$\boldsymbol{C} = \boldsymbol{C}_{\mathrm{mod}} + \boldsymbol{C}_{\mathrm{g}}\,, \tag{4.2}$$

$$\tilde{\boldsymbol{g}} = \boldsymbol{g} + \boldsymbol{C}_{\mathrm{g}}\dot{\boldsymbol{u}}\,. \tag{4.3}$$

With this approach, the modal characteristics are now determined from an *autonomous surrogate* system whose dynamics are governed by

$$\boldsymbol{M}\ddot{\boldsymbol{u}}(t) + \boldsymbol{K}\boldsymbol{u}(t) + \tilde{\boldsymbol{g}}\left(\boldsymbol{u}(t), \dot{\boldsymbol{u}}(t)\right) = \boldsymbol{0}\,. \tag{4.4}$$

While Eq. (4.4) governs the motion of the surrogate system, Eq. (4.1) governs the motions under *operating conditions*.

4.1.2 A new definition of nonlinear modes

The motions of the surrogate system are generally non-periodic, owing to dissipative (friction) terms in $\tilde{\boldsymbol{g}}$, as illustrated in the phase projections in **Fig. 4.1**a. This is in contrast to the motions under operating conditions in the regime of interest, which were assumed to be essentially periodic. In the periodic case, the motions form closed orbits of equal energy in phase space, as illustrated in **Fig. 4.1**b. In this thesis, it is proposed to perceive the nonlinear modes as periodic motions instead of non-periodic motions. Thus, the nonlinear modes are effectively centralized with respect to energy, in order to reproduce expanding or contracting flow under operating conditions with equal accuracy. One means

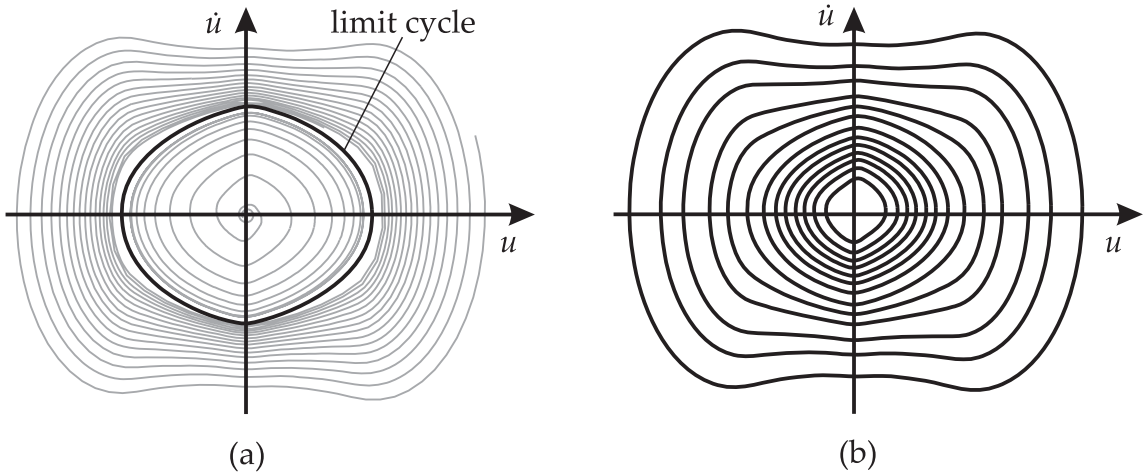

Figure 4.1: Visualization of different conceptions of nonlinear modes of non-conservative systems: (a) damped flow conception followed in [94], (b) periodic flow conception followed in this study

of enforcing periodicity is to compensate the dissipative terms by a mass-proportional damping term $\xi \boldsymbol{M}\dot{\boldsymbol{u}}$,

$$\boldsymbol{M}\ddot{\boldsymbol{u}}(t) - \underbrace{\xi \boldsymbol{M}\dot{\boldsymbol{u}}(t)}_{\substack{\text{artificial term enforcing} \\ \text{periodic motions}}} + \boldsymbol{K}\boldsymbol{u}(t) + \tilde{\boldsymbol{g}}\left(\boldsymbol{u}(t), \dot{\boldsymbol{u}}(t)\right) = \boldsymbol{0}\,. \tag{4.5}$$

If the value of ξ is chosen properly, the flow becomes periodic. To the best of the author's knowledge, this conception has not been proposed so far for non-conservative systems and will serve as novel definition of nonlinear modes in this study:

Definition 2 (nonlinear mode)**.** *A nonlinear mode is a family of periodic motions of an autonomous nonlinear system. If the system is non-conservative, these periodic motions are enforced by mass-proportional damping. The mode must coincide with the corresponding linear mode when the kinetic energy tends towards zero.*

This definition extends the previous definitions of Rosenberg [140] and others to non-conservative systems. In accordance with this definition, the nonlinear modes are regarded as direct extensions of their linear counterpart in the regime of interest, cf. Section 4.1.1.
Although the approach to enforce periodicity by compensating the dissipative terms is appealing, it is actually intrusive: The term $\xi \boldsymbol{M}\dot{\boldsymbol{u}}$ may in general induce artificial modal coupling and thus deteriorate the geometry of the nonlinear mode. In the linear case with modal damping, the modes are orthogonal with respect to the mass matrix. Hence, the additional term does not affect the accuracy in this case. This can also be extended to the nonlinear case, if the vibrational deflection shapes do not change with energy (similar nonlinear modes). In the general case, however, orthogonality does not hold and the method becomes an approximation. This clearly necessitates a thorough investiga-

tion of the range of validity of the proposed approach, which is an important purpose of Chapters 6 and 7.

4.1.3 Computation of modal characteristics

Since nonlinear modes are perceived as periodic motions, conventional methods for periodic flow computation can be applied. In this study, harmonic balance was used. Therefore, the generalized coordinates are expanded in a truncated Fourier series with base frequency ω_0,

$$\boldsymbol{u}(t) \approx a\Re\{\sum_{n=0}^{H} \hat{\boldsymbol{\psi}}_n \mathrm{e}^{\mathrm{i}n\omega_0 t}\}\,. \tag{4.6}$$

Herein, a is the modal amplitude of the considered nonlinear mode. In contrast to the linear case where only $\hat{\boldsymbol{\psi}}_1 \neq \boldsymbol{0}$, the eigenvector consists of multiple harmonics $\hat{\boldsymbol{\psi}}_n \neq \boldsymbol{0}$. Substitution of Eq. (4.6) into Eq. (4.5) and subsequent Fourier-Galerkin projection leads to a set of nonlinear algebraic equations,

$$\left(-\left(n^2{\omega_0}^2 + \xi \mathrm{i}n\omega_0\right)\boldsymbol{M} + \boldsymbol{K}\right)\hat{\boldsymbol{\psi}}_n a + \hat{\hat{\boldsymbol{g}}}_n\left(\omega_0, a\hat{\boldsymbol{\psi}}_0, \ldots, a\hat{\boldsymbol{\psi}}_H\right) = \boldsymbol{0}\ \forall\, n = 0, \ldots, H\,. \tag{4.7}$$

Herein, the nonlinear terms $\hat{\hat{\boldsymbol{g}}}_n$ are evaluated in a straightforward manner, just like in the conventional harmonic balance formulation. The quantity ξ is related to the modal damping ratio D by $\xi = 2D\omega_0$. This relation is derived in Appendix B in order to ensure consistency with the modal properties of linear, damped, multi-DOF systems and with harmonic linearization applied to a single-DOF system. The solution of the eigenproblem in Eq. (4.7) for a modal amplitude range directly yields the amplitude-dependent eigenfrequency $\omega_0(a)$, the modal damping ratio $D(a)$ and the harmonics $\hat{\boldsymbol{\psi}}_n(a)$ of the multi-harmonic eigenvector. It should be noted that only super-harmonics have been considered in the formulation of Eqs. (4.6)-(4.7) utilized in this study, although the approach can be extended in a straightforward manner to account for sub-harmonics.

Normalization

Compared to the application of harmonic balance to an externally forced system, there are two additional unknowns, ω_0 and ξ, which makes Eq. (4.7) under-determined. Just as in the general linear case, two normalization conditions are therefore imposed. A mass normalization of the fundamental harmonic $\hat{\boldsymbol{\psi}}_1$ of the eigenvector was used in this thesis,

$$\hat{\boldsymbol{\psi}}_1^{\mathrm{H}} \boldsymbol{M} \hat{\boldsymbol{\psi}}_1 = 1\,, \tag{4.8}$$

which is also commonly applied in the linear case. The modal amplitude a is therefore a positive, real-valued quantity which corresponds to the modal mass of the fundamental harmonic $a\hat{\boldsymbol{\psi}}_1$ of the eigensolution. Since the absolute phase is arbitrary in an autonomous system, a phase normalization is proposed in addition to Eq. (4.8). Without the loss of

generality, the imaginary part of the k-th component $\hat{\psi}_{1,k}$ of the fundamental harmonic eigenvector is set to zero,

$$\Im\{\hat{\psi}_{1,k}\} = 0\,. \tag{4.9}$$

This condition is unique as long as $\hat{\psi}_{1,k}$ is nonzero. An arbitrary coordinate associated to a nonzero element of the linear eigenvector was selected throughout the numerical examples in this thesis.

As an alternative to mass normalization, a normalization with respect to the kinetic energy can be performed. It is also common to illustrate the modal properties with respect to the kinetic energy rather than the modal amplitude a. A strategy for the computation of the kinetic energy is therefore useful and is derived in the following.

The value of the kinetic energy generally varies during oscillation. Its mean energy per period reads

$$E_{\mathrm{kin}} = \frac{1}{2\pi} \int\limits_{(2\pi)} \frac{1}{2} \dot{\boldsymbol{u}}^{\mathrm{T}}(t)\, \boldsymbol{M} \dot{\boldsymbol{u}}(t) \mathrm{d}\omega_0 t\,.$$

Inserting Eq. (4.6) and utilizing Parseval's theorem (see Appendix A) yields

$$E_{\mathrm{kin}} \approx \frac{1}{2} a^2 {\omega_0}^2 \sum_{n=1}^{H} \Re\{\hat{\boldsymbol{\psi}}_n^{\mathrm{H}} \boldsymbol{M} \hat{\boldsymbol{\psi}}_n n^2\} = \sum_{n=1}^{H} E_{\mathrm{kin},n}\,. \tag{4.10}$$

The $\approx$ sign is inherited from the approximate character of the truncated Fourier series in Eq. (4.6). $E_{\mathrm{kin},n}$ represents the energy contained in the n-th harmonic component of the response. Due to the mass normalization, the energy associated with the fundamental harmonic is $E_{\mathrm{kin},1} = \frac{1}{2} a^2 {\omega_0}^2$.

The proposed mass normalization is convenient and well-adjusted in the case of an isolated nonlinear mode. In the case of internal resonances, however, the proposed mass normalization may become ill-defined: The kinetic energy may become localized in a higher harmonic at an internal resonance and thus $E_{\mathrm{kin},1} = 0$, as it was shown e. g. in [78]. For the proposed mass normalization, the corresponding modal amplitude becomes $a = 0$, which can be easily verified by noting that $\hat{\boldsymbol{\psi}}_1 \neq \boldsymbol{0}$ from Eq. (4.8) and taking into account the definition of $E_{\mathrm{kin},1}$ in Eq. (4.10). This may lead to numerical difficulties considering Eqs. (4.6) and (4.7). In this special case, the author found it useful to replace the product $a\hat{\boldsymbol{\psi}}_n$ by an auxiliary quantity $\hat{\boldsymbol{u}}_n$ internally within the developed numerical code.

4.1.4 Relation to generalized Fourier-Galerkin method

It should be noted that the governing Eq. (4.7) and Eq. (2.11) are very similar. This justifies a discussion of the relation between the method proposed in this thesis and the method proposed by Laxalde and Thouverez [94]. The differences between both methods essentially result from the entirely different conception of nonlinear modes: While nonlinear modes are perceived as periodic motions induced by artificial (possibly negative) damping terms in this thesis, they are viewed as (possibly decaying) pseudo-periodic mo-

tions of the autonomous system in [94]. The conception followed in this study is therefore termed *periodic flow conception*, while the method proposed in [94] is termed *damped flow conception*. The two conceptions are illustrated in the schematic phase projections in **Fig. 4.1**. The consequences of these deviating conceptions are detailed below.

A major advantage of the periodic flow conception is that it allows the use of standard methods for the analysis of periodic flow, including shooting and harmonic balance method. Moreover, this conception permits the application of well known approaches for stability analysis and investigation of bifurcations. In contrast, the damped flow conception is so far restricted to the use of the Fourier-Galerkin procedure with complex eigenvalue. The aspects of stability and bifurcation of the nonlinear modes have not been developed yet for this specific approach.

While this is not mandatory for the periodic flow conception, the periodic motions were approximated in terms of a Fourier series, and the harmonic balance method was utilized for the computation of the nonlinear modes throughout this study. This results in the governing Eq. (4.7) for the nonlinear modes. Only for this particular formulation of the periodic flow method, it makes sense to further discuss the relation to Eqs. (2.11).

The similarities and differences of the governing equations are as follows: (a) They both contain a mass-proportional term which cancels out the non-conservative forces $\hat{\hat{\boldsymbol{g}}}_n$. It is important to note that these terms are, however, not identical for $n > 1$, since they grow with the harmonic index n due to the coefficient $\xi i n \omega_0$ in Eq. (4.7), while they grow with n^2 due to the coefficient $n^2 \Im\{\lambda^2\}$ in Eq. (2.11). (b) For both approaches, the evaluation of the nonlinear terms $\hat{\hat{\boldsymbol{g}}}_n$ is based on the assumption of periodic motions. While this is fully consistent with the ansatz Eq. (4.6) for the periodic flow method, this treatment was proposed as a convenient approximation for the damped flow method. Moreover, the terms $\hat{\hat{\boldsymbol{g}}}_n$ are not identical, since the underlying periodic motions oscillate with the undamped eigenfrequency ω_0 in the periodic flow approach, while they oscillate with the damped eigenfrequency $\omega_0\sqrt{1-D^2}$ in the damped flow approach.

From a strict mathematical point of view, the two above mentioned differences will generally lead to deviating results of both modal analysis methods. There is only one exception where both approaches give rise to identical results, namely when $D = 0$. In particular, this relation holds at limit cycles and in the special case of conservative systems where $D \equiv 0$. Only if $D = 0$, both methods exactly reproduce the autonomous behavior of the nonlinear system. Otherwise, i. e. with $D \neq 0$, both methods differ in general from each other and do not exactly reproduce the autonomous behavior. The extent of the differences from each other and from the exact behavior is briefly investigated for a well known test case below.

Consider the van der Pol oscillator with the equation of motion,

$$\ddot{u} + \left(0.1u^2 - \alpha\right)\dot{u} + u = 0\,. \tag{4.11}$$

The modal characteristics were computed using the periodic and the damped flow method with harmonic order $H = 13$. The results are illustrated in **Fig. 4.2**a and b for the case without linear damping, i. e. $\alpha = 0$. It can be seen that the results differ for large

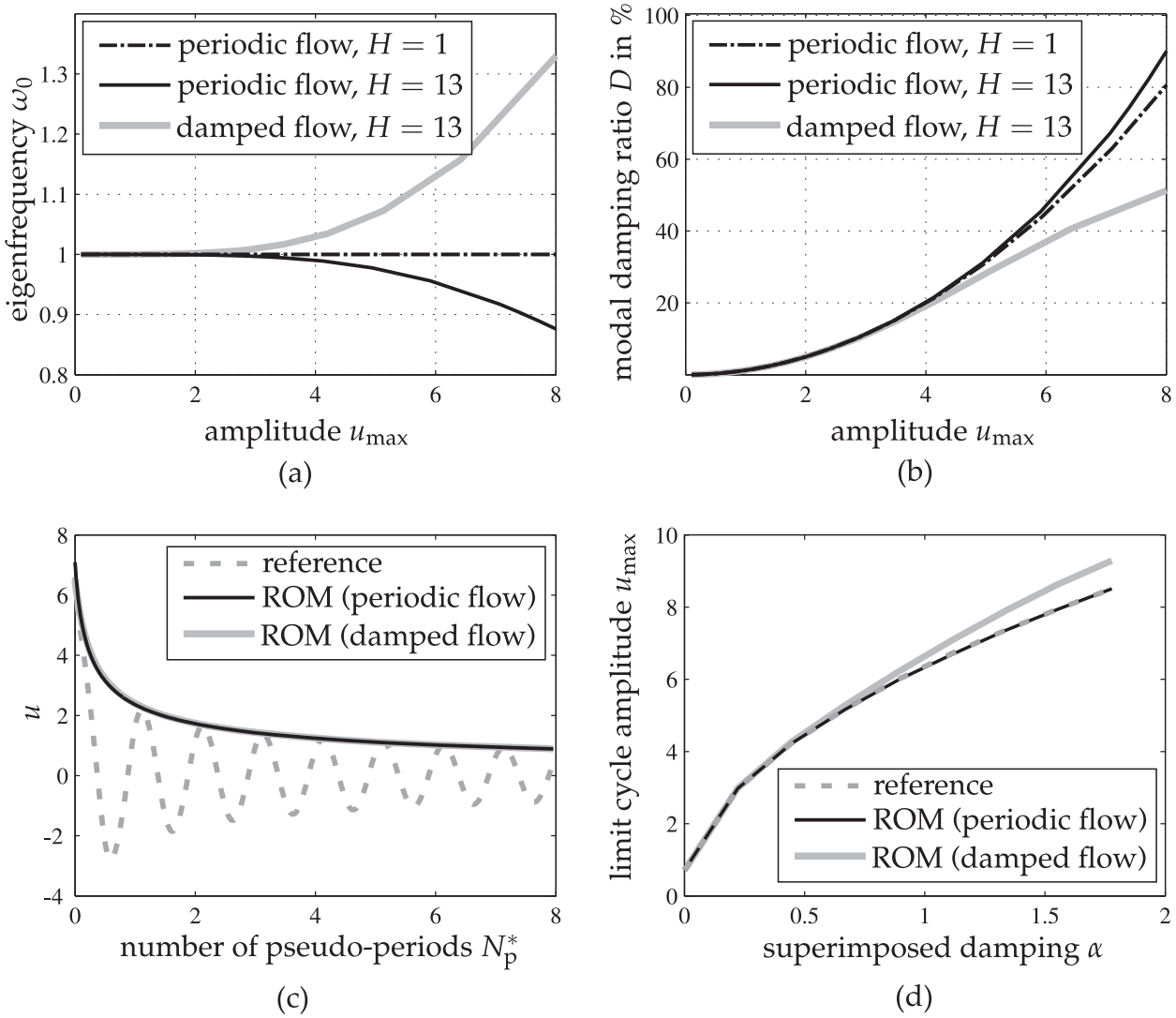

Figure 4.2: Illustration of the differences between periodic and damped flow conception for the van der Pol oscillator: (a) and (b) modal characteristics for $\alpha = 0$, (c) free decay time history for $\alpha = 0$, (d) limit cycle amplitudes for varying α

kinetic energies, i. e. when the nonlinear effects become important. The frequency-energy characteristics exhibit strong deviations in the regime of larger damping ($D > 20\%$). The common harmonic linearization technique was also applied to the system [99]. For this method, the effective stiffness and damping are determined under the assumption of a mono-harmonic (and thus periodic) motion, e. g. $u(t) = \hat{u} \cos \omega_0 t$. Therefore, the results of this method are identical to the periodic flow case with $H = 1$, which is also depicted in **Fig. 4.2**a and b.

The damped flow method aims at reflecting the autonomous vibration behavior. It is therefore expected that this approach is better suited to reproduce the free decay. The free decay of the amplitude was approximated using the differential equation in the modal amplitude a

$$\dot{a} = -D(a)\omega_0(a)a\,, \tag{4.12}$$

Eq. (4.12) represents a special form of the ROM to be derived in Chapter 5. This differential equation was solved using, one after the other, the modal characteristics $D(a)$, $\omega_0(a)$ obtained by the periodic flow and the damped flow method. The results are depicted in **Fig. 4.2**c. The number N_p^* of pseudo-periods was introduced as time variable: It equals $N_\mathrm{p}^* = f_0 t$, where f_0 is the eigenfrequency $f_0 = 1/(2\pi)$ in the linear case. The most significant deviations are expected in the regime with considerable nonlinear damping. However, in this regime the envelopes are almost indistinguishable and in good agreement with the reference which was obtained from direct time integration of Eq. (4.11).
The proposed approach was designed to reproduce periodic motions in the presence of forced or self-excitation. In order to compare the performance of both approaches in this case, limit cycle oscillations for varying α were investigated. The limit cycles were determined by solving the following nonlinear algebraic equation for a:

$$0 = 2D(a)\omega_0(a) - \alpha\,, \tag{4.13}$$

Again, this corresponds to a special case of the ROM to be derived in Chapter 5. The viscous damping with coefficient α was superimposed in Eq. (4.13) in the way that the modal characteristics $D(a)$, $\omega_0(a)$ only had to be determined for $\alpha = 0$. As expected, the proposed method provides excellent prediction quality and performs in this case better than the damped flow method.
In conclusion, it is found that both the damped flow method originally proposed in [94] and the proposed periodic flow method are approximate methods in the general nonlinear, non-conservative case. The exactness is lost by the intrusiveness of the artificial damping term introduced for the periodic flow method and the use of the same complex eigenvalue for all harmonics in the case of the damped flow method. Both methods generally lead to quite similar results, if the nonlinear damping remains moderate. Both approaches reproduce the damped autonomous system behavior with similar accuracy. The periodic flow method clearly outperforms the damped flow method if desiring steady-state vibrations under different operating conditions. But probably the most important advantage of the proposed periodic flow conception is that it makes the approach admissible to the broad class of techniques particularly suited for the computation and analysis of periodic motions.

4.2 Computational improvements

The improvements proposed in this section aim at enhancing the numerical efficiency and robustness of the above described computational approach. These improvements are achieved by exploiting the sparsity of the nonlinear force vector in Eq. (4.7) and the use of analytical gradients. Moreover, a numerical path continuation is carried out in order to continue the solution branch beyond turning points with respect to the energy-dependence of the nonlinear modes. Finally, the efficiency improvements are assessed by numerical investigations.

4.2.1 Exploiting the sparsity of the nonlinear force vector

Friction-damped systems are characterized by localized nonlinearities, i. e. nonlinear forces are confined to certain coupling interfaces at the joints of the underlying structures. As a consequence, the nonlinear forces $\tilde{\boldsymbol{g}}$ typically act and depend on only a subset of the generalized coordinates $\boldsymbol{u}^{\mathrm{N}} \subset \boldsymbol{u}$. It is convenient to arrange the equations of motion in such a manner that the nonlinear force and the generalized displacement vectors can be written as

$$\tilde{\boldsymbol{g}}\left(\boldsymbol{u}, \dot{\boldsymbol{u}}\right) = \begin{bmatrix} \tilde{\boldsymbol{g}}^{\mathrm{N}}\left(\boldsymbol{u}^{\mathrm{N}}, \dot{\boldsymbol{u}}^{\mathrm{N}}\right) \\ \boldsymbol{0} \end{bmatrix}, \quad \boldsymbol{u} = \begin{bmatrix} \boldsymbol{u}^{\mathrm{N}} \\ \boldsymbol{u}^{\mathrm{L}} \end{bmatrix}. \tag{4.14}$$

Herein, $\tilde{\boldsymbol{g}}$ and $\boldsymbol{u}$ have the dimension N_{dof}, whereas $\tilde{\boldsymbol{g}}^{\mathrm{N}}$ and $\boldsymbol{u}^{\mathrm{N}}$ have the dimension N_{nl}. The vector of nonlinear forces is considered as sparse, if $N_{\mathrm{nl}} \ll N_{\mathrm{dof}}$. This sparsity is inherited by the harmonics $\hat{\tilde{\boldsymbol{g}}}_n$ and the associated gradients. The extent of this sparsity also depends on the choice of the generalized coordinates: If the physical coordinates $\boldsymbol{u}^{\mathrm{N}}$, that describe the relative interface motions, are not retained, the sparsity is generally lost.
Taking advantage of this sparsity during the numerical solution process can greatly reduce the required computational effort. It is a common procedure in conjunction with harmonic balance applied to forced systems, to condense the set of N_{dof} nonlinear algebraic equations for each harmonic to a set of N_{nl} equations, see e. g. [82, 60, 10, 26]. This procedure is applied below for the first time in conjunction with nonlinear modal analysis. Special attention is paid to singularities being salient in autonomous systems, and to an efficient factorization scheme which is novel in the context of this condensation procedure.
The condensed set of equations reads

$$\hat{\boldsymbol{\psi}}_n^{\mathrm{N}} a + \boldsymbol{H}_n^{\mathrm{NN}}(\omega_0, D)\hat{\tilde{\boldsymbol{g}}}_n^{\mathrm{N}}\left(\omega_0, a\hat{\boldsymbol{\psi}}_0^{\mathrm{N}}, \ldots, a\hat{\boldsymbol{\psi}}_H^{\mathrm{N}}\right) = \boldsymbol{0} \;\forall\, n = 0, \ldots, H\,. \tag{4.15}$$

Herein, $\boldsymbol{H}_n^{\mathrm{NN}}$ is a portion of the dynamic compliance matrix $\boldsymbol{H}_n$,

$$\boldsymbol{H}_n = \begin{bmatrix} \boldsymbol{H}_n^{\mathrm{NN}} & \boldsymbol{H}_n^{\mathrm{NL}} \\ \boldsymbol{H}_n^{\mathrm{LN}} & \boldsymbol{H}_n^{\mathrm{LL}} \end{bmatrix} = \left(-\left(n^2 + 2Din\right)\omega_0{}^2\boldsymbol{M} + \boldsymbol{K}\right)^{-1}. \tag{4.16}$$

Upon solution of Eq. (4.15) for the reduced set of unknowns $\omega_0, D, \hat{\boldsymbol{\psi}}_0^{\mathrm{N}}, \ldots, \hat{\boldsymbol{\psi}}_H^{\mathrm{N}}$, the remaining portion of the eigenvectors can be determined using the explicit formulation $a\hat{\boldsymbol{\psi}}^{\mathrm{L}} = -\boldsymbol{H}_n^{\mathrm{LN}}\hat{\tilde{\boldsymbol{g}}}_n^{\mathrm{N}}$. It should be noted that this dynamic condensation procedure is mathematically exact, so that it does not suffer from poor accuracy like the static (Guyan) condensation procedure.

Efficient factorization

For each evaluation of the condensed residual (4.15), the dynamic compliance matrix has to be determined in accordance with Eq. (4.16). This involves the expensive computation of a matrix inverse. Since this matrix depends on the unknowns ω_0, D, this inversion has

to be performed each time these values are changed, as e. g. in each iteration of a numerical solution procedure. This could diminish the benefit of the condensation procedure achieved by reducing the number of unknowns.
In order to accelerate the expensive inversion step, it is proposed to express the dynamic compliance matrix in terms of the eigenvectors $\boldsymbol{\varphi}_k$ and the eigenfrequencies ω_k of the linearized system,

$$\boldsymbol{H}_n(\omega_0, D) = \sum_{k=1}^{N_{\mathrm{dof}}} \frac{\boldsymbol{\varphi}_k \boldsymbol{\varphi}_k^{\mathrm{T}}}{\omega_k^2 - (n^2 + 2Din)\,\omega_0{}^2}\,. \tag{4.17}$$

Note that only the corresponding portions of $\boldsymbol{\varphi}_k$ are required to set up $\boldsymbol{H}_n^{\mathrm{NN}}$ in Eq. (4.15). The inversion of the dynamic stiffness matrix is thus replaced by less expensive matrix manipulations. For this *efficient factorization* technique, the linear eigenvectors $\boldsymbol{\varphi}_k$ are required. They are orthogonal with respect to $\boldsymbol{K}$ and $\boldsymbol{M}$ and as usual normalized with respect to $\boldsymbol{M}$:

$$\boldsymbol{\varphi}_k^{\mathrm{T}} \boldsymbol{M} \boldsymbol{\varphi}_j = \delta_{kj}\,, \quad \boldsymbol{\varphi}_k^{\mathrm{T}} \boldsymbol{K} \boldsymbol{\varphi}_j = \omega_k \omega_j \delta_{kj} \;\forall\, j,k \in 1,\ldots,N_{\mathrm{dof}}\,. \tag{4.18}$$

Herein, δ_{kj} is the Kronecker-delta function which is equal to one, if $k = j$ and zero otherwise. The linear eigenvalue problem has to be computed only once. It should be noted that the proposed procedure exploits the symmetry of $\boldsymbol{K}$ and $\boldsymbol{M}$, where the eigenvectors are real-valued and the left and right eigenvectors are identical. An appropriate extension to systems of general structure has been developed in Krack et al. [88].
In special situations, the condensation is not possible because of the singularity of the dynamic compliance matrix. This is obviously the case when the system is linear and at the same time $\boldsymbol{C}_{\mathrm{g}} = \boldsymbol{0}$. Then $\hat{\hat{\boldsymbol{g}}}_n = \boldsymbol{0}$ and $\omega_0 = \omega_k$, $D = 0$, so that the denominator in Eq. (4.17) vanishes for $n = 1$. This special case does not pose any difficulties, since the linear solution is already known and the modal analysis has to be carried out only in the nonlinear regime. Singularity may, however, also occur for $n > 1$ in the special case when $D = 0$ and $n\omega_0 = \omega_k$. In the linear regime, this can only happen if the eigenfrequencies of the linearized system are commensurable. This case has been excluded from this thesis, cf. Section 4.1.1. In the nonlinear regime, this can occur, if a multiple of the eigenfrequency ω_0 of the considered nonlinear mode coincides with the eigenfrequency ω_ℓ of a linear mode ℓ. This case may or may not indicate the presence of an internal resonance. In any case, this singularity should be avoided. This can be achieved by introducing a small damping term in Eq. (4.17). This damping term should be large enough to circumvent numerical singularity and small enough not to influence the accuracy of the modal analysis procedure. Based on empirical investigations, a hysteretic damping value of $10^{-5} - 10^{-9}$ was found to provide a good trade-off throughout the case studies in this thesis. It should be emphasized that this 'trick' is only required to overcome the possible singularities associated with the efficient condensation procedure and is of pure numerical nature.

4.2.2 Solution using analytical gradients

The resulting *eigenproblem* can be summarized as follows:

$$\begin{aligned} \text{solve} \quad & \hat{\boldsymbol{\psi}}_n^{\mathrm{N}} a + \boldsymbol{H}_n^{\mathrm{NN}}(\omega_0, D)\hat{\tilde{\boldsymbol{g}}}_n^{\mathrm{N}}\left(\omega_0, a\hat{\boldsymbol{\psi}}_0^{\mathrm{N}}, \ldots, a\hat{\boldsymbol{\psi}}_H^{\mathrm{N}}\right) = \boldsymbol{0} \;\forall\, n = 0, \ldots, H \\ \text{subject to} \quad & \hat{\boldsymbol{\psi}}_1^{\mathrm{H}} \boldsymbol{M} \hat{\boldsymbol{\psi}}_1 = 1\,, \;\; \Im\{\hat{\psi}_{1,k}\} = 0 \\ \text{with respect to} \quad & \{\omega_0, D, \hat{\boldsymbol{\psi}}_0^{\mathrm{N}}, \ldots, \hat{\boldsymbol{\psi}}_H^{\mathrm{N}}\} \\ \text{for} \quad & a \in [a_{\min}\,,\; a_{\max}]\;. \end{aligned} \tag{4.19}$$

The nonlinear forces $\hat{\tilde{\boldsymbol{g}}}_n^{\mathrm{N}}$ cause a coupling in time and space, in such a way that this condensed set of algebraic equations has to be solved simultaneously with respect to the $N_{\mathrm{dim}} = (2H+1)\,N_{\mathrm{nl}} + 2$ unknowns. Existence and local uniqueness of the solution has to be assumed formally in order to proceed with the methodology.
For the numerical solution of Eq. (4.19), a variant of the Newton method was employed. Specifically, the subroutine 'fsolve' available in the Matlab software environment was utilized [57]. This method requires the computation of the Jacobian matrix, i. e. the gradient of the residual vector with respect to the unknowns, cf. Section 2.1.3, p. 14. The gradient can be approximated by finite differences. For this purpose, the residual has to be evaluated at least N_{dim} times, where the actual number of evaluations depends on the finite difference scheme. This can be computationally intensive, if N_{dim} is large. In this study, the gradient was computed based on analytical expressions which were manually derived prior to the implementation of the method. This manual derivation is a cumbersome, but at the same time quite elementary endeavor. Hence, the actual expressions for the gradient are not provided in this thesis. The interested reader is referred to [10, 155] for details. After each evaluation of the residual function, thus, also its gradient is available, which is then provided to the nonlinear solver. This can greatly reduce the required computational cost compared to the conventional finite difference approximations of the gradient. Moreover, this increases the accuracy of the gradient and therefore improves the convergence behavior.

4.2.3 Numerical path continuation

For a gradient-based solution, an appropriate initial guess has to be specified from which the iterative correction process is initiated. The nonlinear modes are regarded as direct extensions of associated linear modes in this study. Hence, the linear mode is typically an appropriate initial guess for finding the nonlinear mode at small amplitudes $a \approx 0$. A numerical path continuation with respect to the modal amplitude a is proposed to compute the nonlinear mode within the amplitude range of interest. This continuation inherently takes advantage of the invariance property of nonlinear modes. It should be noted that the linear modes are readily available as by-product of the proposed factorization procedure, cf. Eq. (4.18).
As outlined in the state of knowledge, turning points with respect to the amplitude may

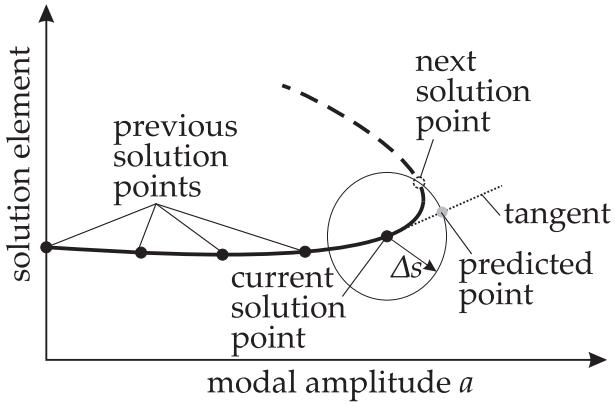

Figure 4.3: Numerical path continuation scheme with tangent predictor step and arc-length parametrization

be encountered, which typically indicates the presence of an internal resonance. Since internal resonances represent the limitation of the ROM, their detection is of interest. In order to overcome turning points, a numerical path continuation was employed. A so-called predictor-corrector scheme with tangent predictor step and arc-length parametrization has been utilized, see **Fig. 4.3**. The details of this scheme can be found e. g. in [148]. Starting at the current solution point, the next point is predicted by going a specified distance Δs in the direction of the analytically determined tangent to the solution branch. Starting from the predicted point, the aforementioned iterative correction procedure was used to find the next solution on the branch. To this end, also the modal amplitude a is considered as unknown. This makes Eq. (4.19) under-determined. Thus, an additional constraint equation is considered which ensures that the next solution point has the specified distance Δs (arc-length) from the current solution point.
The different unknowns associated with the nonlinear mode represent quite different physical quantities and may assume numerical values which are of different order of magnitude. This was found to have a crucial influence on the convergence behavior of a numerical solution procedure. A logarithmic scaling was used for the amplitude, which was found to undergo comparatively large variations during the computation of the nonlinear modes. A linear scaling was applied to the remaining unknowns, so that they had approximately matching orders of magnitude.

4.2.4 Evaluation of the proposed improvements

A numerical study is presented in order to estimate the computational benefits achieved by applying the proposed improvements of (a) condensation, (b) efficient factorization of the dynamic stiffness matrix and (c) using analytical gradients. The goal is to gain insight into which parameters have an influence on the individual benefit of specific steps of the solution procedure. An investigation of the overall benefit is later presented when the developed modal analysis procedure is applied.
A suitable model of a friction-damped structure is required for the numerical assessment

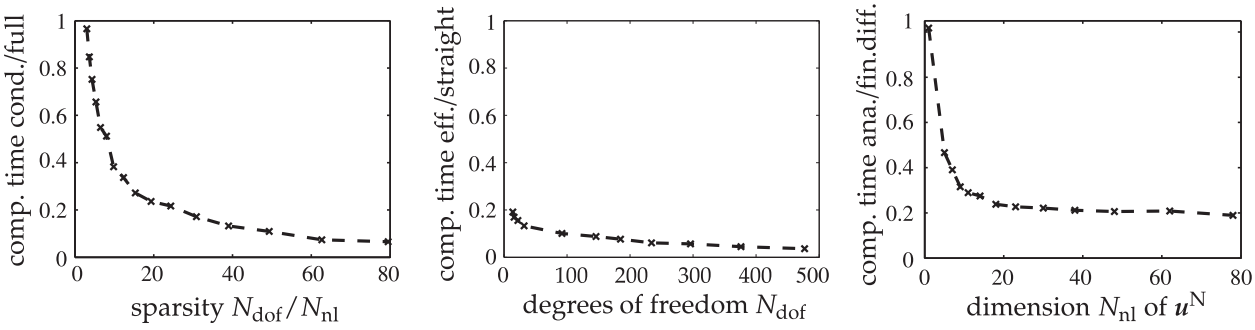

(a) (b) (c)

Figure 4.4: Computational benefits achieved by the proposed improvements: (a) condensation procedure for exploiting sparsity of nonlinear force vector vs. full formulation, (b) efficient vs. straight inversion, (c) analytical gradients vs. finite-difference approximations

of the proposed improvements. This model should be representative regarding the degree of detail required in engineering applications. To this end, a finite element model of a turbomachinery blade with contact interfaces was considered.[1] The model comprised 25,641 nodal degrees of freedom. The Craig-Bampton reduction was carried out with 1 to 100 contact degrees of freedom (constraint modes) and 6 to 600 fixed-interface normal modes. The number of harmonics was set to $H = 7$. Details about the computational resources are listed in Appendix E.

The computation of a single Newton step using (2.8) represents the basis for the investigations. The iteration can be divided into three sub-steps: Determine residual $\boldsymbol{R}$, set up gradient $\frac{\partial \boldsymbol{R}}{\partial \boldsymbol{Z}^{\mathrm{T}}}$ and solve for $\Delta \boldsymbol{Z}^{+}$.

Condensation

The computational benefit achieved by exploiting the sparsity of the nonlinear force vector is illustrated in **Fig. 4.4**a. The condensation procedure is not much faster when the system is barely sparse, i. e. when $N_{\mathrm{nl}} \approx N_{\mathrm{dof}}$, but becomes increasingly advantageous for greater sparsity, i. e. for $N_{\mathrm{nl}} \ll N_{\mathrm{dof}}$. A maximum improvement factor of ten was ascertained for the considered sparsity range. It should be noted that the sparsity strongly depends on the considered model of the friction-damped system. In particular, it is influenced by the degree of detail of the spatial discretization of the contact interface and the underlying structure. It is difficult to give a realistic range. For the case studies presented in this study, the value $N_{\mathrm{dof}}/N_{\mathrm{nl}}$ ranges between six and two after application of Component Mode Synthesis.

Efficient factorization

The computational benefit achieved by using the efficient instead of the straight inversion of the dynamic stiffness matrix is depicted in **Fig. 4.4**b. A significant reduction of the computational effort by 5-20 can be ascertained. The proposed procedure becomes more

[1] This particular model also served as test case for the overall methodology proposed in this thesis and is described in more detail in Section 7.1.

beneficial for larger numbers of unknowns. The efficient factorization procedure requires the linear eigenproblem to be solved. This overhead was not considered.

Analytical gradients

The investigation was limited to the computation of the gradients of the nonlinear terms, which typically represents the bottleneck. The computational effort required for evaluating the gradients analytically is compared to approximating them by finite differences in **Fig. 4.4**c. The benefit depends on the dimension N_{dim} of the vector of unknowns $\boldsymbol{Z}$, which determines the size of the gradient matrix. A forward finite difference scheme has been utilized, for which $N_{\text{dim}} + 1$ function evaluations are required in each iteration, in contrast to only one function evaluation when the gradients are calculated analytically. N_{dim} was varied between 20 and 2000 in this case. As it can be deduced from **Fig. 4.4**c, the computational effort is only reduced by a smaller factor of up to five. The reason is the overhead caused by evaluating the additional lines of program code which are associated with the analytical gradient evaluation.

Discussion of the computational benefit

The benefits of the individual improvements are considerable. It is thus concluded that the additional preparation effort required to follow the proposed strategies, pays off quickly. The proposed improvements are particularly beneficial, if extensive parameter studies have to be performed for large and considerably sparse problems.
The scope of this conclusion is bounded by the restrictions of the investigations. Only a single iteration of the nonlinear solver was considered. The analysis also involves model preparation, assembly of linear components of the residual, other solver-related tasks such as line search and finally the expansion of the reduced solution. Depending on the test case, these steps can also play a considerable role in the overall computational cost. Moreover, it should be kept in mind that the Newton method served as basis for the investigations. The computational benefit might be different for other solution methods like secant methods or pseudo-time solvers, which are beyond the scope of this study.

5 A model reduction approach based on nonlinear modes

In the linear case, the general solution of the equations of motion (of a spatially discretized system) can be expressed exactly as synthesis of a finite set of fundamental and particular solutions. Unfortunately, this procedure is not possible in the nonlinear regime, since the superposition principle is no longer valid. Hence, further assumptions have to be accepted in order to derive a suitable approximation. The model reduction approach proposed in this chapter is based on the assumption that the response can be approximated by an isolated nonlinear mode, in accordance with the dynamic regime of interest defined in Chapter 4.
This chapter is organized as follows: In Section 5.1, the ROM is derived in its general form. The attributes of this ROM are analyzed in Section 5.2. Finally, variants of the general approach are derived for relevant special cases in Section 5.3. Parts of the theoretical developments of the ROM have already been published in Krack et al. [88, 89]. The scale invariance introduced in Section 5.2 was first published in Krack et al. [92].

5.1 Derivation of the general ROM

5.1.1 Reconstruction of the invariant manifold

The model reduction idea is to describe the flow on only the invariant manifold, which is a subspace of the entire phase space, as depicted in **Fig. 5.1**. This invariant manifold corresponds to the geometry of the nonlinear mode. The problem is thus reduced from computing the flow in the original $2N_{\mathrm{dof}}$-dimensional phase space associated with Eq. (4.1), to computing the flow in a two-dimensional subspace.
For this purpose, the invariant manifold can be expressed as the union of the computed closed orbits in accordance with Eq. (4.6),

$$\begin{aligned} \boldsymbol{u}(t) &\approx \quad a(t)\Re\{\sum_{n=0}^{H} \hat{\boldsymbol{\psi}}_n(a(t))\mathrm{e}^{\mathrm{i}n\vartheta(t)}\} \quad &&= \boldsymbol{U}(a,\vartheta)\,, \\ \boldsymbol{v}(t) &\approx a(t)\Omega\Re\{\sum_{n=0}^{H} \mathrm{i}n\hat{\boldsymbol{\psi}}_n(a(t))\mathrm{e}^{\mathrm{i}n\vartheta(t)}\} &&= \boldsymbol{V}(a,\vartheta)\,. \end{aligned} \tag{5.1}$$

Amplitude a and phase ϑ are thus utilized as coordinates on the manifold $\boldsymbol{U}(a,\vartheta), \boldsymbol{V}(a,\vartheta)$. Mathematically, Eq. (5.1) defines a nonlinear coordinate transformation from the state

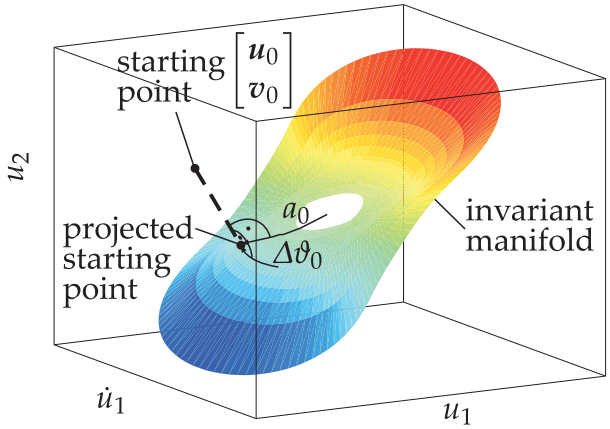

Figure 5.1: Definition of manifold coordinates and projection of initial conditions

space coordinates to the invariant manifold coordinates.
The fundamental oscillation frequency Ω is either locked to the frequency Ω_e of the external force or it coincides with the eigenfrequency ω_0,

$$\Omega = \begin{cases} \Omega_e & \text{externally forced} \\ \omega_0(a) & \text{autonomous} \end{cases} . \tag{5.2}$$

It should be noted that the modal analysis was only carried out for the eigenfrequency ω_0. When $\Omega \neq \omega_0$, it is simply assumed that the velocity-related subspace $\boldsymbol{V}$ of the manifold is *squeezed or stretched* with a factor Ω/ω_0, cf. Eq. (5.1). This is of course only an approximation and hence a possible source of inaccuracy when the system is driven at considerable distance from resonance.

5.1.2 Governing equations for the unsteady flow on the manifold

The time derivative of ϑ is essentially the fundamental oscillation frequency Ω. Introducing a possible phase lag $\Delta\vartheta$, the absolute phase ϑ can be expressed as

$$\vartheta(t) = \int_0^t \Omega(\bar{t})\mathrm{d}\bar{t} + \Delta\vartheta(t) . \tag{5.3}$$

In order to facilitate the prediction of unsteady flow on the manifold, amplitude and phase lag are allowed to vary with time. This time variation is assumed to be slow compared to the underlying oscillation with Ω, i. e. $\dot{\vartheta} \ll \Delta\dot{\vartheta}$. It is then possible to apply an *averaging formalism* in order to derive a set of ODEs governing the slowly varying amplitude and phase lag. To this end, the invariant manifold defined in Eq. (5.1) was substituted into the equations of motion (4.1) under operating conditions. This produces a residual vector, which then was made orthogonal to the fundamental harmonic component of the nonlinear mode. This corresponds to setting the inner product of the residual and the vector $\hat{\boldsymbol{\psi}}_1$ to zero and subsequent averaging over the fast time scale related to Ω. Details about the mathematical development can be found in Appendix C.

The above mentioned approximations will generally produce an error. Poor predictions are expected beyond the regime of interest, i. e. in particular if (a) amplitude and phase lag actually vary fast compared to the underlying oscillation, and (b) the dynamics is not dominated by the fundamental harmonic component of the nonlinear mode.
The resulting set of first order ODEs in a and $\Delta\vartheta$ that govern the averaged (or slow) flow on the manifold reads

$$\dot{a} = \quad -\tilde{D}\omega_0 a \quad + \quad \frac{1}{2\Omega}\Im\{\hat{f}_{\mathrm{e,mod}}\mathrm{e}^{-\mathrm{i}\Delta\vartheta(t)}\}\,, \tag{5.4}$$

$$\Delta\dot{\vartheta} = \quad \tfrac{1}{2\Omega}\left(\omega_0{}^2 - \Omega^2\right) \quad - \frac{1}{2\Omega a}\Re\{\hat{f}_{\mathrm{e,mod}}\mathrm{e}^{-\mathrm{i}\Delta\vartheta(t)}\}\,. \tag{5.5}$$

Note that linear modal damping and harmonic forcing terms, which were neglected during the modal analysis step, have now been re-introduced by simply *superimposing* these terms like in the linear case: $\hat{f}_{\mathrm{e,mod}} = \hat{\boldsymbol{\psi}}_1^{\mathrm{H}}\hat{\boldsymbol{e}}_1$ is the modal excitation force associated with the fundamental harmonic $\hat{\boldsymbol{e}}_1$ of the external force. The term $2\tilde{D}\omega_0 = 2D\omega_0 + \hat{\boldsymbol{\psi}}_1^{\mathrm{H}}\boldsymbol{C}_{\mathrm{mod}}\hat{\boldsymbol{\psi}}_1$ accounts for the possible damping matrix $\boldsymbol{C}_{\mathrm{mod}}$. For reasons of readability, the time dependence of $a(t)$ and $\Delta\vartheta(t)$ and the amplitude dependence $\omega_0(a)$, $\tilde{D}(a)$, $\hat{\boldsymbol{\psi}}_1(a)$ were not explicitly denoted.
The similarity of Eqs. (5.4)-(5.5) to the equations of motion of a single-DOF system in amplitude-phase formulation should be noted. This clearly indicates that the nonlinear system behaves like a single nonlinear modal oscillator in the presence of an isolated resonance.
Starting from initial conditions $a(t=0) = a_0, \Delta\vartheta(t=0) = \Delta\vartheta_0$, the unsteady flow on the manifold can be computed from Eqs. (5.4)-(5.5) using conventional integration schemes. In practice, the initial condition may not be given in manifold coordinates but in the generalized coordinates $\boldsymbol{u}(0) = \boldsymbol{u}_0, \boldsymbol{v}(0) = \boldsymbol{v}_0$. In this case, it is proposed to perform a closest point projection to find a corresponding point $a_0, \Delta\vartheta_0$ on the manifold,

$$a_0, \Delta\vartheta_0 = \underset{a,\Delta\vartheta}{\arg\min} \left\| \boldsymbol{u}_0 + \tfrac{1}{\mathrm{i}\Omega}\boldsymbol{v}_0 - a\boldsymbol{Y}\left(a, \Delta\vartheta\right) \right\| . \tag{5.6}$$

Here, $\boldsymbol{Y}$ is the complex-valued auxiliary function as defined in Appendix C, which in turn depends on the manifold defined in Eq. (5.1). It should be noted that the minimization problem in Eq. (5.6) is not necessarily convex. Local methods for the minimization in Eq. (5.6) may get stuck in a local minimum, and the global minimum might even not be unique. It should be kept in mind, however, that the isolated nonlinear mode assumption implies that the initial state vector lies on the invariant manifold. In this case, there exists a unique solution, and the minimum in Eq. (5.6) becomes zero.
The ODEs (5.4)-(5.5) were numerically integrated using an explicit Runge-Kutta quadrature formula implemented in the subroutine 'ode45' available in the Matlab software environment. A continuous representation of the nonlinear mode with respect to amplitude is convenient for the numerical treatment of the ROM. For this purpose, a one-dimensional interpolation of the discrete data points obtained from the preceding numerical modal analysis can be used. Both piecewise linear and piecewise cubic interpolation schemes were found to perform well according to the experiences gained from the numer-

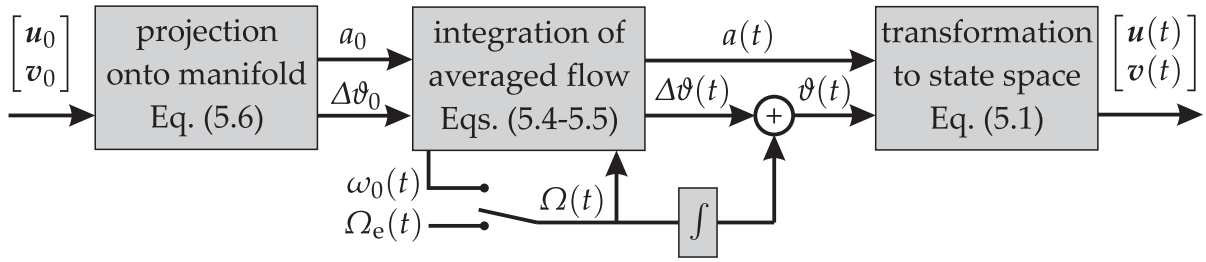

Figure 5.2: Signal flow chart for the numerical prediction of the unsteady flow on the manifold

ical studies throughout this thesis. The signal flow chart of the overall method is depicted in **Fig. 5.2**.

5.1.3 Governing equations for limit cycles on the manifold

In the case of steady-state vibrations, the amplitude and phase lag are constant, and consequently $\dot{a} \equiv 0 \equiv \Delta\dot{\vartheta}$. In this case, Eqs. (5.4)-(5.5) degenerate to a set of two real-valued nonlinear algebraic equations which can be conveniently written in complex arithmetic,

$$\left(\omega_0{}^2(a) - \Omega^2 + 2\tilde{D}(a)\,\omega_0(a)\,\mathrm{i}\Omega\right) a\mathrm{e}^{\mathrm{i}\Delta\vartheta} = \hat{f}_{\mathrm{e,mod}}\,. \tag{5.7}$$

A solution of this equation corresponds to a periodic motion, i. e. a limit cycle[1] on the manifold. Various global and local methods are generally suited for solving Eq. (5.7). In this study, the gradient-based method already described in Section 4.2.3 was employed for solving Eq. (5.7). Once again, path continuation and analytical gradients have been utilized.

5.1.4 Synthesis with off-resonant modes

Following the ideas of the single nonlinear mode theory [29, 55], the contribution of off-resonant modes can be taken into account in the ROM. In the dynamic regime of interest, the energy is mainly confined to the considered, resonant nonlinear mode, while the level of the off-resonant modes is comparatively low. Hence, they were only considered in their linear forms in this study. It should be noted that these *linearized modes* are readily available from the modal analysis step, cf. Eq. (4.18).
In this thesis, the contribution of each linear mode was determined individually and thus independent of both the nonlinear and the remaining linear modes, just as in a linear modal synthesis procedure. This step is exemplified for the steady-state case. The

[1] Note that throughout this thesis, stable periodic motions are referred to as limit cycles (in phase space). In contrast to some other authors, the system is not required to be autonomous. See also the glossary for more information.

complex-valued modal amplitude $\hat{q}_k$ of the k-th linear mode can be expressed explicitly as

$$\hat{q}_k = \frac{\boldsymbol{\varphi}_k^{\mathrm{T}} \hat{\boldsymbol{e}}_1}{\omega_k^2 - \Omega^2 + \boldsymbol{\varphi}_k^{\mathrm{T}} \boldsymbol{C}_{\mathrm{mod}} \boldsymbol{\varphi}_k \mathrm{i}\Omega} \,. \tag{5.8}$$

The linearized modes were simply superimposed in the proposed approximate procedure. It should be noted that this approach makes the ROM fully consistent with and exact in the linear case, which is an important feature.

5.2 Remarks on the ROM's attributes

Multi-harmonic character of the predictions

The conception of the nonlinear modes as invariant manifolds in accordance with Eq. (5.1) inherently gives rise to a multi-harmonic character of the predicted flow. The multi-harmonic character is an important dynamic feature. It should be noted that it is obtained only at the cost of the a posteriori synthesis, but no additional equations have to be solved, thanks to the projection onto only the fundamental harmonic component involved in the derivation of the governing equations.
Higher temporal harmonics and non-resonant linear modes, as well as their coupling induced by nonlinearity are automatically taken into account in the modal analysis. Compared to a straight reduction to a single linear mode and the fundamental harmonic, the proposed model reduction approach thus requires a potentially costly preliminary analysis, but the ROM is expected to be more accurate.

Efficiency

The predictions based on the ROM are significantly less expensive than the ones based on direct analysis of the full-order model governed by Eq. (4.1) for several reasons. Firstly, the problem is reduced to a very small dimension. This dimension equals the dimension of the subspace on which the dynamics are assumed to take place, namely the two-dimensional invariant manifold. Hence, this dimension is independent of the spatial and temporal discretization of the original problem or the type and distribution of nonlinearities. Averaging aims at rotating the coordinate system with the principal component of the flow. The coordinates, a and $\Delta\vartheta$, are therefore varying comparatively slowly, which permits larger step sizes in the computational procedures. Finally, the nonlinear forces $\boldsymbol{g}$ in the original space, which may be expensive to evaluate, do not occur in the reduced equations anymore. Instead, only the amplitude-dependent modal properties $\omega_0(a), D(a), \hat{\boldsymbol{\psi}}_1(a)$ have to be evaluated. Those are available in the form of discrete data points directly obtained from the preceding modal analysis. Comparatively inexpensive interpolation was carried out for determining the modal properties for arbitrary a.

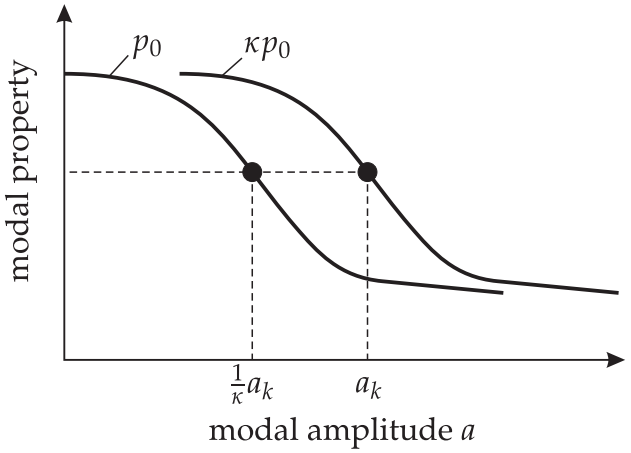

Figure 5.3: Determination of modal characteristics for varied parameter p_0 taking advantage of scale invariance

Parameter space

The parametric character of the ROM is essential for making the proposed methodology attractive to parameter studies. Considerable computational savings are possible when the modal characteristics do not have to be re-computed for altered parameters. Since the linear damping and harmonic forcing terms were only considered in the ROM, this is the case for the following parameters:

- external forcing magnitude and phase distribution described by $\hat{\boldsymbol{e}}_1$
- external forcing frequency Ω_e
- (modal) damping parameters associated with $\boldsymbol{C}_\mathrm{mod}$

It should be noted that the viscous damping term shall be deemded as 'wild card'. Hysteretic and modal damping can be readily taken into account in the proposed approach. Furthermore, the *scale invariance* of specific nonlinearities can be exploited. In this thesis, such a scale invariance is established for systems in which nonlinearity stems solely from the piecewise linear elastic unilateral contact and elastic Coulomb dry friction laws (cf. **Fig. 2.3**, p. 10). Suppose the modal characteristics are known for a specific normal preload level p_0 in the contact interface. The scale invariance relates the modal characteristics for preload κp_0 scaled with a real-valued positive scalar $\kappa > 0$ to those already obtained:

$$\{\omega_0, D, \hat{\boldsymbol{\psi}}_0, \ldots, \hat{\boldsymbol{\psi}}_H\}\big|_{\kappa p_0}(a) = \{\omega_0, D, \hat{\boldsymbol{\psi}}_0, \ldots, \hat{\boldsymbol{\psi}}_H\}\big|_{p_0}\left(\frac{1}{\kappa}a\right). \tag{5.9}$$

Hence, this scale invariance permits the immediate determination of modal characteristics for varied preload, i. e. without actual re-computation. This relationship is illustrated in **Fig. 5.3**. A formal proof of this invariance is given in Appendix D. It should be emphasized that the above mentioned contact formulations are widely used in the field of friction damping, see e. g. [76, 154, 128, 51]. This scale invariance further applies in the special cases of pure unilateral contact interaction or friction with constant normal load. For other parameters, the modal characteristics have to be re-computed in general. In-

stead of carrying out the modal analysis during the ROM simulation, it is proposed to determine the modal characteristics a priori for discrete parameter values, and to interpolate between these points. Details and an example for this procedure involving the friction coefficient can be found in Krack et al. [92].
It should be remarked at this point that although the above mentioned parameters can in principle be varied arbitrarily, the parameter range in which the ROM provides satisfying accuracy, will generally be limited. For instance, a sufficiently large forcing magnitude might drive the system into a regime with strong nonlinear modal interactions, where the assumption of an isolated resonance is no longer valid. Similarly, if the excitation frequency Ω_e is far from the eigenfrequency ω_0, another mode might be driven into its respective nonlinear regime.

5.3 Derivation of special cases for the design of friction-damped systems

In order to demonstrate the versatility of the proposed ROM, special cases of Eqs. (5.4)-(5.5) and (5.7) are derived below, which are particularly relevant for the design of friction-damped systems.

5.3.1 Steady-state dynamics

Forced response to harmonic excitation

Frequency-response functions
A particularly relevant case is the computation of frequency-response functions, where the frequency Ω_e of the harmonic forcing is varied. In this case, the oscillation frequency is $\Omega = \Omega_\mathrm{e}$. Since the modal properties do not depend on the phase lag, Eq. (5.7) can be solved for a and $\Delta\vartheta$ in a sequential manner: The amplitude a is computed iteratively from a single real-valued equation,

$$\left| {\omega_0}^2(a) - {\Omega_\mathrm{e}}^2 + 2\tilde{D}(a)\,\omega_0(a)\,\mathrm{i}\Omega_\mathrm{e} \right| a = \left| \hat{\boldsymbol{\psi}}_1^{\mathrm{H}}(a)\,\hat{\boldsymbol{e}}_1 \right| . \tag{5.10}$$

If needed, the phase lag $\Delta\vartheta$ can be evaluated in a subsequent non-iterative step upon solution, by substituting the result into Eq. (5.7). After finding an initial solution point, continuation with respect to Ω_e was performed. Finally, off-resonant modes were superimposed in accordance with Eq. (5.8).
The interested reader might note the similarity of Eq. (5.10) with the forced response equation derived in [94]. The approach proposed in the present thesis exceeds the work reported in [94] by the consideration of the multi-harmonic character of the vibrational deflection shape, the approximate synthesis of the off-resonant linearized modes and the

superposition of the linear damping term. These benefits are accompanied by comparatively low additional computational burden.

Direct analysis of external resonances

It is further noted that resonances can be directly analyzed. In this case, the external forcing frequency coincides with the eigenfrequency, i. e. $\Omega_\mathrm{e} = \omega_0$, and Eq. (5.10) simplifies to

$$\left(2\tilde{D}\left(a\right)\omega_0{}^2\left(a\right)\right)a = \left|\hat{\boldsymbol{\psi}}_1^\mathrm{H}\left(a\right)\hat{\boldsymbol{e}}_1\right| . \tag{5.11}$$

The phase lag can then be identified as $\Delta\vartheta = \arg\left(\hat{\boldsymbol{\psi}}_1^\mathrm{H}\left(a\right)\hat{\boldsymbol{e}}_1\right) - \pi/2$, and the a priori unknown resonance frequency is a by-product of the solution of Eq. (5.11). Again, continuation with respect to a specific control parameter of the ROM is carried out. This facilitates the computation of the *backbone curve*, i. e. the line which connects the maxima of a group of frequency-response curves obtained for a varied control parameter. This is particularly relevant for the design of friction-damped systems, since this permits the direct computation of the damper performance or optimization curve, cf. **Fig. 2.6** on p. 19. These characteristics are crucial to accomplish an effective vibration reduction.

In the field of friction-damped turbomachinery blades, it is common practice to directly analyze forced resonance regimes with respect to certain system parameters. This is achieved by considering the excitation frequency as an additional unknown and augmenting the governing set of equations in generalized coordinates by a so-called resonance condition [122, 125, 91, 85, 86]. As it was demonstrated in Krack et al. [85], these strategies fail in the presence of internal resonances, similar to the approach proposed in this thesis. Therefore, these techniques have a similar range of applicability. The solution of Eq. (5.11) thus represents an apt and possibly more efficient alternative to the aforementioned techniques.

Limit cycles in the presence of negative damping

In the absence of external forcing, the right hand side of Eq. (5.7) vanishes and the oscillation frequency coincides with the eigenfrequency $\Omega = \omega_0$. This leads to a single real-valued equation,

$$2\tilde{D}(a)\omega_0(a)a = \left[2D(a)\omega_0(a) + \hat{\boldsymbol{\psi}}_1^\mathrm{H}(a)\boldsymbol{C}_\mathrm{mod}\hat{\boldsymbol{\psi}}_1(a)\right]a = 0\,. \tag{5.12}$$

The phase lag $\Delta\vartheta$ does not have a relevant physical meaning in the absence of external forcing, and therefore does not occur in Eq. (5.12). Non-trivial solutions of Eq. (5.12) may for instance occur when $\boldsymbol{C}_\mathrm{mod}$ induces negative damping which is compensated by friction damping with $D > 0$. The variation of the modal deflection shape $\hat{\boldsymbol{\psi}}_1(a)$ may also have an influence on the limit cycle amplitude. In fact, this effect alone may lead to stabilization even when nonlinear damping is absent [127].

Again, these self-excited limit cycles can be continued with respect to a specific parameter. This is particularly relevant for the design of friction-damped systems, since this

facilitates the direct computation of stability maps in the presence of negative damping, cf. **Fig. 2.6**c on p. 19.
It should be noted that the isolated nonlinear mode assumption implies that the off-resonant modes are damped away. Otherwise they would grow unboundedly or at least into the regime in which they would necessarily cause nonlinear modal interactions. In this case, the kinetic energy would no longer be confined to an isolated nonlinear mode anymore. Such a situation is, by definition, beyond the regime of interest in the present study. Hence the off-resonant modes are not considered for the prediction of self-excited limit cycles to be in full accordance with the limitations of the proposed ROM.

5.3.2 Unsteady dynamics

Externally forced case
Again, the oscillation frequency is locked to the external excitation, $\Omega(t) = \Omega_\mathrm{e}(t)$. A slow variation of the excitation frequency can be taken into account to investigate resonance passages. If the external excitation is left constant, the transition to a limit cycle induced by steady harmonic forcing can be studied.

Autonomous case
Two relevant situations should be mentioned: The free decay from resonance and the transition to a limit cycle in the presence of negative damping. Again, the phase lag is constant and does not have a relevant physical meaning in the absence of external forcing. Eqs. (5.4)-(5.5) thus simplify to

$$\dot{a}\left(t\right) = -\tilde{D}\left(a\left(t\right)\right)\omega_0\left(a\left(t\right)\right)a\left(t\right) \ . \tag{5.13}$$

6 Application to simple models with contact interfaces

The purpose of this chapter is to investigate the performance of the proposed procedure composed of the modal analysis developed in Chapter 4 and the model reduction developed in Chapter 5. Simple structural dynamical models are considered in order to systematically study the influence of the basic nonlinearities relevant for friction-damped systems: friction and preloaded unilateral contact. Parts of the presented results have already been published in Krack et al. [88, 89].

As a first test case, a cantilevered beam was studied as illustrated in **Fig. 6.1**. At its free end, nonlinear elements can be attached. Two different elements were considered, a unilateral spring and an elastic Coulomb element, with stiffness k_n and k_t, respectively.

The one-dimensional nonlinear elements can be considered as degenerate variants of a three-dimensional contact model: If the contact dynamics feature a predominant direction aligned with either the normal direction or the tangential plane, the interaction will primarily have a friction or a unilateral character, respectively. These extreme cases typically occur, if the normal load does not vary significantly or if the friction coefficient is negligibly small.

The cantilevered beam was spatially discretized by means of ten Euler-Bernoulli beam elements. Only the displacement in the x-direction was taken into account. The Craig-Bampton method was applied to reduce the order of the underlying linear model. In accordance with a preliminary convergence study, the system dynamics in the considered frequency range are described with sufficient accuracy in the reduced basis composed of the static constraint mode associated to the tip displacement coordinate and the first five

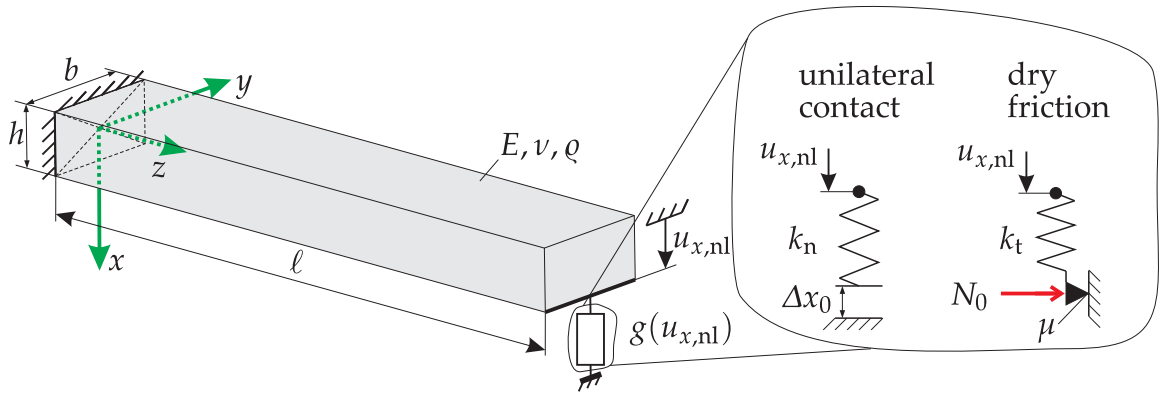

Figure 6.1: Cantilevered beam with either unilateral contact or dry friction at its free end, $E = 210 \cdot 10^3$ MPa, $\nu = 0.3$, $\varrho = 7800$ kg/m^3, $\ell = 200$ mm, $b = 40$ mm, $h = 3$ mm

fixed interface normal modes.
In spite of the simplicity of the models investigated in this chapter, a closed-form analytical solution of the differential equations of motion cannot be derived in general. Because of the piecewise linear character of the nonlinear forces, an analytical solution can of course be obtained for the different contact states. It can, however, easily be shown that a closed-form solution of the transition conditions between these contact states is not possible.

Normalization:
In the figures presented throughout this chapter, physical quantities have been normalized, which is indicated by a superscript '': Frequencies have been normalized by the eigenfrequency of the considered mode in the linear case, i. e. where the nonlinear element is replaced by its linearization around the equilibrium. Generalized coordinates and the kinetic energy have been normalized by their value at the kinetic energy where the purely linear regime turns into a nonlinear regime, i. e. where the first contact-separation or stick-slip transition takes place.*

Reference results:
In order to assess the quality of the ROM predictions, reference results were determined using numerical time integration applied directly to the equations of motion (4.1) of the full-order model.

6.1 System with preloaded unilateral contact

The unilateral contact element was first attached to the beam in **Fig. 6.1**. A preload in the spring was realized by an initial compression of length $|\Delta x_0| = 0.05\, l$. Although the investigations in this thesis are restricted to opening (preloaded) contact, analogous results are generally expected for closing (initially open) contact.

6.1.1 Modal characteristics

Internal resonances

The modal characteristics of the first bending mode were computed using the proposed modal analysis technique, i. e. by solving Eq. (4.19). In addition to the zeroth and the fundamental harmonic, the first superharmonics up to $H = 40$ were retained in this analysis. The results are depicted in **Fig. 6.2** for different stiffness values k_n of the unilateral spring. The values k_n were normalized by the bending stiffness $3EI_{yy}/l^3$ of the clamped beam, where $I_{yy} = bh^3/12$ is the second moment of the cross section area with respect to the y-axis.

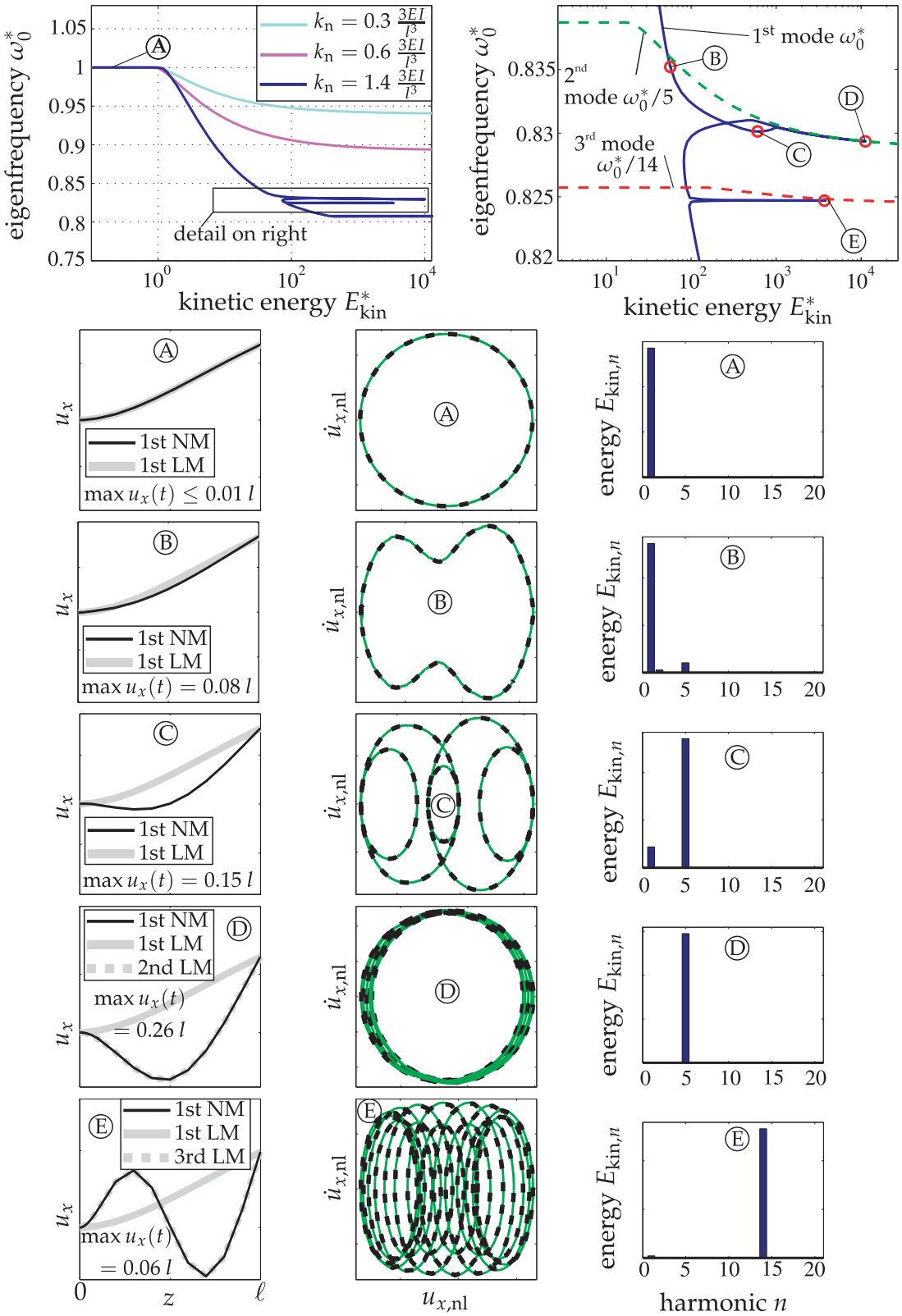

Figure 6.2: Energy dependence of the first nonlinear mode of the beam with preloaded unilateral contact. Top left plot: frequency-energy plot for different k_n values, $\Delta x_0/l = -5\,\%$. Top right plot: detail of the first two folds. Bottom plots: modal deflection shape, phase projection (solid green: reference, dashed black: modal analysis) and frequency content of kinetic energy for the largest k_n value.

In order to provide a better understanding of the underlying dynamics, modal deflection shape, phase projection of the beam tip coordinate and frequency content of the kinetic energy are shown for the indicated points (A) through (E). Since the system is conservative, the modal damping ratio is identical to zero, $D \equiv 0$, and not depicted in the figure.
Depending on the kinetic energy and the system parameters, linear, weakly nonlinear and strongly nonlinear regimes can be encountered, which are described below. For small energies, the preload in the spring k_n is not exceeded. This results in a *linear regime* where the eigenfrequency and the modal deflection shape are constant. This is the case for point (A) in **Fig. 6.2**. Beyond a certain energy level, the contact undergoes lift-off during vibration and the system exhibits nonlinear behavior henceforth. This results in a softening effect, i. e. the eigenfrequency decreases. For the largest considered stiffness k_n, the linear regime ends when the beam's tip displacement amplitude exceeds 1 % of the beam's length.
In the *weakly nonlinear regime*, the eigenfrequency varies with energy and may significantly deviate from its corresponding value in the linear regime, cf. point (B) in **Fig. 6.2**. The modal deflection shape of the first nonlinear mode (NM) varies to a certain extent, but can still be uniquely related to its linear counterpart (LM). The periodic motion is still dominated by its fundamental harmonic component, but first 'wrinkles' appear in the phase projection, which indicates the presence of super-harmonics. This finding can also be obtained from the frequency content of the kinetic energy $E_{\mathrm{kin},n}$, which is defined in Eq. (4.10) and is depicted in the right plots in **Fig. 6.2**.
The contact stiffness k_n influences the strength of the nonlinear forces in relation to the elastic and the inertia forces of the underlying structure. If the contact stiffness is sufficiently small, only the weakly nonlinear regime is reached for large energies. In this case, the eigenfrequency approaches a decreased, constant value. For increasing k_n the softening effect becomes more prominent. For sufficiently large k_n, a *strongly nonlinear regime* is encountered. This regime is characterized by bifurcations, as they occur here in the form of turning points. This behavior is induced by internal resonances.
The $5:1$ internal resonance with the second mode and the $14:1$ internal resonance with the third mode are highlighted in the top right plot in **Fig. 6.2**. In order to show the frequency coincidence, the eigenfrequency characteristics of the corresponding higher modes are also depicted. Their eigenfrequencies were divided by 5 and 14, respectively, which is the ratio of the eigenfrequencies present at the tip points (D) and (E) of the folds. In the linear case, the ratio between the eigenfrequencies of second and first mode is 4.2 and 11.6 between third and first mode. Hence, the internal resonances are not present in the linear regime, but they are caused by the energy dependence in the nonlinear regime. The bifurcations introduce a qualitatively different vibration behavior. The modal deflection shape exhibits a peculiar form which cannot be uniquely related to the first linear bending mode anymore, cf. points (C)-(E) in **Fig. 6.2**. In fact, the modal deflection shape typically coincides with the corresponding higher mode at the tip of the folds. Thus, an accordingly higher harmonic content becomes apparent. It should be noted that the maximum displacement amplitude is small for point (E) considering the large kinetic energy per period. This can be explained with the higher frequency content at this point. Between

the internal resonances, intermediate regimes may exist where the frequency content is again dominated by the fundamental harmonic component.
The complicated system behavior is well-resolved by the proposed modal analysis technique, which can be ascertained by comparing the phase projections computed by modal analysis (dashed black) with the ones obtained from numerical time integration (solid green) in the five middle plots in **Fig. 6.2**. For the numerical time integration, the results of the modal analysis were specified as initial conditions.
The approach proposed in this thesis was designed for the regime of an isolated resonance, i. e. where internal resonances are absent. The dynamic regime of interest is therefore composed of the linear and weakly nonlinear regime. It is, however, relevant to identify the limit between weakly and strongly nonlinear regime, which is defined by the first bifurcation.

Convergence with respect to harmonic order

The presence of internal resonances encountered in the analysis of the beam impedes the validation of the proposed approach. To avoid internal resonances, the beam could be investigated for a comparatively small k_n only, as it was done in Krack et al. [88]. In this study, the two-DOF system illustrated in **Fig. 6.3**a is considered instead of the beam for the subsequent investigations. Note that the dynamic behavior of the beam could in principle be described by a two-DOF system if e. g. a modal truncation to the first two modes was applied. This procedure would involve to artificially neglect the physically meaningful internal resonances. In order to emphasize that the considered two-DOF system is not related to the beam, its properties are given in dimensionless form below **Fig. 6.3**. For the second mode of this system, no internal resonances were encountered, even for comparatively large k_n. This allowed the validation of the ROM for strongly nonlinear forces.
The frequency-energy characteristic of the system's second mode is illustrated in **Fig. 6.3**b. The qualitative behavior is similar to the one of the beam. The influence of

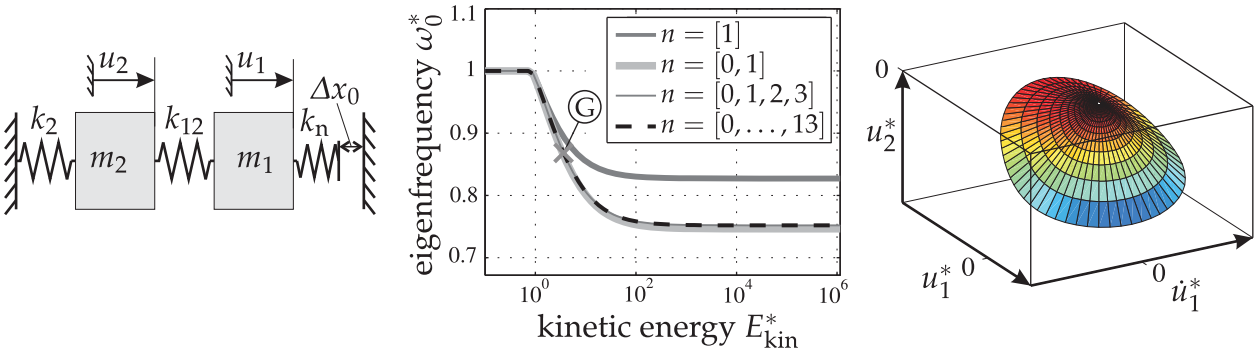

(a) (b) (c)

Figure 6.3: Two-DOF system with preloaded unilateral contact, $m_1 = 0.02$, $m_2 = 1$, $k_{12} = 40$, $k_2 = 600$, $\Delta x_0 = -1$, $k_\mathrm{n} = 70$: (a) model definition, (b) frequency-energy plot of second mode, (c) two-dimensional invariant manifold of second mode

the harmonics retained in the modal analysis was investigated. A comparatively small harmonic order is sufficient to achieve asymptotic convergence of the frequency-energy characteristic. It is important to retain the zeroth-order term ($n = 0$). This term controls the static deflection of the system, which is obviously nonzero when the unilateral contact changes its status between open and closed during vibration. This static deflection also has an influence on the effective preload in the unilateral spring. Note that this effect already inhibits the derivation of an analytical approximation in terms of the harmonic balance method with $n = [0, 1]$ [183], which justifies the numerical character of the proposed approach.
While the linear mode spans a plane in phase space, the dynamics of the nonlinear mode takes place on a curved manifold. This manifold is no longer symmetric around the static equilibrium with regard to its coordinates. This can be well ascertained from **Fig. 6.3**c. Apparently, the unilateral contact has a significant influence on the energy-dependent modal deflection shape of the system.

6.1.2 Autonomous response

In order to assess the ability of the developed method to reproduce the dynamic behavior of the full-order model in the regime of interest, the system was investigated under various operating conditions. This is essential for a thorough validation of the approximate procedure. The response of the system was first investigated in its autonomous configuration. A constant, mass-proportional damping was specified, so that the second mode had a damping ratio of 1% in the linear case.
Starting from point (G) indicated in **Fig. 6.3**b, the system was left to itself, in such a way that it approached its static equilibrium point. The ROM prediction is based on the time integration of Eq. (5.13). The time history of the second mass's displacement u_2^* is illustrated in **Fig. 6.4**a. The number N_p^* of pseudo-periods was introduced as time variable: It equals $N_\mathrm{p}^* = f_0 t$, where f_0 is the eigenfrequency of the considered (second) mode in the linear case.
The asymmetrical upper and lower envelope of the response should be noted. In accordance with the manifold in **Fig. 6.3**c, there is an offset, so that the mean value of u_2^* is negative in the nonlinear regime. This mean value becomes smaller with decreasing amount of lift-off and finally vanishes when no lift-off occurs anymore. In order to obtain a deeper insight into this behavior, the time dependent amount of lift-off was quantified. To this end, the time spans between the transitions from contact to lift-off and vice versa were determined by finding the zero crossings of the unilateral spring's deflection $u_1^* - \Delta x_0$. The amount of lift-off is defined as the ratio between the time span in which this deflection is negative (lift-off) to the entire time span between two positive zero crossings. The results are depicted in **Fig. 6.4**b. In general, the ROM predictions are in quite good agreement with the reference results.

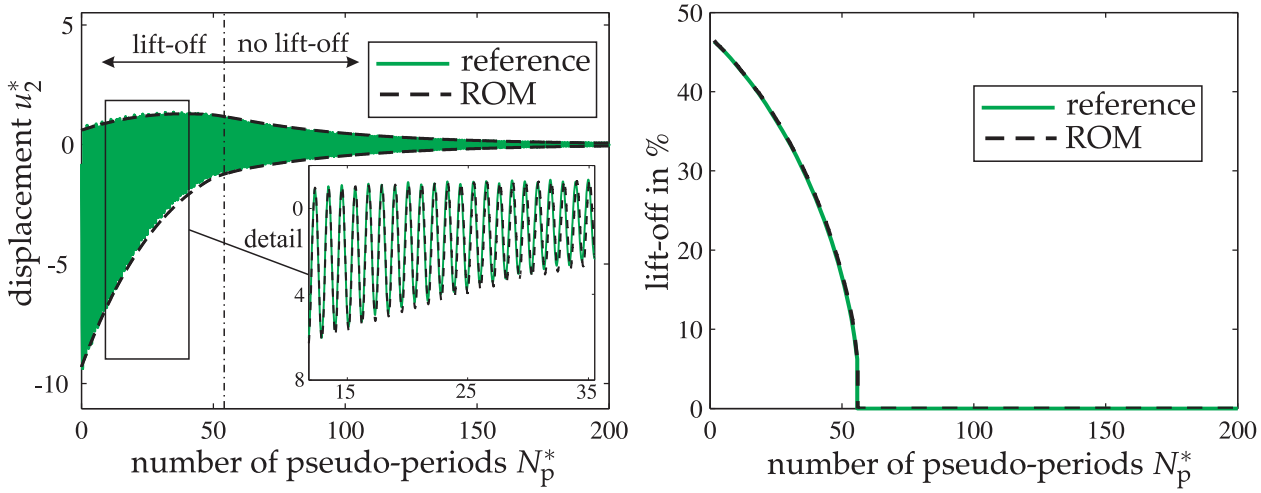

Figure 6.4: Time history of a free decay of the two-DOF system with preloaded unilateral contact, starting point (G) as defined in **Fig. 6.3**b: (a) displacement of the second mass, (b) amount of lift-off

6.1.3 Forced response

An external harmonic force was applied to the mass m_2 illustrated in **Fig. 6.3** in order to investigate the steady and unsteady dynamics in the presence of forced excitation.

Steady-state forced response

The steady-state response of the system in the frequency range around the second eigenfrequency was studied. The linear damping was adopted from the autonomous setting. The ROM results were obtained by solving Eq. (5.10) for frequency-response functions and Eq. (5.11) for backbone curves. The reference results were determined by means of direct time integration of the equations of motion of the full-order model. The excitation level was varied in a wide range. For each frequency step, the simulation was carried out until the vibration amplitude was constant according to a sufficiently small tolerance. The state vector at the end of the simulation for the current frequency step were adopted as initial values for the next frequency step. The results are depicted in **Fig. 6.5**a.
For an increasing excitation level, the forced resonance amplitude increases and the softening effect becomes apparent, in full accordance with the results in **Fig. 6.3**b. The frequency-response curves bent towards the left. This results in a multi-valued response for some of the curves. It is generally known that the overhanging branches, depicted in **Fig. 6.5** are locally unstable. Hence, they could not be obtained from the time domain simulation. The reference computation was carried out for increasing and for decreasing frequencies in order to compute the lower and the upper branch, respectively. The ROM prediction of the forced response is in very good agreement with the reference results. Particularly in the vicinity of the resonance, the accuracy of the proposed ROM is excellent.

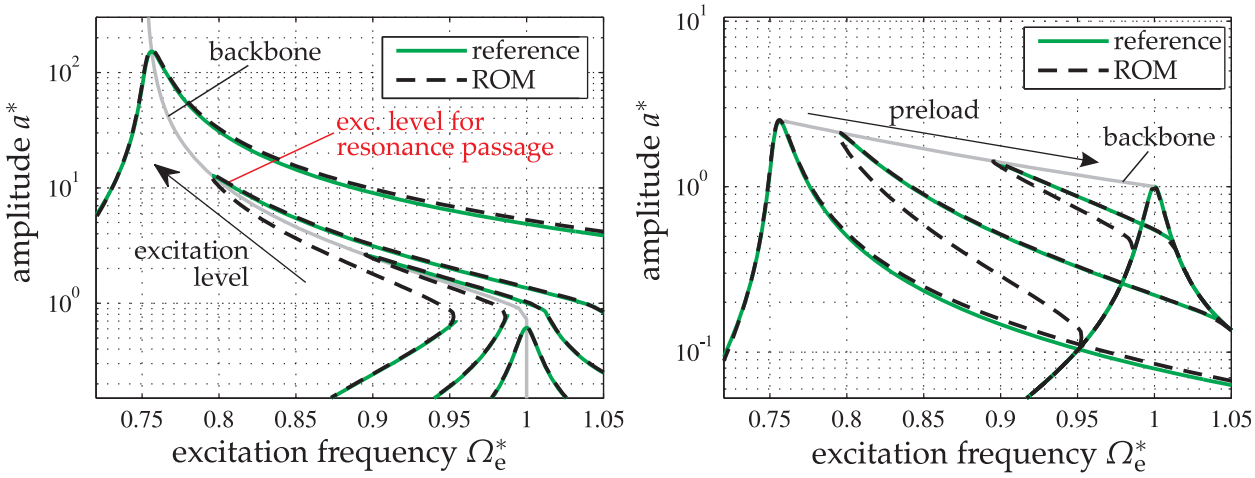

Figure 6.5: Steady-state forced response near the second mode of the two-DOF system with preloaded unilateral contact: (a) variation of excitation level, (b) variation of preload

Moreover, the backbone curve, which corresponds to the frequency-energy characteristic depicted in **Fig. 6.3**, matches well with the maxima of the frequency-response curves.
Next, the excitation level was kept fixed and the preload was varied. The resulting frequency-response functions are depicted in **Fig. 6.5**b. For an increasing preload, the lift-off phases become shorter within one cycle of oscillation. When the preload is large enough, it entirely prevents the contact from lifting off, resulting in a linear behavior. The ROM predictions were computed by taking advantage of the scale invariance as explained in Section 5.2. Thus, the nonlinear modal analysis had to be carried out only once for a fixed preload in order to obtain the results shown in **Fig. 6.5**b (and also **Fig. 6.5**a). Again, a great prediction quality of the ROM can be stated.

Resonance passages

The unsteady vibration behavior of the externally forced system was also investigated. For this purpose, a sine sweep excitation was specified where the excitation frequency $\Omega_e(t)$ varies linearly with time. In **Fig. 6.6**, the results are shown both for increasing and decreasing frequency. The specified excitation level corresponds to the one indicated in **Fig. 6.5**a. The ROM results were obtained by time integration of the averaged differential equations (5.4)-(5.5) governing the flow on the manifold, while the reference results are based on direct time integration of the equations of motion of the full-order model. The time dependence is expressed in normalized form as $\Omega_e^*(N_p^*)$. A normalized angular acceleration of magnitude 0.0003 was used for the up-sweep as well as for the down-sweep. The meaning of this value can be numerically illustrated as follows: The excitation frequency varies by 0.3% every ten pseudo-periods, or equivalently, it takes 33 pseudo-periods until the frequency has changed by 1%. Note that the depicted time history does not start from $N_p^* = 0$, but it is restricted to the part around the largest amplitudes. The counter ΔN_p^* starts from zero at the beginning of the depicted time span.

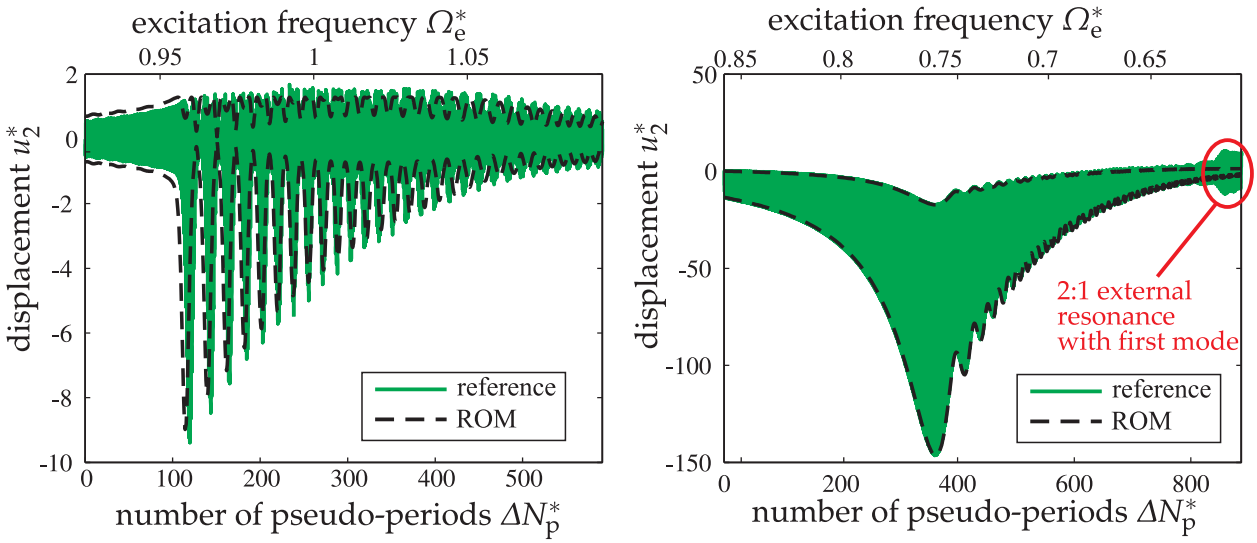

Figure 6.6: Time history of resonance passages through the second mode of the two-DOF system with preloaded unilateral contact, starting from equilibrium point: (a) up-sweep $\Omega_e^*(N_p^*) = 0.0003N_p^*$, (b) down-sweep $\Omega_e^*(N_p^*) = 1.75 - 0.0003N_p^*$

There exists a strong qualitative discrepancy between the responses in **Fig. 6.6**a and b. This effect is caused by the multi-valued response phenomenon encountered in the steady state in **Fig. 6.5**a. Coming from either side of the resonance frequency, a jump phenomenon occurs when the frequency hits the respective first turning point of the frequency-response curve. In the time history of the resonance passage, this causes a comparatively fast change of the medium envelope in conjunction with a strong beating phenomenon, cf. **Fig. 6.6**. Larger amplitudes are reached in the down-sweep, where the response follows the upper branch of the frequency-response curve, compared to the up-sweep, where the response follows the lower branch.

Mostly, a good agreement between the ROM and the reference can be stated. In the presence of fast amplitude changes, which can be particularly observed in the up-sweep, the response only agrees qualitatively and apparently fails to accurately track the phase lag of the actual response. In the down-sweep case depicted in **Fig. 6.6**b, a second 'burst' in the amplitude is encountered at $\Omega_e^* \approx 0.62$. The first eigenfrequency is about one third of the second eigenfrequency in the linear case, and a resonance would thus be expected for $\Omega_e^* \lessapprox 0.33$. It is conjectured that this behavior is caused by a $2:1$ external resonance with the first mode. In full accordance with the restriction of the ROM, the dynamics are only predicted well in the vicinity of the $1:1$ external resonance of the considered second mode, and the other amplitude burst is missed.

6.2 System with dry friction contact

In this section, the beam illustrated in **Fig. 6.1** is considered again. Now the elastic Coulomb element is attached to its free end.

6.2.1 Modal characteristics

The energy-dependent eigenfrequency and modal damping ratio of the first bending mode are depicted in **Fig. 6.7** for different tangential stiffness values k_t. Like in the case of the unilateral contact, the values k_n were normalized by the bending stiffness $3EI_{yy}/l^3$ of the clamped beam, where $I_{yy} = bh^3/12$ is the second moment of the cross section area with respect to the y-axis of the beam depicted in **Fig. 6.1**. The results generally resem-

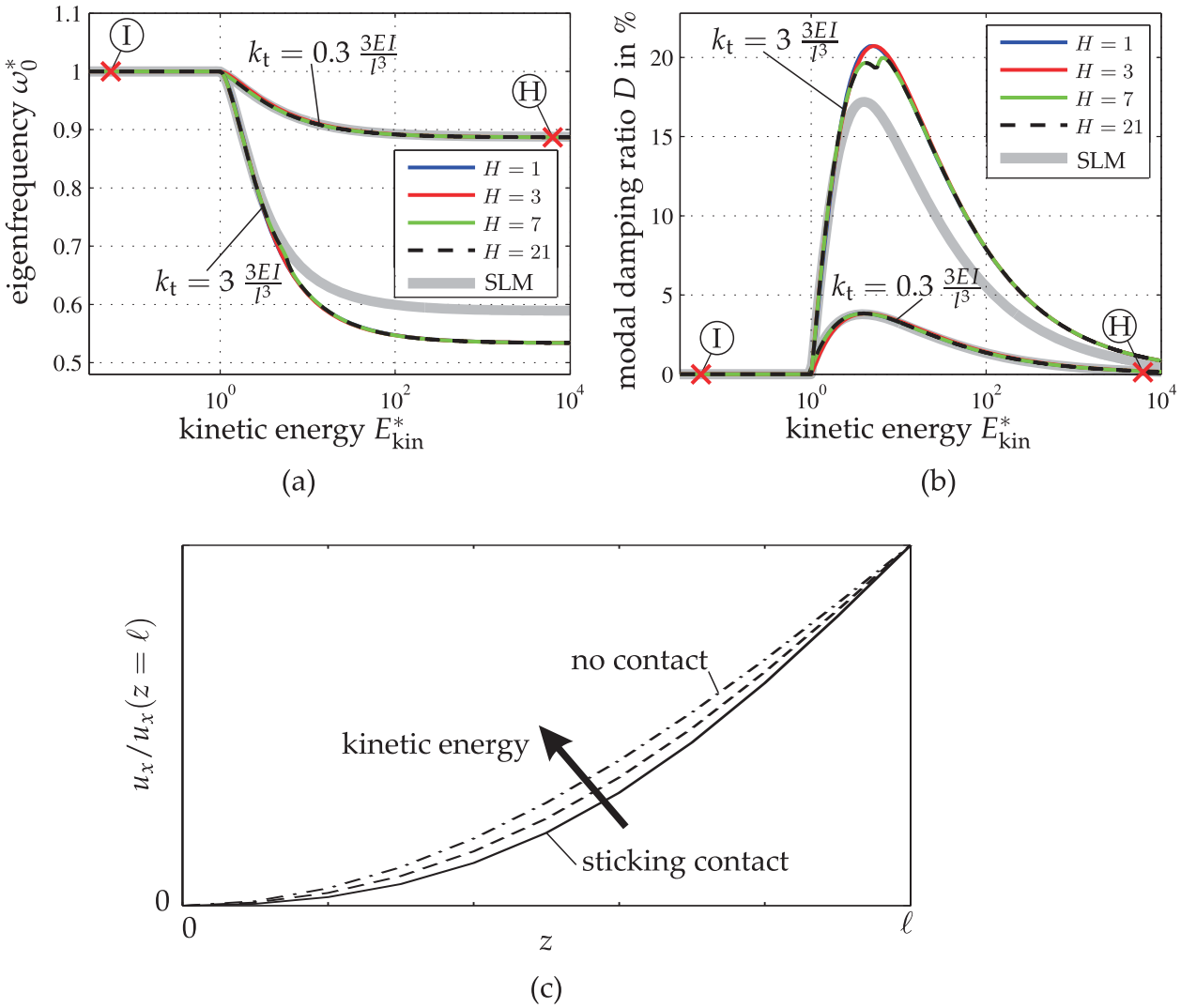

Figure 6.7: Modal characteristics of the first mode of the beam with friction nonlinearity, $\mu = 0.3$, $N_0 = 100$ N: (a) eigenfrequency, (b) modal damping, (c) variation of the beam's vibrational deflection shape for $k_t = 3\ \frac{3EI}{l^3}$

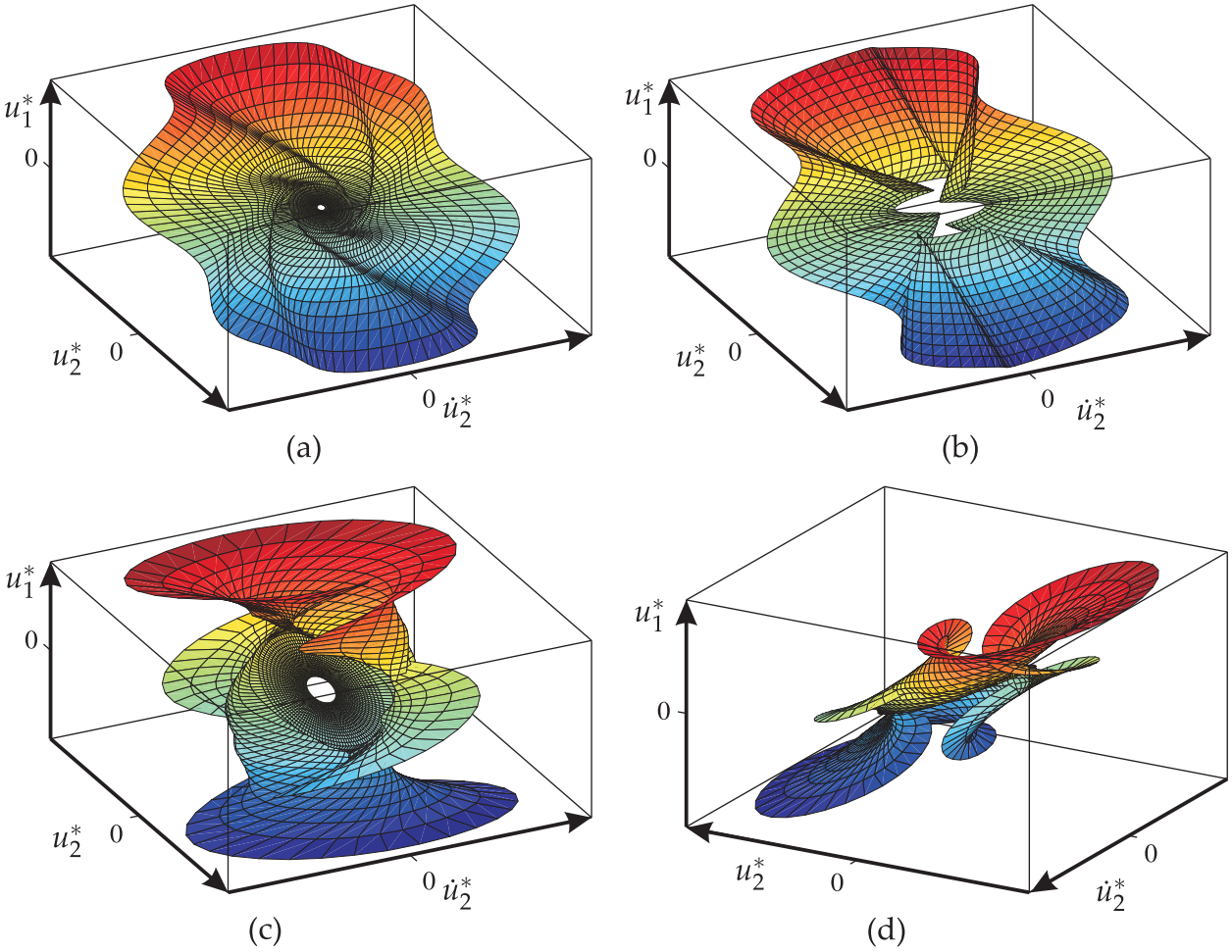

Figure 6.8: Two-dimensional invariant manifolds of the first mode of the beam with friction nonlinearity: (a) $k_t = 0.3\ \frac{3EI}{l^3}$ for $0.1 < E^*_{kin} < 300$ (b) $k_t = 3\ \frac{3EI}{l^3}$ for $6 < E^*_{kin} < 300$, (c) and (d) $k_t = 3\ \frac{3EI}{l^3}$ for $0.01 < E^*_{kin} < 1$

ble modal characteristics of friction-damped systems previously reported by other researchers, see e. g. [176, 187, 94]. There exists a linear energy regime, where the friction contact is permanently sticking and no energy is dissipated, i. e. $D = 0$. As soon as the energy is large enough, the contact also undergoes slip friction. As a consequence, the modal damping ratio increases. Moreover, the system behavior becomes softer, resulting in a decrease of the eigenfrequency. The decrease of the modal damping ratio for larger kinetic energies may seem counter-intuitive at first, but it can be easily made plausible: For a viscous damping source, the dissipated energy grows quadratically with amplitude, which leads to a constant modal damping ratio. The energy dissipated in the dry friction contact, in contrast, increases only linearly with amplitude, thus leading to a decreasing modal damping ratio for large amplitudes present for large kinetic energies. When E_{kin} tends towards infinity, the modal properties asymptotically approach towards the values associated to the linear case without contact.

Akin to the case of the unilateral spring, the contact stiffness influences the strength of the nonlinearity compared to the underlying linear structure. Thus, the relative frequency shift and the maximum modal damping ratio increase with k_t. Apparently, several har-

monics are required to achieve asymptotic convergence of the modal characteristics for larger k_t. This is particularly true in the vicinity of the maximum damping value, cf. **Fig. 6.7**b. This indicates that the abrupt changes between stick and slip of the friction contact induce higher harmonic vibration content.
It is common to derive analytical approximations of the steady-state vibration behavior of friction-damped systems based on the single-term harmonic balance method. For this strategy, it is generally necessary to assume a constant vibrational deflection shape and thus to simplify the system to a single-DOF (modal) oscillator, see e. g. [83, 134]. This has also been done for the beam assuming that the vibrational deflection shape for sticking contact is retained. The results are also depicted in **Fig. 6.7** a and b with the label 'SLM' (single linear mode). The differences between SLM and the proposed method for $H = 1$ is caused by the variation of the modal deflection shape. This variation is illustrated in **Fig. 6.7**c. The benefit of having an explicit solution, in the case of the SLM assumption, apparently is provided at the cost of lower accuracy. In contrast to this strategy, the variation of the vibrational deflection shape due to nonlinear effects is inherently taken into account in the proposed numerical procedure.
The friction nonlinearity thus causes a distortion of both the spatial and the temporal spectrum of the nonlinear modes, compared to the linear case where only a single linear mode and a single harmonic are present. This can also be observed from the invariant manifolds illustrated in **Fig. 6.8**a and b. The motions clearly deviate from ellipses for larger energies, indicating the presence of higher harmonics (in time). On the other hand, the nonlinear mode does not span a plane as in the linear case, but rather forms a curved manifold in phase space, indicating the contribution of other linear modes, i. e. harmonics in space.
It is important to note that the manifolds for the two different k_t values feature a qualitative topological difference: In contrast to the lower k_t value, the manifold is folded in the case of $k_t = 3\,\frac{3EI}{l^3}$. This folding occurs in the lower energy regime in the vicinity of the maximum damping ratio. The beginning of this folding can be clearly seen beyond the linear regime (plane in phase space) in **Fig. 6.8**c and d. This behavior is accompanied by a significant super-harmonic component of the periodic motion. Hence, the fundamental harmonic component of the flow does no longer dominate and the resonance cannot be regarded as isolated anymore in accordance with the definition on p. 33. For the subsequent investigations, only the smaller stiffness $k_t = 0.3\,\frac{3EI}{l^3}$ is considered, for which such strong modal interactions are absent, and the nonlinear mode can be regarded as isolated.

6.2.2 Autonomous response

Similar to the system with unilateral contact, the developed method was assessed regarding its capability of reproducing the dynamic behavior of the original model under various operating conditions. This is essential for a thorough validation of the approximate procedure. Special attention is paid to situations which are commonly of interest for

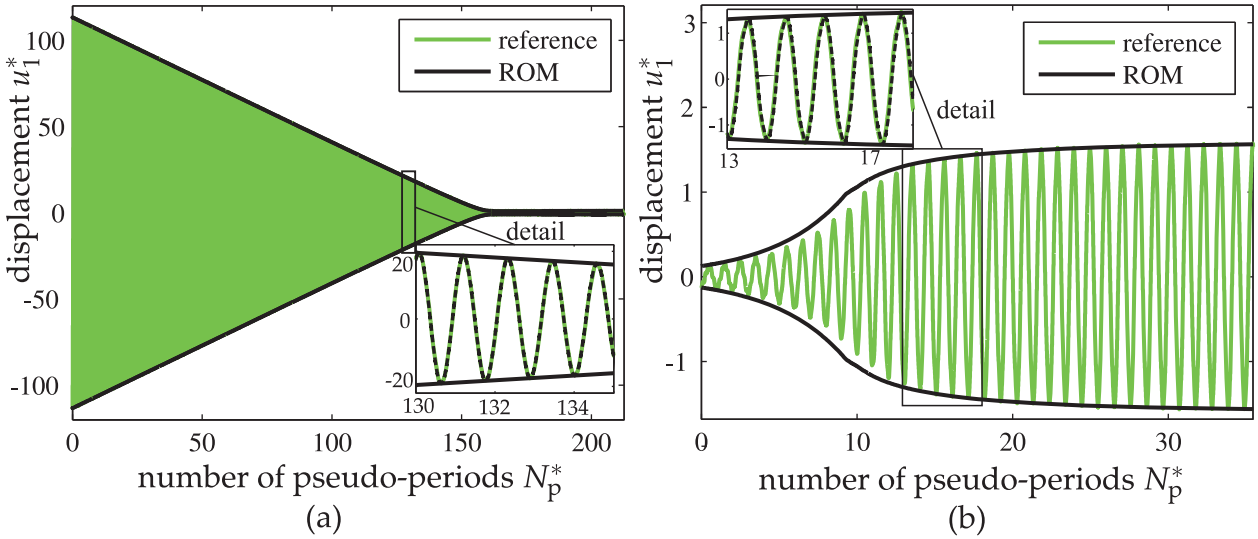

Figure 6.9: Time history of the autonomous beam with friction nonlinearity: (a) free decay with $\boldsymbol{C}_{\text{mod}} = \boldsymbol{0}$ from starting point (H), (b) transition into limit cycle induced by negative damping with $\boldsymbol{C}_{\text{mod}} = \boldsymbol{C}_{-2\%}$ from starting point (I)

the design of friction-damped systems. The autonomous behavior of the friction-damped beam was investigated first.

Free decay

Starting from point (H) indicated in **Fig. 6.7**a and b, the free decay towards the equilibrium point was simulated. The results were computed by time integration of the equations of motion of the original model (reference) as well as the ROM equation (5.13). The time history of the beam's tip displacement u_1^* is depicted in **Fig. 6.9**a.
In contrast to the exponential decay of the amplitude which is characteristic for the linear case, the envelope exhibits a linear decay. This is a typical feature of dry-friction damped systems and it indicates again the amplitude dependence of the damping ratio. This behavior is well predicted by the ROM, as compared to the reference results.

Transition into a limit cycle in the presence of negative damping

The effect of negative damping was investigated next. To this end, a constant damping matrix $\boldsymbol{C}_{\text{mod}}$ was imposed. It was defined in such a way that the first linear mode had a negative damping ratio $D_1 < 0$, while the remaining linear modes had a positive damping ratio of 1%. While the amplitude of the first mode would grow unboundedly for a slight perturbation from the static equilibrium point in the linear case, the nonlinear friction damping can stabilize the system in a limit cycle. The time history of the transition from the starting point (I) towards such a limit cycle is illustrated for $D_1 = -2\%$ in **Fig. 6.9**b. For the ROM predictions, the linear damping was superimposed in Eq. (5.13) to

obtain the results.
An acceptable accuracy of the ROM can be ascertained. Slight deviations occur in particular during the time span with comparatively fast amplitude increase. In fact, the amplitude doubles within about three pseudo-periods. Hence, the amplitude variation and the oscillation take place on rather proximate time scales. Since the ROM derived in Chapter 5 is based on averaging, deviations in this range are expected.

Analysis of limit cycles in the presence of negative damping

The autonomous behavior in the presence of negative damping was further investigated. For this purpose, limit cycles were computed using Eq. (5.12) of the ROM. Reference results were obtained by means of time integration of the original equations of motion, starting from small initial values until the vibration amplitude was constant (considering a sufficiently small tolerance). The limit cycle amplitude and frequency are illustrated with respect to the modal damping ratio D_1 in the left plots of **Fig. 6.10**.
In the presence of negative damping, the trivial solution, i. e. the static equilibrium point is unstable. The illustrated limit cycle amplitudes are non-trivial solutions of Eq. (5.12). They are characterized by vanishing effective modal damping, i. e. the damping caused by the joint effect of friction and the superimposed (negative) linear damping. Stable and unstable regimes are indicated in **Fig. 6.10**a and c. The local stability was determined by considering the effective damping ratio and analyzing the slope at the zero crossing: If the effective modal damping increases with respect to the amplitude, the limit cycle is stable, otherwise it is unstable. Whether the system reaches a stable limit cycle obviously depends on the initial amplitude.
For sufficiently low damping, e. g. $D_1 < -4\%$, no limit cycles exist at all and the amplitudes would grow unboundedly. For positive damping values (not illustrated), the limit cycle would obviously degenerate to the static equilibrium point. It should be noted that the stability map is not only influenced by the modal damping characteristic, but it also depends on the modal deflection shape, which in turn affects the negative damping caused by $\boldsymbol{C}_{\mathrm{mod}}$, see Eq. (5.12). The ROM predictions of the stable limit cycles are in excellent agreement with the reference results. The reference results were obtained from the equations of motion of the full-order model using direct time integration, starting from small initial values. Only the stable limit cycles were thus obtained. It should be remarked that the unstable limit cycles could have been obtained e. g. by integration backwards in time or by the shooting method. This was, however, not performed in this study. The results generally resemble the results reported in previous studies, see e. g. [156, 157, 62].
In the right plots of **Fig. 6.10**, the amplitude and the frequency of the limit cycles are depicted with respect to the preload N_0. The value N_0^* is normalized by its nominal value of 100 N. Apparently, the frequency is constant and the amplitude increases linearly with N_0^*. This resembles the results reported by other researchers, see e. g. [127]. The linear relationship between limit cycle amplitude and preload follows directly from the scale invariance established in this thesis and expressed in Eq. (5.9).

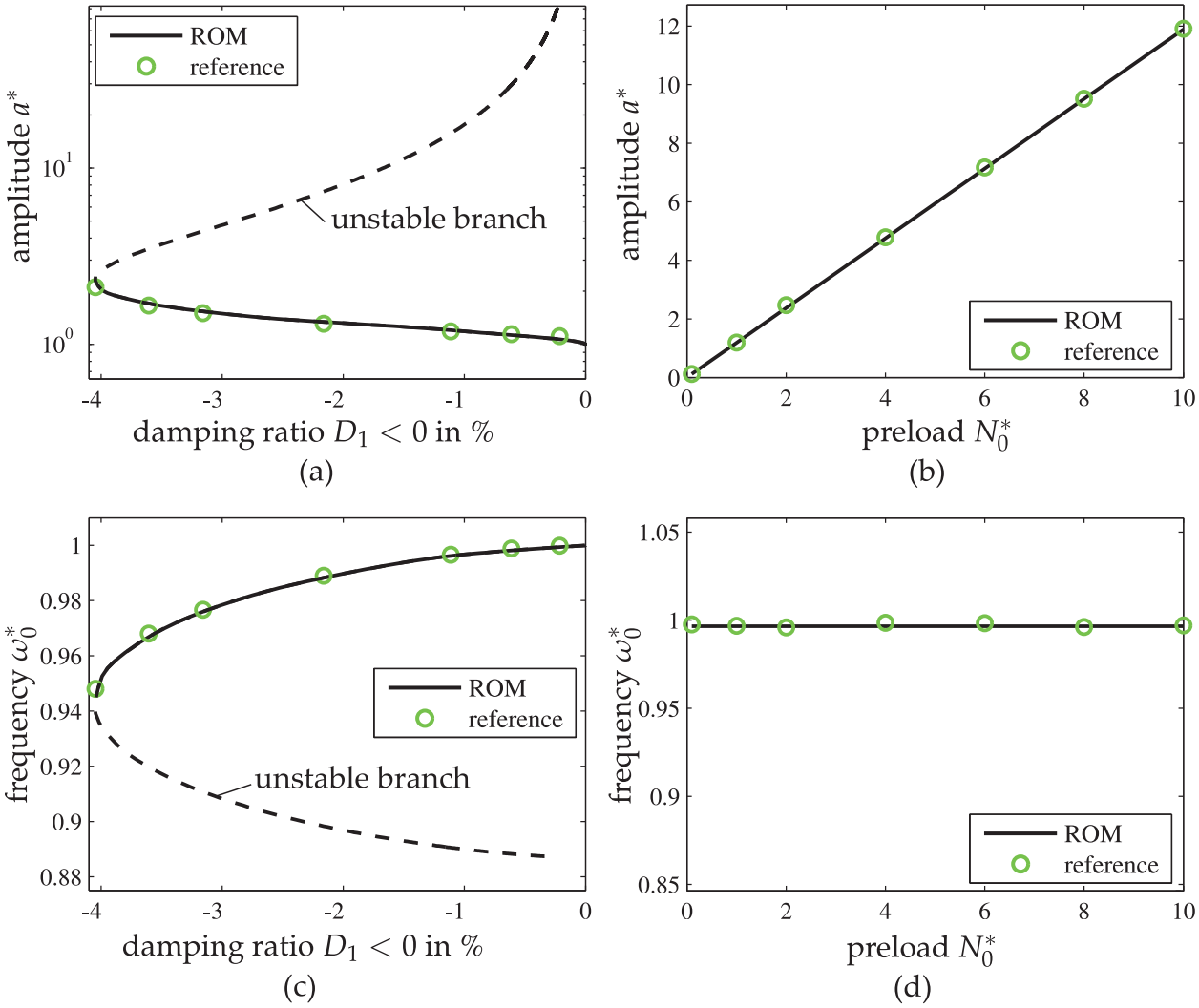

Figure 6.10: Limit cycles of the beam with friction nonlinearity in the presence of negative damping: (a) and (c) amplitude and frequency vs. negative damping ratio D_1 for $N_0^* = 1$, (b) and (d) amplitude and frequency vs. preload for $D_1 = -1\%$

6.2.3 Forced response

In order to investigate the performance of the proposed method with regard to the non-autonomous behavior of the friction-damped beam, a harmonic external forcing was applied to its free end. A positive hysteretic background damping ratio of 0.1% was specified. While this background damping is not mandatory, it limits the resonant forced response in the linear case.

Analysis of limit cycles in the presence of harmonic forcing

First, the steady-state forced response was studied in the frequency range around the first eigenfrequency. To this end, the ROM Eq. (5.10) was considered for frequency-response functions and Eq. (5.11) was solved in order to obtain directly the resonances with respect

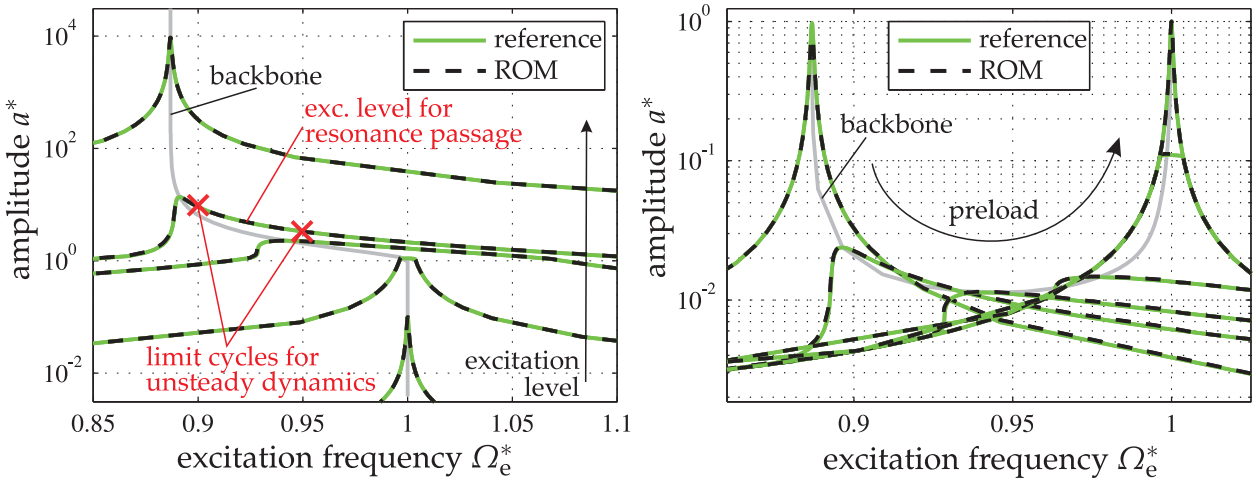

Figure 6.11: Steady-state frequency response of the beam with friction nonlinearity: (a) variation of excitation level, (b) variation of preload

to the varied parameters. The reference results were obtained by time integration directly applied to the equations of motion of the original model. Excitation level and preload were varied in a wide range. The results are illustrated in **Fig. 6.11**. In general, the results are in agreement with those obtained by conventional methods in previous studies, see e. g. [40, 19, 10].

The maximum response amplitude and thus the energy increase with the excitation level. The softening effect deduced from the modal characteristics is reflected in the forced response. The results for varied preload are related to the ones for varied excitation level by the scale invariance. For large N_0^*, the contact is permanently sticking. For vanishing N_0^*, the contact can slip freely. The resonant forced response is minimized for an optimal value of the preload.

The influence of the background damping on the optimization curve, i. e. the relationship between resonance amplitude and preload was further investigated. The background hysteretic damping was varied between 0.01% and 10%. The results are illustrated in **Fig. 6.12**. It might seem counter-intuitive that a^* increases with increasing background damping. The reason for this is the normalization: For each background damping value, the amplitude is normalized by the individual corresponding value in the sticking case, and thus $a^* \equiv 1$ for large preload values independent of the background damping. Hence, **Fig. 6.12** only depicts the relative decrease of the resonance amplitude with respect to the preload.

The effective damping ratio is composed of both the background and the friction damping. Since the friction damping was determined from the configuration without linear damping, it does not depend on the background damping. As the background damping is increased, the relative contribution of friction to the effective damping ratio is reduced. Hence, the relative amplitude reduction between sticking and optimum preload decreases. The ROM predictions agree well with the reference results. Note that this

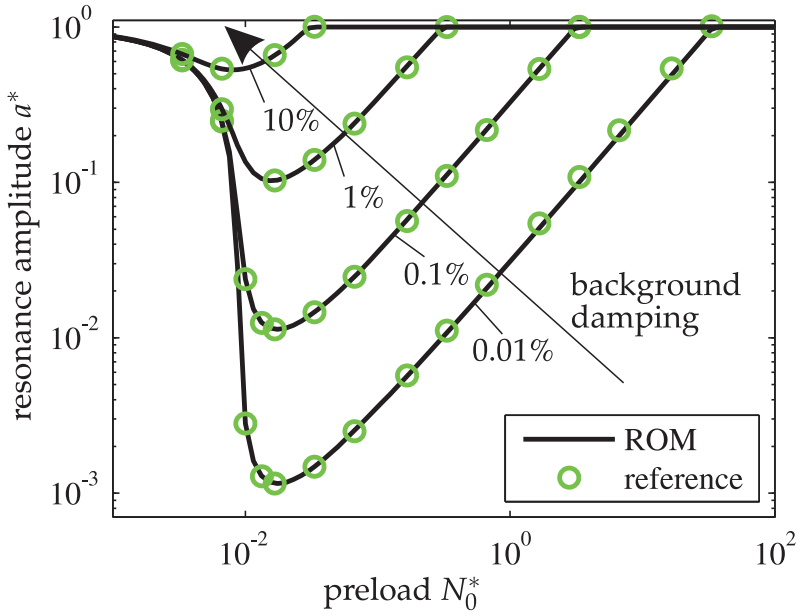

Figure 6.12: Resonance amplitude of the beam with friction nonlinearity vs. preload for varying background damping

agreement still holds for damping values as large as 10%, in spite of the proposed superposition of linear damping in the ROM.

Transition into a limit cycle in the presence of harmonic forcing

In the presence of steady harmonic forcing, the periodic steady-state response is typically of interest. This results in periodic motions addressed in the previous paragraphs, i. e. the motion takes place on a limit cycle in phase space. If the motion does not start from the corresponding point on this limit cycle, a transient motion is initiated. This unsteady response can be predicted by the proposed ROM using Eqs. (5.4)-(5.5) as long as the starting point lies on the invariant manifold. The response has been computed for different starting points and different frequencies of the harmonic forcing. The resulting time histories of the beam's tip displacement are illustrated in **Fig. 6.13**. The excitation frequency and limit cycles correspond to the points indicated in **Fig. 6.11**a. In **Fig. 6.13**a, the motion was initiated from point (I) indicated in **Fig. 6.7** with an amplitude smaller than the amplitude of the steady-state response. In contrast, the motion was initiated from point (H) in **Fig. 6.13**b with an amplitude larger than the amplitude of the steady-state response. Since the excitation frequencies are different for the two cases depicted in **Fig. 6.13**, also different steady-state amplitudes are reached after the unsteady regime. Beating phenomena occur in both cases. Dissipation due to friction and background damping is the reason for the decay of the envelope modulation and the transition into the limit cycle. Despite the comparatively small initial amplitude, it can be seen in **Fig. 6.13**a that the amplitude overshoots the steady-state amplitude by a factor of about two. This phenomenon is par-

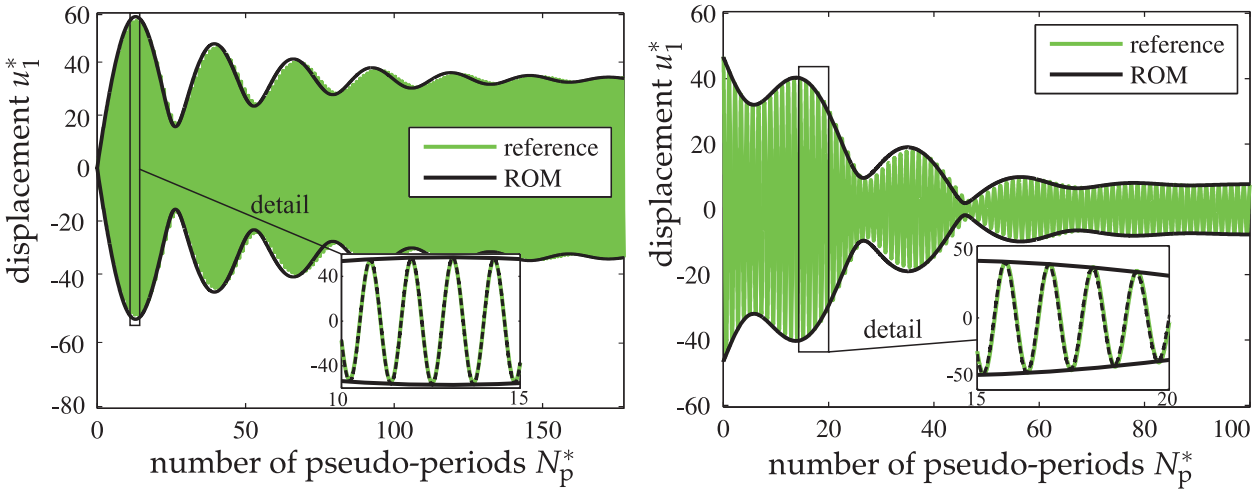

Figure 6.13: Time histories of the beam with friction nonlinearity subject to harmonic forcing: (a) $\Omega_e^* = 0.90$, starting point (I), (b) $\Omega_e^* = 0.95$, starting point (H)

ticularly interesting from a design point of view, and it is qualitatively and quantitatively well predicted by the proposed ROM.

Resonance passage

Finally, the passage through the first resonance of the beam with friction nonlinearity is studied. A linearly increasing excitation frequency with different angular accelerations $\Omega_e^*(N_p^*) = 0.0003N_p^*$ to $0.03N_p^*$ was considered. The excitation level was specified as for the steady-state frequency-response curve indicated in **Fig. 6.11**a. The corresponding time histories of the beam's tip displacement are depicted in **Fig. 6.14**.
Again, a beating phenomenon occurs in the response. The maximum amplitude of the first pulse decreases with increasing angular acceleration. This maximum occurs for a certain instantaneous excitation frequency Ω_e^* which will be termed transient resonance frequency in the following. In the up-sweep through the resonance of a linear system, it would be expected that the transient resonance frequency is slightly larger than the eigenfrequency $\Omega_e^* \gtrsim 1$ [67, 14]. However, it can be seen from **Fig. 6.14**a-d that the transient resonance frequency is $\Omega_e^* < 1$, which at first glance seems to be counter-intuitive. The reason for this behavior is that the eigenfrequency decreases for larger amplitudes, cf. **Fig. 6.7**a. Larger amplitudes are reached for smaller angular accelerations, which makes this effect more prominent. The maximum amplitude and the transient resonance frequency, which are of particular importance for design considerations, are accurately predicted by the ROM. Not only the modulated envelope but also the fast oscillations of the physical coordinate can be predicted. The agreement with the reference results is slightly worse for considerably large angular acceleration. In this case, the oscillation and amplitude modulation take place on very proximate time scales. As a consequence, the averaged character of the ROM leads to inaccurate results.

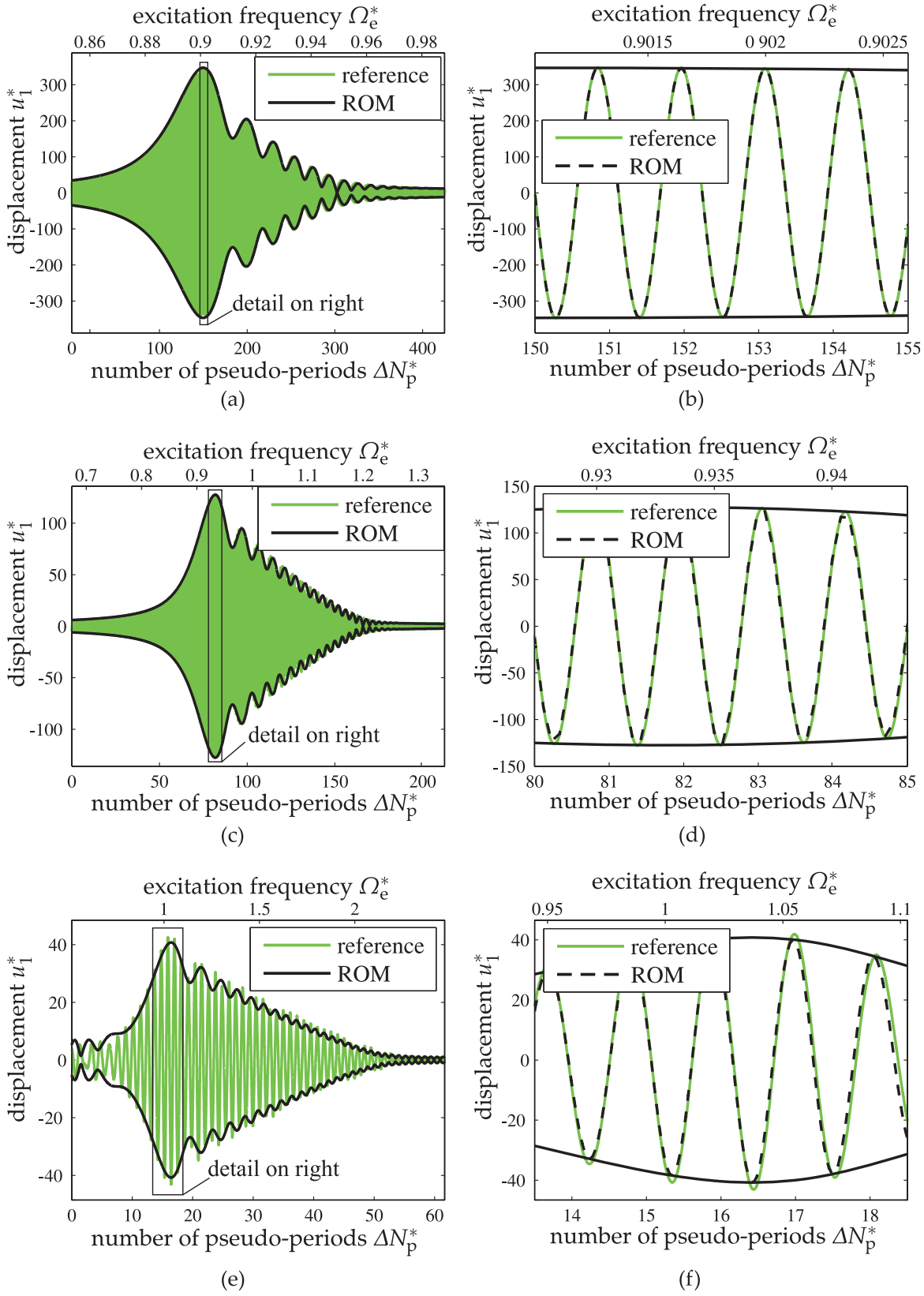

Figure 6.14: Time histories of resonance passages of the beam with friction nonlinearity, starting point (I) defined in **Fig. 6.7**: (a) and (b) $\Omega_e(N_p^*) = 0.0003N_p^*$, (c) and (d) $\Omega_e(N_p^*) = 0.003N_p^*$, (e) and (f) $\Omega_e(N_p^*) = 0.03N_p^*$

6.2.4 Computational benefit of the ROM for unsteady dynamics

The computation times consumed by the ROM and the time integration of the full-order model are listed **Table 6.1**. The problem dimension of the original model is twice the number of retained generalized coordinates (six coordinates, associated with one constraint mode and five fixed interface modes) plus one for modeling the friction hysteresis. Thus, the system dimension equals $2 \cdot 6 + 1 = 13$. The problem dimension of the ROM is only two (amplitude a and phase lag $\Delta\vartheta$ are unknown) in the externally forced case and one (only the amplitude a is unknown) in the autonomous case.
The same time integration scheme and error tolerances were specified for both methods. It can be easily ascertained from **Table 6.1** that the computational effort required to obtain the transient time histories presented in this section can be significantly reduced by the proposed ROM. It should be remarked that the extent of the computational benefit of the proposed method generally depends on many aspects, including the system parameters, the operating conditions and the parameters of the time integration scheme.

Table 6.1: Computational effort for the prediction of the unsteady behavior of the beam with friction nonlinearity; the CPU time is normalized (*) by the CPU time consumed by the ROM for the prediction of the resonance passages in **Fig. 6.14** (bold-faced element in last column)

Problem	ODE *dim.* (reference)	normalized CPU *time** (reference)	ODE *dim.* (ROM)	normalized CPU *time** (ROM)
Fig. 6.9a	13	170	1	< 0.1
Fig. 6.9b	13	37	1	< 0.1
Fig. 6.13	13	150	2	0.2
Fig. 6.14	13	830	2	**1.0**

7 Application to detailed models of friction-damped systems

Rotating bladed disks in stationary gas or steam turbines and aero engines are exposed to considerable thermal and centrifugal loading which cause high static stresses. Possible vibrations may thus lead to damage and fatigue related costs. Two of the primary vibration mechanisms are of aero-elastic type: forced response and flutter [158]. Forced response is primarily caused by the rotation of the bladed disk in the stationary, inhomogeneous pressure field which leads to externally forced vibrations, synchronous to the rotational speed. Flutter, on the other hand, represents an aero-elastic instability and leads to self-excited vibrations with an eigenfrequency of the bladed disk.
The most established means of passive vibration reduction in this field is certainly friction damping [42]. Therefore, friction interfaces are introduced in various forms. An appropriate design of the friction joints may significantly increase the durability of the structure. At the same time, it can increase the tolerable range of operating conditions and the feasible blade design space, and thus contribute to an increased efficiency of turbomachines. The structural dynamical design process of friction-damped bladed disks is typically associated with considerable computational cost. In practice, the affordable cost is bounded, which in turn strictly limits the affordable modeling fidelity and depth of the design optimization. It is therefore particularly important to investigate the potential of the proposed procedure to reduce the computational burden of the analysis and the design of such systems. Two of the most common forms of friction joints are addressed in this chapter. In Section 7.1, tip shrouds are investigated, while underplatform dampers are subject of Section 7.2. In contrast to the rather academic models studied in Chapter 6, these test cases shall demonstrate the applicability of the proposed approach to more realistic structures described in terms of solid finite elements. Moreover, these test cases necessitate the discussion of the specific modeling aspects of cyclically symmetric systems in the context of the proposed modal analysis procedure.

7.1 Modal analysis and model reduction of a bladed disk with shroud joints

In this section, a bladed disk with shroud joints is investigated. This example is particularly suited to assess the performance of the proposed procedures in the presence of

strongly nonlinear, three-dimensional contact forces. The stick, slip, and lift-off contact situations are resolved in a spatially local manner, so that the vibration-induced variation of the contact area can be taken into account. A focus of this section is also on specific aspects of the ROM, which become important only for more detailed models and thus could not be properly addressed in Chapter 6. Special attention is paid to characteristics which are especially useful for the structural dynamical design process. Parts of the presented results have already been published in Krack et al. [90].

7.1.1 Description of the model

Consider the blade integrated disk illustrated in **Fig. 7.1**. It comprises 30 blades and is built as an integral part, which means that blades and disk belong to the same structure. The hub of the disk was fixed in such a manner that a potential excitation by the rotor was not taken into account. Small deflections around the static equilibrium were considered, and in general the nonlinearity was assumed to stem only from the contact interactions.
The so-called mistuning refers to the blade-to-blade variation of structural mechanical properties and can generally lead to the localization of vibration energy. Due to the strong coupling of adjacent blades by the shroud joints, however, this effect is commonly neglected, as it was also done in the present study. Thus, the geometry and the operating conditions were considered as perfectly cyclically symmetric. Previous authors have shown that even in this case, the effect of nonlinear forces may cause localization phenomena [171]. It is generally difficult to estimate a priori if and under what conditions this effect occurs [54]. Appropriate strategies for finding all stable localized and non-localized vibration modes are still under research [59]. In the present study, this effect was excluded by assuming that the cyclic symmetry of the response is retained. It is therefore valid to consider only a single segment of the full system with appropriate boundary conditions, which can greatly simplify the dynamic analysis.
The segment was discretized with three-dimensional, tetrahedral elements having four nodes per element. The FE model comprises 25,641 nodal DOFs. Gyroscopic effects were neglected, so that the resulting structural matrices of the segment were hermitian upon application of the cyclic symmetry boundary conditions. A Craig-Bampton reduced order model of the segment was constructed. Only the DOFs involved in the contact formulation were retained as boundary coordinates. In accordance with a preliminary convergence study, the first 50 fixed interface normal modes were considered in the reduced basis.
During operation, the rotating bladed disk is subjected to centrifugal forces which cause the blade to untwist. A pressure builds up in the shroud contact interface between adjacent blades. The normal pressure distribution is generally inhomogeneous. It can exhibit high local pressures which prevent relative motions in certain portions of the contact interface, while other portions may undergo slip and lift-off phases. The accurate prediction of the centrifugal effects on the deflection shape and the initial pressure distribution represents a challenging task in itself. In this study, the illustrated geometry

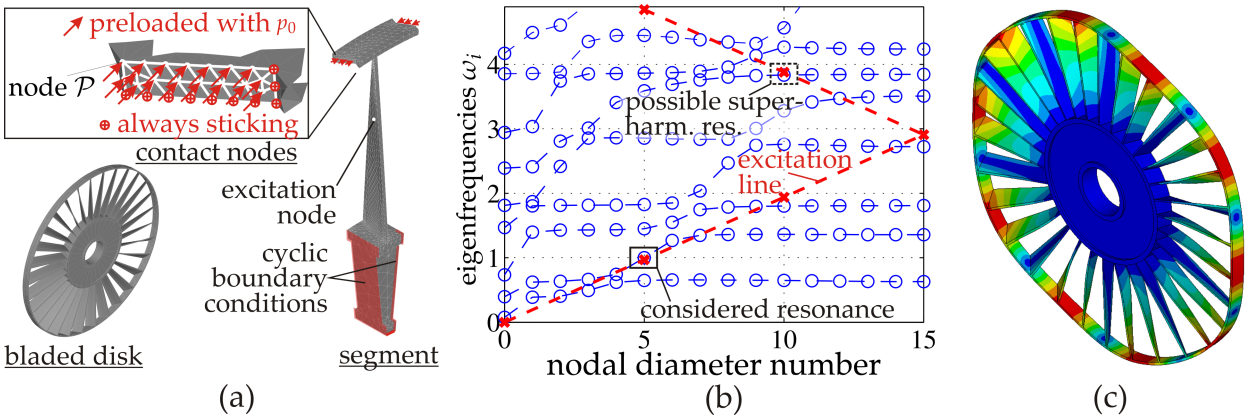

Figure 7.1: Bladed disk with shroud contact: (a) model definition, (b) nodal diameter map for sticking contact, (c) deflection shape of the considered mode for sticking contact

was considered as the static deflection shape at a particular rotational speed. The effect of centrifugal stiffening was not accounted for. An *idealized pressure distribution* was specified as follows: Contact was defined to occur only in the central part of the Z-shaped shroud interface. A very high local pressure was specified at a portion of the contact nodes, so that they were permanently sticking as indicated in **Fig. 7.1**a. A uniform initial pressure p_0 was specified at the remaining nodes. This type of pressure distribution limits the relative displacements in the contact interface to partial slip and partial lift-off. On the other hand, gross slip and high-energy snubbing phenomena, which are typically not desired in the regime of interest [111, 1] and could be encountered for another type of initial pressure distribution, are excluded.

The contact interactions at the shroud interface were modeled by three-dimensional contact constraints: Coulomb dry friction was considered in the tangential plane, and impenetrability was taken into account in the normal direction. Hence, stick, slip, and lift-off conditions are possible, and the effect of the contact normal dynamics on the stick-slip behavior is captured by this modeling approach. Elastic formulations of the contact laws were considered with a homogeneous and isotropic contact stiffness distribution. The contact interactions were modeled locally at each vertex node of the conforming triangular surface elements. Thus, the vibration-induced variation of the contact area of the extended shroud interface was taken into account.

Tuned bladed disks typically exhibit traveling-wave type vibrations in the case of forced response and flutter [79, 152]. These vibrations are characterized by their spatial order of symmetry around the circumference. This order is typically quantified by either the number of circumferential waves or, equivalently, by the number of (traveling) diametral lines of material points having zero deflection. This latter number is termed nodal diameter number. The lowest eigenfrequencies in the linear case with sticking of all shroud contact nodes are illustrated in **Fig. 7.1**b with respect to the nodal diameter number. The second mode with five (backward) traveling nodal diameters was considered in the subsequent investigations. Its modal deflection shape is illustrated in **Fig. 7.1**c. It should be noted that typically the first couple of mode families are of particular interest for the structural dynamical design of bladed disks [158]. The nodal diameter number has an

influence on the phase lag between adjacent blades and thus determines the extent of relative displacement in the shroud contact interfaces. Hence, the quantitative vibration behavior and in particular the friction damping potential depend on this number.

Normalization:
In the figures presented throughout this section, physical quantities have been normalized, which is indicated by a superscript '': Frequencies have been normalized by the eigenfrequency of the considered second mode with five nodal diameters in the linear case, i. e. where the entire set of contact nodes is permanently sticking. Generalized coordinates and the kinetic energy have been normalized by their value just before leaving the linear regime, i. e. when the first contact node is not permanently sticking anymore.*

7.1.2 Modal characteristics

The modal characteristics were computed using the proposed modal analysis technique, and the results are depicted in **Fig. 7.2**. The qualitative energy dependence is similar to the one of the clamped beam with friction nonlinearity, cf. **Fig. 6.7**. Apparently, a moderate harmonic order H has to be retained in the analysis to accurately resolve the strongly nonlinear contact interactions and to achieve asymptotic convergence of the modal characteristics. In this case, more harmonics are required for the convergence of the modal damping than for the eigenfrequency. It is noteworthy that the behavior is not predicted well with $H = 1$ or $H = 3$, even for large energies. A harmonic order $H = 7$ was deemed sufficient and was therefore used in the subsequent investigations, if not otherwise specified.
In the bottom plots of **Fig. 7.2**, the contact status is illustrated for different energy levels. The 'slip' state also includes possible sticking phases, and likewise the 'lift-off' state includes possible sticking and slipping phases during vibration. Beyond the linear regime with sticking contact, a small portion of the contact area undergoes stick-slip and partial lift-off. This portion increases with energy as it can be ascertained from **Fig. 7.2**c-f.
Compared to the results in **Fig. 6.7**b, the modal damping evolves less smoothly with respect to the kinetic energy. It is assumed that this behavior is caused by the abrupt changes of the contact situation of individual contact nodes at different energies. This behavior can be explained as follows: Suppose a set of contact nodes is permanently sticking, while the remaining nodes undergo slip and lift-off. Suppose further that no change of the contact status occurs, i. e. these sets are invariant within a considered energy range. This particular situation corresponds to a specific evolution of the modal properties with respect to energy. Now, if one permanently sticking node is moved to the set of sliding/lifting-off nodes, this changed situation will clearly result in a different evolution of the modal properties. A change of the contact status from permanently sticking to sliding/lifting-off will cause a jump between these two non-coincident modal characteristics. This hypothesis can be supported by the contact situation for different energy levels illustrated in **Fig. 7.2**.

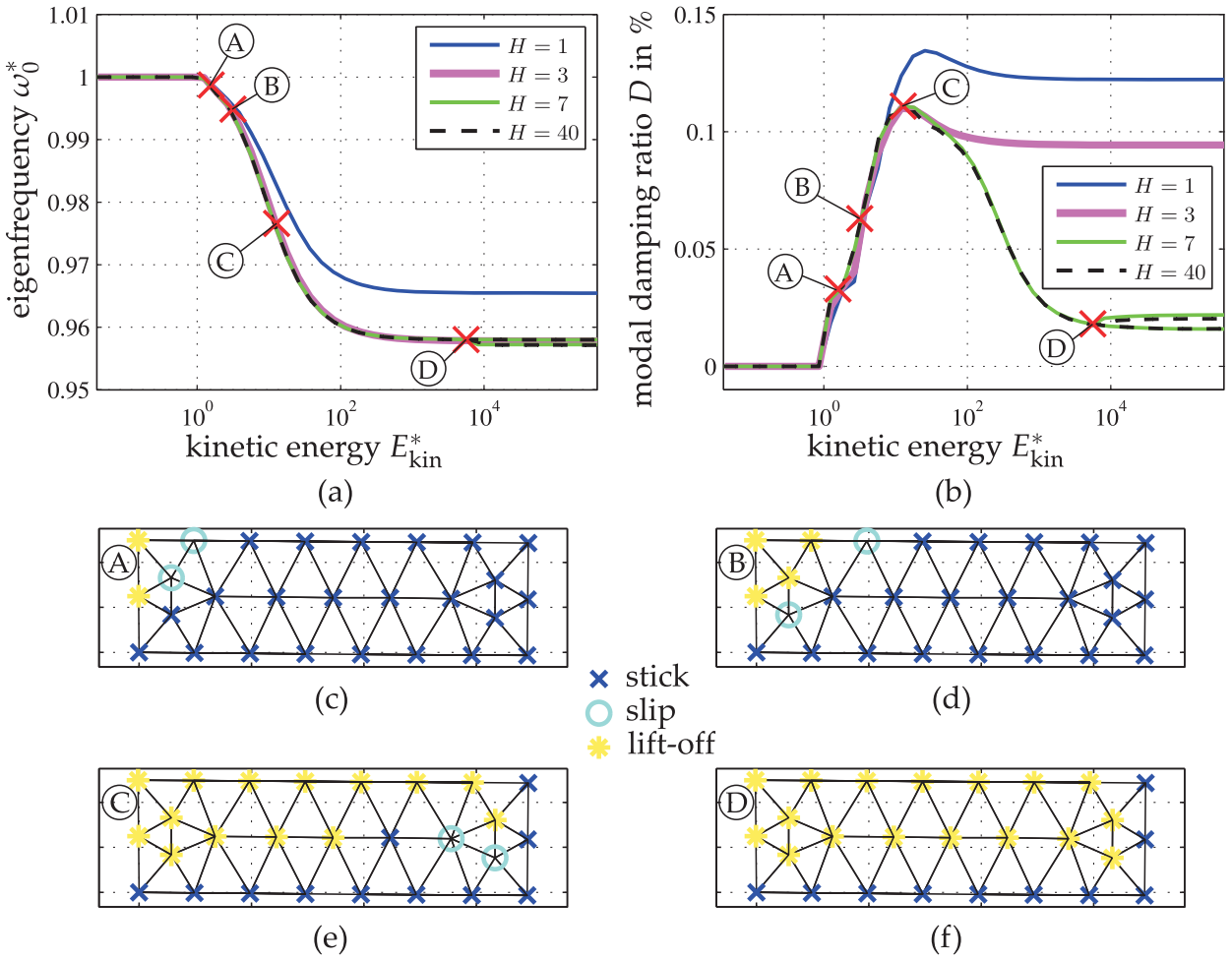

Figure 7.2: Modal characteristics of the considered mode of the bladed disk with shroud contact; stiffness per area $3.7 \cdot 10^4$ N/mm^3, $\mu = 0.3$, $p_0 = 1$ N/mm^2: (a) eigenfrequency, (b) modal damping ratio, (c)-(f) contact status of shroud for different energy levels

Indeed, the contact status of a specific number of contact nodes is different on either side of a jump in the modal characteristic. It is therefore conjectured that the modal properties would evolve smoother with respect to energy, if the mesh density in the shroud joint was considerably increased.

Quantitatively, it can be stated that the damping ratio of the mode considered here is smaller than the one of the first bending mode of the friction-damped beam. Of course, the modal characteristics depend on many aspects such as the mode family, the nodal diameter number, the geometry of the blade and the shroud interface and the material properties. The proposed modal analysis method is regarded as an apt alternative to the common approach to estimate the damping performance indirectly on the basis of forced response data [153]. Detailed design investigations are, however, considered to be beyond the scope of the present study. The interested reader is referred to [185] for a thorough design analysis of shroud joints with regard to friction damping.

It can be deduced from the modal characteristics that the solution is not unique over the entire energy range. Beyond a certain energy level, e. g. $E_{kin}^* > 10^4$, two coexisting solutions were found, as depicted in **Fig. 7.2**a and b. The two distinct solution branches

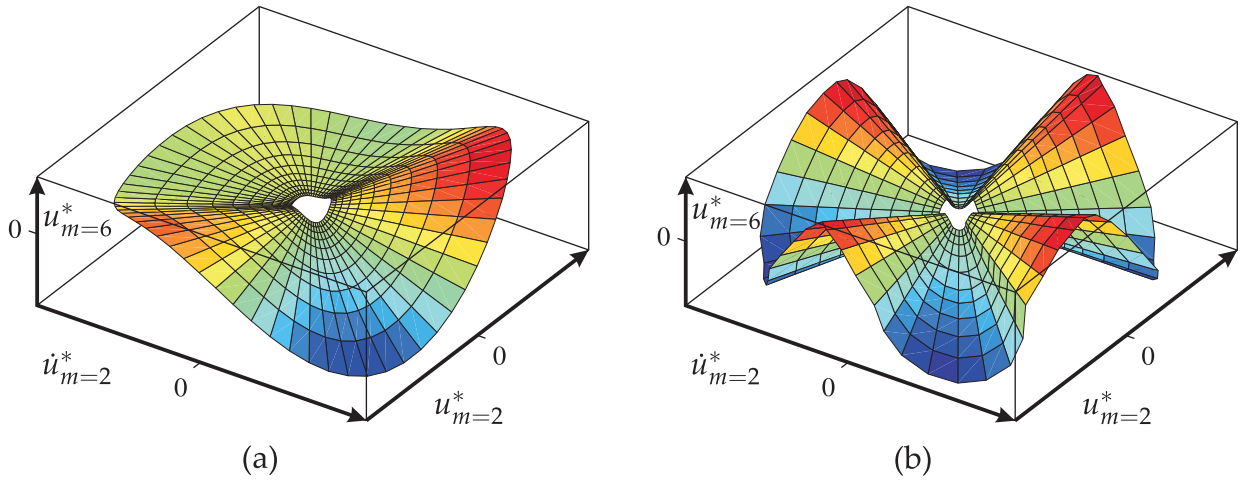

Figure 7.3: Two-dimensional invariant manifolds of the considered mode of the bladed disk with shroud contact, $u^*_{m=2}$ and $u^*_{m=6}$ are the coordinates of the second and sixth linear mode, respectively: (a) $H = 3$, (b) $H = 40$ harmonics retained in modal analysis

were obtained by performing the path continuation with slightly different continuation parameters. This bifurcation indicates the presence of an internal resonance and will be investigated below.

The nodal diameter map depicted in **Fig. 7.1**b is useful to identify possible internal resonances. For instance, it can be deduced from the map that the fourth multiple of the considered eigenfrequency is close (but not equal) to the linear eigenfrequency of the sixth mode with ten nodal diameters. The associated two modes are therefore candidates for a 4 : 1 super-harmonic internal resonance in the nonlinear regime. This conjecture can be confirmed by a look at the invariant manifolds illustrated in **Fig. 7.3**: If only $H = 3$ harmonics are considered, the geometry of the invariant manifold is dominated by its fundamental harmonic component. If more (e. g. $H = 40$) harmonics are considered, in contrast, the fourth harmonic dominates the modulation of the coordinate $u^*_{m=6}$ associated to the sixth linear mode family.

7.1.3 Steady-state forced response

In state-of-the-art forced response analyses of bladed disks, the steady pressure field acting on the rotating blade surface is determined using a computational fluid dynamics software. In a second step, this pressure field is integrated over the blade surface in order to obtain the nodal forces consistent with the structural dynamical FE model. In this case study, a discrete representative excitation force was considered instead. For this purpose, a force in the circumferential direction was applied to the node at the location indicated in **Fig. 7.1**a. The force was defined as mono-harmonic with a constant phase lag between adjacent blades (traveling-wave type forcing), so that the considered mode with five nodal diameters was excited. The forced response was computed in the frequency range near the considered mode. The excitation frequency is typically directly proportional to the rotational speed, which determines the centrifugal forces. These forces influence the struc-

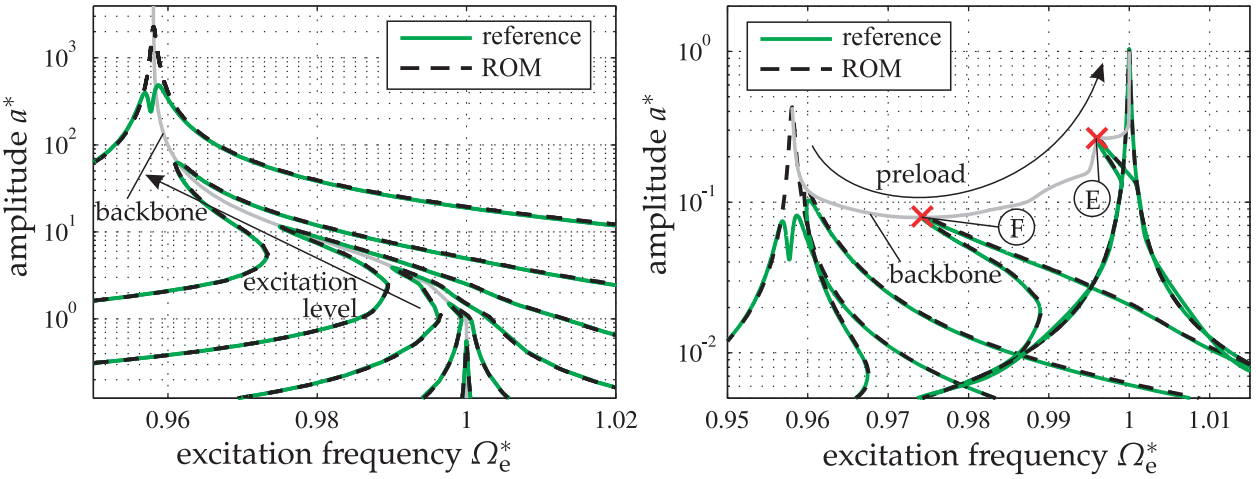

Figure 7.4: Frequency response of the bladed disk with shroud contact: (a) variation of excitation level, (b) variation of preload

tural dynamic properties of the assembly. For instance, the preload generally depends on the centrifugal loading. Moreover, the variation of the rotational speed of a designed turbomachine is accompanied by a variation of the blade loading. Hence, a variation of the excitation frequency is generally associated with a variation of other operating conditions as well. These effects were neglected in the present study, i. e. the excitation frequency was varied independently of all other system parameters. An actual fluid-structure interaction was not taken into account in the forced response analysis. Instead, only a hysteretic background damping of 0.1% was considered to mimic the joint effect of material and fluid damping. The results were determined for different excitation levels and are depicted in **Fig. 7.4**a. To this end, Eq. (5.10) was solved for the computation of frequency-response curves, and Eq. (5.11) was solved for the direct computation of the resonances, i. e. the backbone curve.

The excitation level governs the kinetic energy of the system. Therefore, the forced response results are in accordance with the modal characteristics. The results are also in qualitative agreement with the corresponding results of the systems with either purely unilateral contact or friction studied in Chapter 6, cf. **Fig. 6.5**a- and **Fig. 6.10**a.

The results obtained by the ROM were compared with a high-fidelity numerical reference. Throughout this chapter, the reference results were computed by solving the equations of motion of the segment model in generalized coordinates by means of the high-order harmonic balance method. This method is regarded as a suitable reference, as this method is widely used in the design of friction-damped bladed disks where numerical time integration often leads to prohibitive computational effort [128, 15, 155]. The results are in excellent agreement up to certain amplitudes. For large amplitudes, an additional maximum occurs in the frequency-response functions. This indicates the presence of an internal resonance, which confirms the results of the modal analysis. As a consequence, the reduction to an isolated nonlinear mode is no longer valid, and the proposed ROM provides a poor approximation of the actual dynamical behavior.

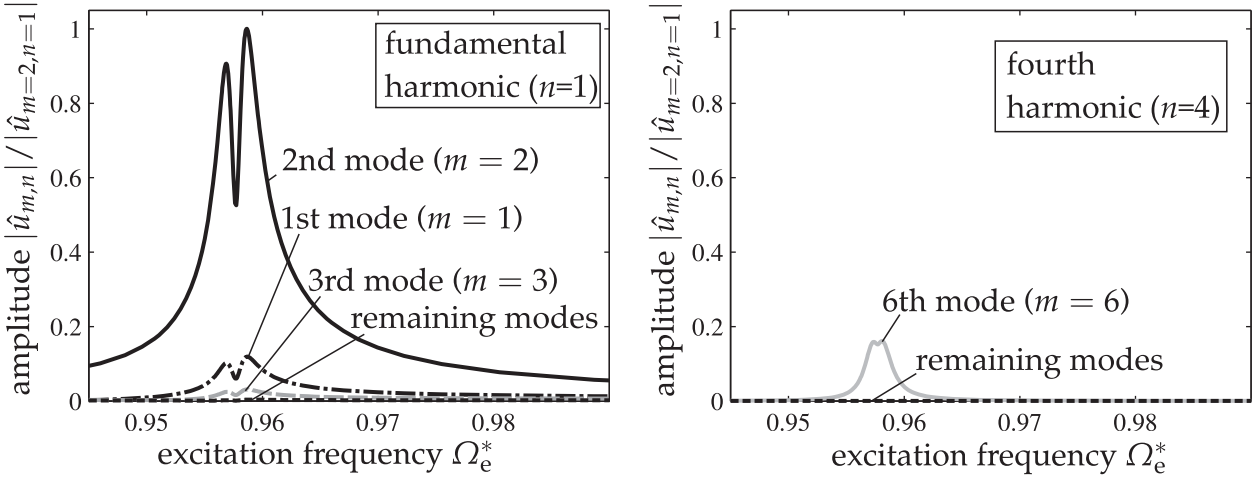

Figure 7.5: Steady-state frequency response of the temporal harmonic amplitudes, index n of the linear modes, index m: (a) fundamental harmonic, (b) fourth harmonic

The forced response was also calculated for varying preload in the shroud joint. For the ROM computation, the modal characteristics were thus required for different preload values. These characteristics have been obtained from the ones for only a specific preload and taking advantage of the scale invariance, as proposed in Chapter 5. The results are depicted in **Fig. 7.4**b. These forced response results are also directly linked to the ones depicted in **Fig. 7.4**a via the scale invariance. For moderate preload, the resonance amplitude is significantly reduced by means of friction damping. For a certain (optimal) preload, the resonance amplitude is minimized. The resonance amplitude then increases again. Below a certain value of the preload, the frequency-response curves exhibit a second maximum as well. This again indicates the presence of an internal resonance, and consequently the ROM fails.

In order to further investigate the multiple maximum phenomenon, the frequency response to the largest excitation level depicted in **Fig. 7.4**a was analyzed with respect to its temporal and spatial spectrum. The fundamental ($n = 1$) and the fourth ($n = 4$) harmonic amplitudes of the linear modes are depicted in **Fig. 7.5**a and b, respectively. The amplitudes have been normalized by the maximum fundamental harmonic amplitude $\hat{u}_{m=2,n=1}$ of the second linear mode. Note that this is the only nonzero amplitude at resonance in the linear case. This mode still dominates the response in the depicted nonlinear case. In contrast to the linear case, however, the sixth linear mode participates to a significant extent in the fourth harmonic of the response. This confirms the internal resonance identified from the modal analysis. It can moreover be seen from **Fig. 7.5**a that the nonlinearity enriches the modal content of the fundamental harmonic of the response: In addition to the expected second linear mode, also the first and the third linear mode have a significant contribution. In other words, the nonlinearity distributes the vibration energy among other modes.

The accuracy of the proposed ROM depends on different aspects. The influence of some of these aspects was investigated for the frequency-response curve marked with an (F)

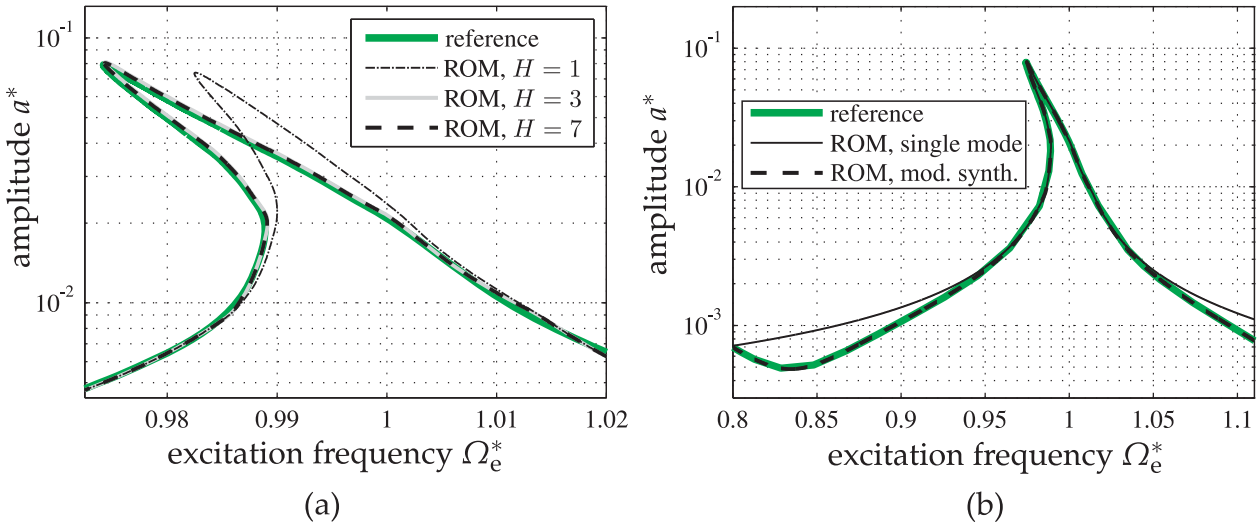

Figure 7.6: Two aspects that influence the accuracy of the ROM: (a) influence of the number of harmonics H retained in the modal analysis, (b) influence of the off-resonant modes

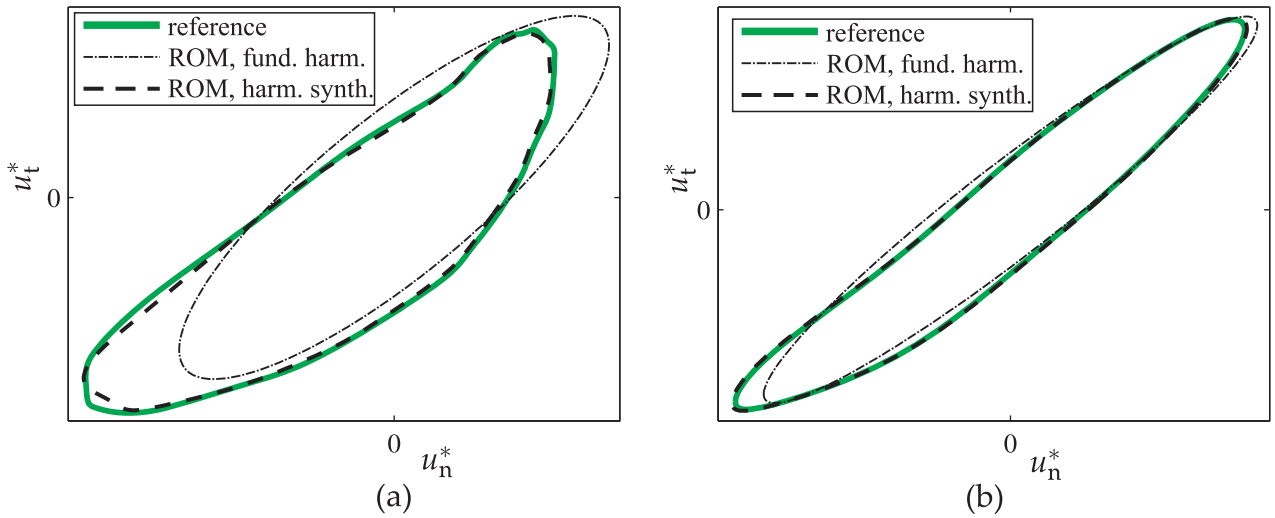

Figure 7.7: Relative motion of contact node $\mathcal{P}$ as defined in **Fig. 7.1**a projected onto the plane of predominant dynamics: (a) point (E), (b) point (F) indicated in **Fig. 7.4**b

in **Fig. 7.4**b. The harmonic order H considered in the modal analysis obviously has an influence on the prediction quality. The ROM predictions for different harmonic orders are compared to the reference results in **Fig. 7.6**a. A number of $H = 3$ or $H = 7$ should be retained in the modal analysis, in order to achieve convergence of the ROM predictions and ensure sufficient agreement with the reference results in this case. This finding is generally in accordance with the harmonic convergence behavior of the modal characteristics illustrated in **Fig. 7.2**.

Furthermore, the consideration of the off-resonant modes affects the accuracy of the ROM predictions. In the proposed procedure, a simple modal synthesis is performed in which the off-resonant modes are superimposed in their linear form. The frequency-response curves have been computed with the ROM (a) only considering the isolated nonlinear mode by solving Eq. (5.10) and (b) additionally applying the synthesis procedure using

Eq. (5.8). The results are illustrated in **Fig. 7.6**b and compared with the reference. Obviously the consideration of the off-resonant modes does not significantly influence the accuracy of the ROM very close to resonance. However, the synthesis procedure successfully enriches the residual dynamic compliance and thus considerably increases the prediction quality farther away from resonance. Note that this linear synthesis is a non-iterative post-processing step and, hence, does not significantly increase the computational cost.
The strongly nonlinear contact forces can induce a considerable multi-harmonic vibration content. This is particularly true for the coordinates which describe the relative motion at the contact interface. The contact interactions have an essential influence on the resulting effective stiffness and damping introduced by the interface. That is why it is important to accurately predict the local dynamics of the contact nodes. In **Fig. 7.7**, the relative motion of the contact interface is illustrated for the upper left node $\mathcal{P}$ indicated in **Fig. 7.1**a. The results are depicted for two different resonance situations marked in **Fig. 7.4**b. The relative motion in the radial direction was negligible for the considered cases. For the sake of clarity, the three-dimensional trajectories were thus projected onto the axial-circumferential plane and are illustrated in the local contact coordinate system. Apparently, the multi-harmonic ROM achieves good agreement with the reference. It can be ascertained from the results that the proposed multi-harmonic synthesis significantly increases the accuracy compared to only considering the fundamental harmonic of the nonlinear mode.

7.1.4 Computational benefit of the ROM for steady-state predictions

For the presented case study, the modal analysis was carried out with (efficient) and without (conventional) the proposed numerical improvements. The required computation times are listed in **Table 7.1**. The joint benefit achieved by using the improvements (condensation, efficient factorization and analytical gradients) leads to a reduction of the computation time by a factor of 300. This benefit is within the bounds estimated on the basis of the investigations in Section 4.2.4.
The computational effort for the forced response analysis of the bladed disk with shroud contact is also listed in **Table 7.1**. The computation time for the efficient modal analysis of an isolated nonlinear mode represents the overhead of the proposed procedure. For the presented case study, this expense is in the same order of magnitude of a single frequency-response or backbone curve computation using the reference method (high-order harmonic balance). This is plausible, since the mathematical problem dimension is almost the same for each solution point, and a similar number of solution points is required for both analysis types. While the reference method computes the branches of the frequency-response curve left and right from resonance, the modal analysis effectively determines the resonant amplitude-frequency relationship, i. e. the backbone curve.
By taking advantage of the proposed superposition strategy and applying the scale invariance, the expensive overhead does not have to be paid again when the associated

Table 7.1: Computational effort for conventional and proposed procedure

Problem	normalized CPU time	N_{dim}
conventional modal analysis	620	1517
efficient modal analysis	2.0	767
frequency-response function (ROM)	< 0.0002	1
backbone (ROM)	< 0.0002	1
frequency-response function (reference)	1.0	765
backbone (reference)	0.9	766

parameters are varied. Thus, the modal analysis had to be carried out only once in order to obtain all ROM predictions presented throughout this section. The computational cost for the individual ROM predictions is almost negligible compared to the reference computations or the modal analysis itself. In this case, the overhead for the modal analysis already pays off after two frequency-response function evaluations.
It should be noted that the absolute computational effort strongly depends on the dimension N_{dim} of the set of algebraic equations. It is composed of the harmonic order H and the number N_{nl} or N_{dof} of the condensed or full generalized coordinates vector, respectively. The condensation was applied in the case of the efficient modal analysis and the reference method. For the considered three-dimensional contact model, $N_{\mathrm{nl}} = 3 \cdot 17 = 51$ equals the number of relative interface coordinates for the 17 contact nodes, cf. **Fig. 7.1**a. For the conventional modal analysis, no condensation was applied. Thus, the equations still contain the additional 50 generalized coordinates associated with the fixed interface modes. This results in $N_{\mathrm{dof}} = N_{\mathrm{nl}} + 50 = 101$. For the frequency-response function computation, this results in a total algebraic dimension of $N_{\mathrm{dim}} = (2 \cdot H + 1)\, N_{\mathrm{nl}} = 765$, with a number of $H = 7$ harmonics. Using the reference method for the computation of the backbone curve, the oscillation frequency represents an additional unknown, so that N_{dim} is increased by one. For the modal analysis, eigenfrequency and modal damping ratio represent the two additional unknowns, leading to a total dimension of $N_{\mathrm{dim}} = (2 \cdot H + 1)\, N_{\mathrm{nl}} + 2 = 767$ and $N_{\mathrm{dim}} = (2 \cdot H + 1)\, N_{\mathrm{dof}} + 2 = 1517$ for the efficient and the conventional variant, respectively. In contrast, the ROM predictions only have $N_{\mathrm{dim}} = 1$, since the modal amplitude is the only unknown in this case.

7.2 Robust design of a bladed disk with underplatform dampers

It appears to be common practice in the field of friction damping to tune the design for only a single set of nominal parameters, i. e. to perform a so-called Single-Point Optimization, regardless of the parameter uncertainties [185, 112, 95]. If the variability of uncertain parameters is not properly taken into account in the design process, even high-fidelity models cannot yield optimum designs with respect to robustness [102, 179]. Should the actual parameters deviate from the assumed nominal ones, the performance of the *localized optimal design* may be considerably lower than for nominal parameters. In this section, a strategy is presented to find a reliable design by explicitly taking into account parameter uncertainties. Such a strategy necessitates the vibration prediction for a considerable number of parameter sets. If conventional methods were employed, this would commonly result in prohibitive computational cost. Hence, this test case is particularly well-suited to demonstrate the ability of the proposed model reduction approach to significantly decrease the prediction effort and thus to facilitate robust design optimization. Parts of the presented results have already been published in Krack et al. [92].

7.2.1 Description of the model

The model of the bladed disk with underplatform dampers is illustrated in **Fig. 7.8**a. This section should be regarded as a proof-of-concept study. The simplifications applied in the previous section were adopted analogously: Fixed hub, nonlinearity stems solely from contact between damper and platform, cyclically symmetric response, no gyroscopic effects, no centrifugal stiffening, simplified modeling of forcing and fluid-structure interaction. The first mode with two (backward) traveling nodal diameters was considered in the subsequent investigations, and its deflection shape is illustrated in **Fig. 7.8**b. The forcing was applied in the circumferential direction at the node indicated in **Fig. 7.8**a. A background, hysteretic damping with $\boldsymbol{C}_{\mathrm{mod}} = \mathrm{i}\eta\boldsymbol{K}$ was specified. The FE model comprises $2,250$ nodal DOFs. A Craig-Bampton reduced order model of the segment was constructed. Only the DOFs involved in the contact formulation were retained as boundary coordinates. In accordance with a preliminary convergence study, the first 50 fixed interface normal modes were considered in the reduced basis.
The underplatform wedge dampers were assumed to be rigid, which is a common simplification. The damper mass has a significant influence on the normal preload in the contact interfaces, which in turn has an important effect on the damping performance. This influence on the normal preload was taken into account in the present case study. In practice, the variation of the damper mass is achieved by variation of damper geometry or material properties. In general, these modifications have an influence on inertial and elastic forces within the assembly, and may affect its dynamic behavior. These influences were found to play a minor role for the relevant mass ranges in the considered parameter studies. This

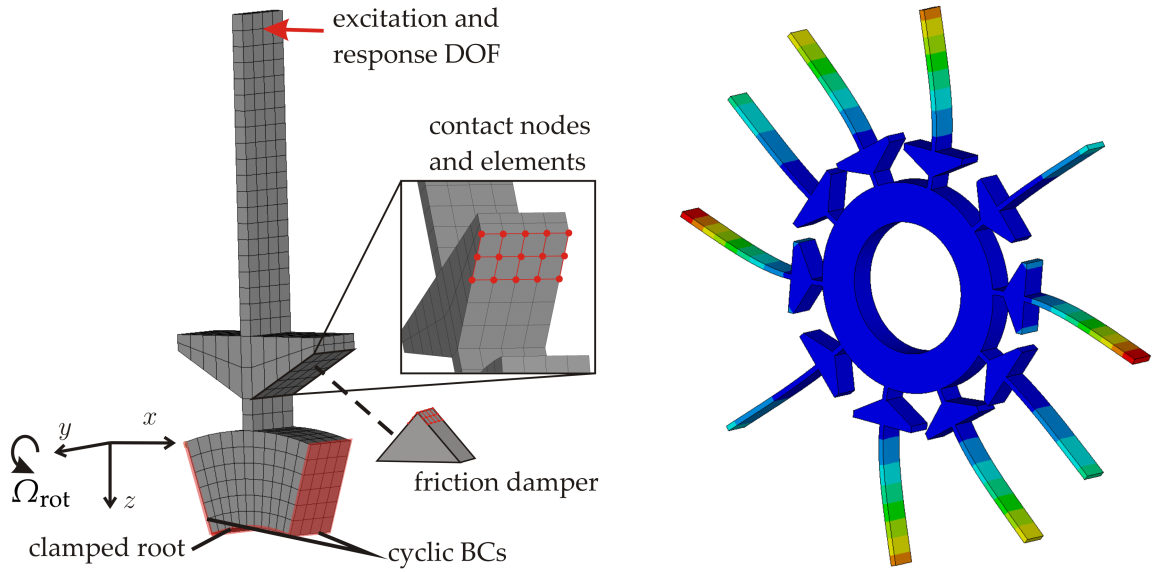

(a) (b)

Figure 7.8: Bladed disk with underplatform dampers: (a) model definition, (b) deflection shape of the considered mode for sticking contact

has also been found by other researchers [143, 69]. Hence, only the nominal damper mass, as defined later, was considered for the derivation of the structural dynamical properties. During variation of the mass in the following parameter study, only its influence on the normal preload was therefore taken into account. The normal preload of the contact interfaces was determined from the static equilibrium with the centrifugal force $mr_{\text{cg}}\Omega_{\text{rot}}^2$, where m is the damper mass, Ω_{rot} is the rotational speed and r_{cg} is the distance from the rotation axis to the center of gravity of the dampers. The preload was distributed among the contact nodes indicated in **Fig. 7.8**a assuming a homogeneous initial normal pressure field. The contact model was adopted from the shroud joints, as described in the previous section.

7.2.2 Modal characteristics

The modal properties were computed using the proposed modal analysis method. The results are depicted with respect to the friction coefficient and the kinetic energy in **Fig. 7.9**. The eigenfrequency ω_0^* was normalized by its corresponding value in the linear case without dampers. The qualitative energy dependence is similar to the one of the clamped beam with friction nonlinearity, cf. **Fig. 6.7**. In the case of constant normal load, this characteristic would only be shifted along the kinetic energy axis for varying friction coefficient. In this case, however, the dynamics in the contact normal direction influence the stick-slip transitions. For larger friction coefficients, also larger relative motion amplitudes of the adjacent blades are required to achieve the same amount of slipping. For larger amplitudes, however, also longer lift-off phases occur during one vibration cycle

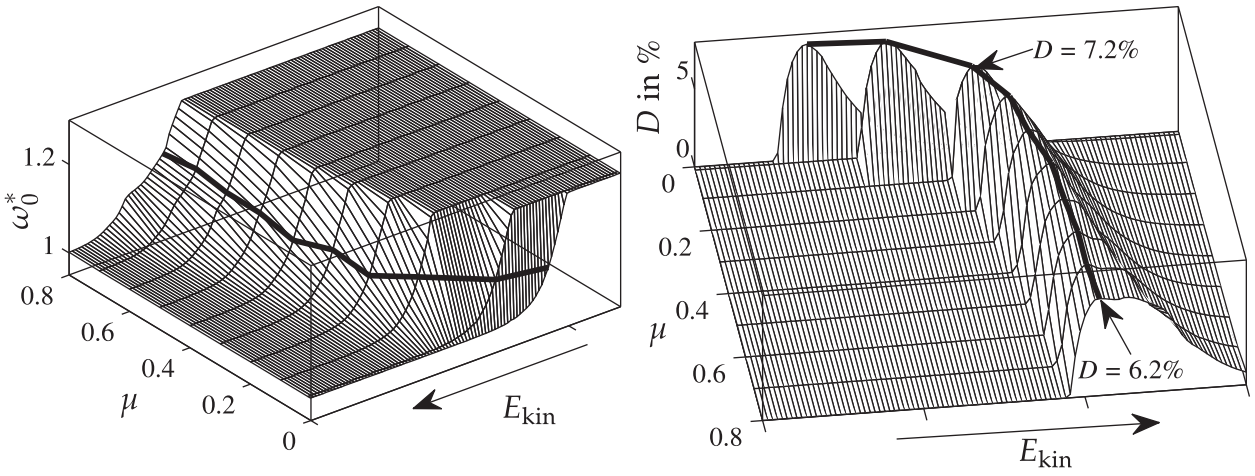

(a) (b)

Figure 7.9: Modal properties as a function of kinetic energy E_{kin} and friction coefficient μ: (a) eigenfrequency, (b) modal damping ratio

in case of variable normal load. Thus, the maximum damping capacity is decreased for larger friction coefficients.

7.2.3 Sensitivity analysis of the resonant forced response

In order to estimate the influence of different parameters on the dynamic behavior of friction-damped bladed disks, it is common practice to carry out sensitivity analyses of the forced response. In this study, the influence of the damper mass m, the friction coefficient μ, the excitation level ε and the background damping factor η was investigated. These parameters were individually varied in a wide range, i. e. the remaining parameters were left constant during this variation. For this purpose, a nominal set of parameter values $\boldsymbol{X}_0 = [m_0\, \varepsilon_0\, \eta_0\, \mu_0]^{\mathrm{T}}$ was specified with $\boldsymbol{X}_0 = \left[m_{\text{opt,c}} \quad 1 \quad 0.15\% \quad 0.3\right]^{\mathrm{T}}$. $m_{\text{opt,c}}$ refers to the mass which minimizes the resonant forced response amplitude a_{resp} of the response DOF indicated in **Fig. 7.8**a for otherwise nominal parameters. The resonant forced response was computed with the proposed ROM procedure by solving Eq. (5.11). The results are depicted in **Fig. 7.10**. a_{resp}^* was normalized by its value for sticking dampers and nominal parameters.

The damper performance curve and the optimization curve, i. e. the dependence of the resonant vibration level on the excitation level and the damper mass, respectively, have a typical form, see **Fig. 2.6**a-b and its explanation for details. The influence of the background damping factor is small near its nominal value of $\eta_0 = 0.15\%$, since it is virtually negligible compared to the friction-induced damping of several percents, see **Fig. 7.9**b. The effect of the friction coefficient is qualitatively similar to the influence of the damper mass, which both determine the limiting friction force.

As long as all parameters are precisely known, the design optimization simply consists of minimizing a_{resp}. Suppose the damper mass is the only design variable, which is a

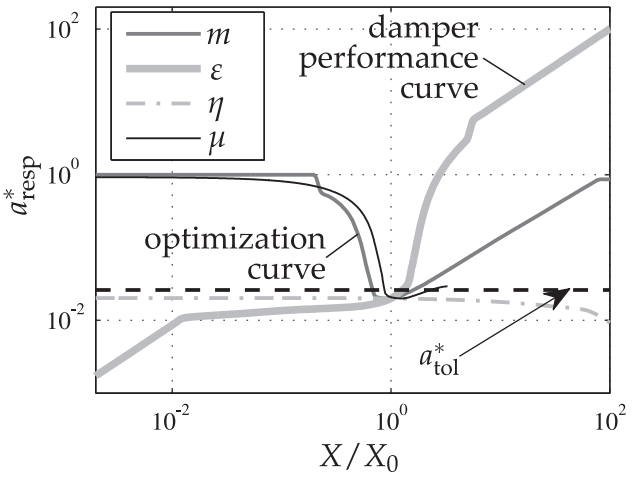

Figure 7.10: Sensitivity of the resonant forced response amplitude with respect to different parameters

common situation. In this case, $m = m_{\mathrm{opt,c}}$ would be the optimal choice. However, a finite level of uncertainty is usually associated with the system parameters. It should be remarked that friction coefficient, excitation level and background damping are often regarded as uncertain in this field [125]. If, for instance, the actual excitation level (friction coefficient) was slightly larger (smaller) than its respective nominal value, the response amplitude would be significantly larger, as it can be deduced from **Fig. 7.10**. In the next paragraph, a strategy is presented for finding a *robust design*, i. e. a design which provides high performance and, at the same time, low sensitivity with respect to parameter variability.

7.2.4 Reliability optimization

Definition of the robust design problem

A common strategy to simultaneously optimize robustness and performance is the maximization of the expected value of the reliability [66]. This expected reliability is defined as the so-called *probability of success*, i. e. the probability that a specified performance is achieved. In this study, a tolerable amplitude a_{tol} was specified as performance. This threshold value defines whether a design is deemed to be feasible. An appropriate value for a_{tol} should take into account strength or fatigue considerations and certainly depends on the application-specific requirements. The a_{tol} specified in this study is indicated in **Fig. 7.10**. Hence, the objective is to maximize the probability $\Pr\left[a_{\mathrm{resp}} \leq a_{\mathrm{tol}}\right]$ that the maximum displacement amplitude a_{resp} does not exceed the tolerable amplitude a_{tol}.
Uncertainties in the excitation level ε, the background damping factor η and the friction

coefficient μ were taken into account. The damper mass m was considered as the only design variable. The design problem can thus be stated as,

$$\begin{aligned} \text{maximize} \quad & \Pr\left[a_{\text{resp}}\left(\boldsymbol{X}\right) \leq a_{\text{tol}}\right] \\ \text{with respect to design variable} \quad & X_{\text{DV}} = m \\ \text{subject to uncertain parameters} \quad & \boldsymbol{X}_{\text{UC}} = \left[\varepsilon \ \eta \ \mu\right]^{\text{T}} . \end{aligned} \tag{7.1}$$

Herein, $\boldsymbol{X}$ is the entire set of parameters, which comprises the set of design variables X_{DV} as well as the set of uncertain parameters $\boldsymbol{X}_{\text{UC}}$, i. e. $\boldsymbol{X} = \begin{bmatrix} m & \varepsilon & \eta & \mu \end{bmatrix}^{\text{T}}$.
The probability in Eq. (7.1) can be expressed as expectation integral over the entire domain of all $N_{\text{UC}} = 3$ uncertain parameters,

$$\Pr\left[a_{\text{resp}}\left(\boldsymbol{X}\right) \leq a_{\text{tol}}\right] = \int_{X_{N_{\text{UC}},\text{min}}}^{X_{N_{\text{UC}},\text{max}}} \cdots \int_{X_{1,\text{min}}}^{X_{1,\text{max}}} \left[a_{\text{resp}}\left(\boldsymbol{X}\right) - a_{\text{tol}}\right]_{+} \, f_1(X_1)\mathrm{d}X_1 \cdots f_{N_{\text{UC}}}(X_{N_{\text{UC}}})\mathrm{d}X_{N_{\text{UC}}} . \tag{7.2}$$

Herein, $\left[()\right]_{+}$ is the Heaviside function which returns the argument, if it is positive and zero otherwise. f_i are the probability density functions (PDFs) of the uncertain parameters $X_i \in \boldsymbol{X}_{\text{UC}}$.
In practice, it is certainly not trivial to determine realistic PDFs by means of measurements, error estimations and experience. It is thus relevant to vary these parameters and estimate their influence on the robust design, as it was done in Krack et al. [91, 92]. In this study, a Gaussian stochastic distribution around the mean value $\boldsymbol{X}_0$ was assumed for all parameters. Hence the probability integral in Eq. (7.2) would have to be evaluated on an infinite domain. In this study, the numerical integration is restricted to the $3-\sigma$ range corresponding to the 99.73rd percentile of the parameter domain. It is important to note that the Gaussian distribution is of course also defined for negative parameters, which might lead to physically questionable results in case of e. g. the friction coefficient. However, negative parameters were found to be beyond the $3-\sigma$ range in this study.

Reliability analysis using nonlinear modes

In general, the evaluation of the probability integral cannot be carried out analytically, and numerical integration schemes have to be used instead. The adaptive recursive Simpson's integration rule was employed in this study [38]. This is a standard method for the numerical computation of arbitrary integrals. In general, the integrand needs to be evaluated for a considerable number of points in the three-dimensional space spanned by the parameters $\boldsymbol{X}_{\text{UC}}$. For each parameter point, the frequency-response curve needs to be calculated in order to determine $a_{\text{resp}}\left(\boldsymbol{X}\right)$. This commonly results in prohibitive computational cost, if conventional methods are employed. Instead, this task is performed using the proposed ROM approach to decrease the computational burden.
In order to use the proposed ROM for the evaluation of $a_{\text{resp}}\left(\boldsymbol{X}\right)$ in Eq. (7.1), it has to be

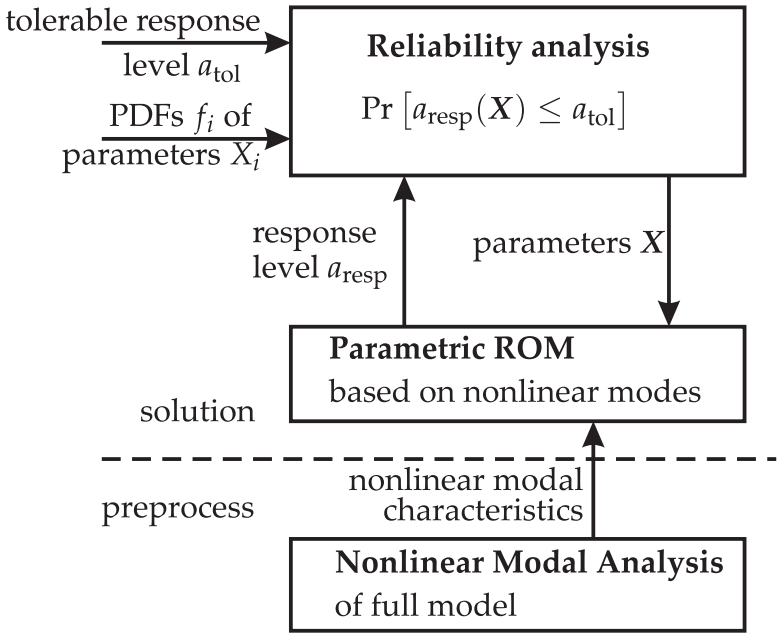

Figure 7.11: Signal flow chart of the reliability analysis based on nonlinear modes

ensured that the ROM is available within the entire parameter domain. As explained in Chapter 5, this is inherently fulfilled for the excitation level ε and the damping coefficient η. This also applies to the damper mass m, due to the scale invariance of the considered contact model and the assumptions detailed in Section 7.2.1. Only the friction coefficient μ is not ad hoc available as a parameter of the ROM. Thus, the modal analysis was carried out for ten sampling points of μ, as indicated in **Fig. 7.9**. The results for arbitrary μ values were obtained by piecewise cubic interpolation (analogous to the interpolation with respect to the amplitude explained in Chapter 5).
A signal flow chart of the overall approach is illustrated in **Fig. 7.11**. It consists of two parts: In the preprocessing part, the modal analysis is performed. Owing to the inherent parametric character, the nonlinear modal characteristics only had to be re-computed for varying friction coefficients. From these characteristics, a parametric ROM is constructed that can be evaluated at any point $\boldsymbol{X}$ within the parameter space. In the solution part, the probability integral is computed using a numerical integration scheme. The integration scheme automatically selects the required sampling points $\boldsymbol{X}$. It utilizes the parametric ROM like a black box for the evaluation of $a_{\text{resp}}(\boldsymbol{X})$ and thus to determine the integrand at any point $\boldsymbol{X}$.

Results for the test case

In **Fig. 7.12**, the reliability-mass characteristic is illustrated for individual and cumulative parameter uncertainties. The standard deviation of all parameters was set to 15%. In the limit case without uncertainties, the reliability-mass characteristic would be a step function, for which the reliability changes between 0 and 100% where the graphs of $a_{\text{resp}}(m)$ and a_{tol} intersect in **Fig. 7.10**. The stronger the parameter variability and the higher the

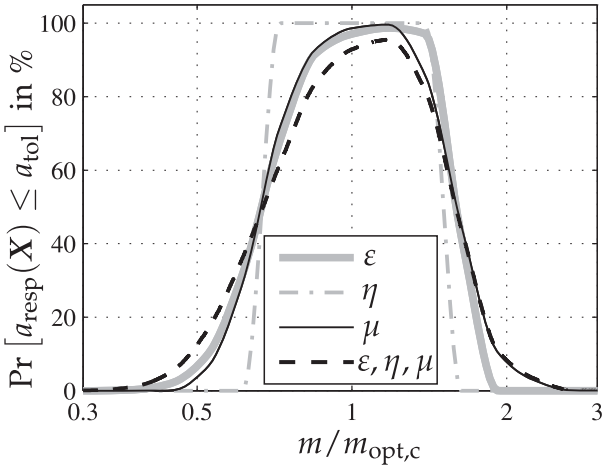

Figure 7.12: Reliability for different sets of uncertain parameters vs. damper mass

sensitivity of a_{resp} with respect to the uncertain parameters, the more will the characteristic deviate from a step function and become smoother. Because of the skewness of the reliability curve, the mass which maximizes the reliability, i. e. the *robust mass* does in general not coincide with $m_{\mathrm{opt,c}}$. Because of the comparatively low sensitivity with respect to η as illustrated in **Fig. 7.10**, the reliability-mass characteristic is merely a step function for uncertainty in η. The cumulation of uncertainties leads to a smoother shape of the resulting reliability characteristic compared to the individual characteristics.
In case all parameters are uncertain with a standard deviation of 15%, the robust damper mass is 17% larger than the optimum damper mass $m_{\mathrm{opt,c}}$ without uncertainties. Compared to $m_{\mathrm{opt,c}}$, the robust mass improves the reliability by 2.6% from 93% to 96%, but it increases the nominal value of a_{resp} by 6.7% in this case. It should be noted that these values clearly depend on the considered system, the tolerable amplitude a_{tol} and the parameter variabilities. This was investigated in more detail in Krack et al. [92].
It is common practice to design the damper mass larger than its theoretical optimal value $m_{\mathrm{opt,c}}$ (for nominal parameters) [35]. The proposed reliability analysis not only gives rise to a probabilistic justification of this practice, but it also provides a suitable objective for a systematic approach towards robust design of friction-damped systems.

Computational benefit achieved by the proposed procedure

In the course of computation, it was generally found that there is a sufficient agreement between ROM and the reference calculations ($< 1\%$ deviation). The numerical reference was obtained by solving the equations of motion of the segment model in generalized coordinates by means of the high-order harmonic balance (HBM). This is a suitable numerical reference as explained in Section 7.1.3. The ROM is therefore qualified for the reliability optimization.
In **Table 7.2**, the computation times for different tasks are listed. It was found that the average computational effort for computing a single frequency-response function (FRF) using the reference method is in the order of magnitude of a single nonlinear modal analysis

Table 7.2: Computational effort normalized to overhead caused by a single NMA, the asterisk in the last column denotes that the value was estimated based on the single FRF computation times

task	no. of FRF evaluations	comp. time NMA overhead	comp. time ROM	comp. time reference
single FRF	1	1.0	0.03	1.7
Fig. 7.12	$2.9 \cdot 10^6$	10.0	$8.9 \cdot 10^4$	$5.0 \cdot 10^6$ *

(NMA). In the present case, the reference computation of a single FRF takes longer than the NMA computation. It is thus already beneficial to follow the ROM approach for a single FRF computation, despite the NMA overhead.
The benefit of the ROM approach becomes more prominent as soon as multiple FRF calculations are required for different parameter sets. The NMA was carried out for ten sampling points of the friction coefficient, and an interpolation was used between these points to obtain the results in **Fig. 7.12**. Hence, the NMA overhead was ten times as large as the one for a single NMA. Nevertheless, it can be concluded from **Table 7.2** that the NMA overhead is negligible compared to the actual computations required to produce the probabilistic analysis results. Considering the computational effort listed in **Table 7.2**, it can be concluded that reliability analysis can easily become prohibitive in conjunction with conventional analysis methods.
Finally, it has to be remarked that the actual computation times depend on many influences such as the problem dimension, type of nonlinearity and the considered dynamic regime. The number of deterministic function evaluations in the probabilistic analysis depends on the number of uncertain parameters and on the integration method utilized for the evaluation of the expectation integral.

8 Discussion of the results

Dynamic regime of interest

In order to assess the modal characteristics of friction-damped systems, the concept of nonlinear modes has been utilized in the present study. The overall method was designed for a particular dynamic regime, namely the regime of an isolated resonance. This clearly represents the limitation of the proposed method. The proposed modal analysis method is thus only suitable to reproduce the vibration behavior of a system, as long as the fundamental harmonic dominates its response.
At this point, it makes sense to highlight examples for which the proposed approach is not suitable: If the system is exposed to multi-harmonic, broad-band or impulsive excitation, the response is typically not dominated by a fundamental harmonic component. Another situation where the approach is not capable of reproducing the dynamic behavior is when the nonlinear character of the coupling forces causes strong interactions among multiple modes. Such situations were also encountered for the presented case studies, when the nonlinear contact forces became strong compared to the elastic and inertia forces present in the underlying structure. In these situations, the approach was at least capable of detecting the modal interaction and identifying the corresponding modes.
A literature review of the design of friction-damped systems revealed that the regime of an isolated resonance is commonly of primary interest. Modal interactions caused by nonlinearity, on the other hand, often indicate undesired dynamical behavior like high-energy rubbing phenomena in the contact joints. Furthermore, it should be stressed that commonly applied and established approaches in the field of friction damping are also strictly limited to the regime of isolated resonances: The widely used single-term harmonic balance method is a well known example. Also, the direct computation of the resonant forced response proposed in [122], is obviously limited to isolated resonances [85]. For these reasons, the proposed approach is deemed in fact to be very useful, notwithstanding its apparent limitation.

Definition of nonlinear modes

The periodic motion concept was extended to the class of non-conservative systems in the present thesis. In the case of dissipative systems (such as friction-damped structures), a negative mass-proportional damping term was introduced to compensate the non-conservative forces and thus to enforce periodic motions. The modal properties are

directly related to the vibratory properties of these motions. In spite of their entirely different concept of nonlinear modes, the mathematical similarity of the proposed approach to the work of Laxalde and Thouverez [94] was highlighted in Chapter 4. In contrast to their approach, the proposed technique permits the use of conventional methods for the actual modal analysis, including the shooting and the harmonic balance method. Moreover, the proposed definition makes the approach admissible to the powerful class of common stability and bifurcation analysis methods developed for the investigation of periodic motions.
The artificial damping term renders the approach intrusive, and thus the autonomous behavior of the nonlinear system is generally not captured in an exact manner. However, the approach has been proven to be fully consistent with the linear case (including harmonic linearization). In fact, the linear modes have been used as starting guess for the continuation of the modes in the nonlinear regime. The significance of the modal characteristics in the nonlinear regime should still be interpreted with care. Like every other definition of nonlinear modes, its link to reality resides in its ability to reproduce the vibration behavior in the dynamic regime of interest. This was verified by assessing the accuracy of the associated ROM (discussed later).

Efficient computation of modal characteristics

The (high-order) harmonic balance method has been employed for the direct computation of the energy-dependent eigenfrequency, modal damping ratio and the harmonic components of the eigenvector. Harmonic balance is generally known for its efficiency compared to time domain methods in the presence of strongly nonlinear or even non-smooth forces. Moreover, harmonic balance is applicable to a wide range of nonlinearities. In particular, the regularized contact constraints considered in this thesis were treated in the usual manner. This had the additional benefit that, in contrast to many other modal analysis methods, the possibly involved formulation of the nonlinear forces does not have to be adjusted, but their conventional harmonic balance formulations can be readily used.
In general, the computational method provided great numerical robustness throughout the numerical examples presented in this study. The computational efficiency was further improved by exploiting the sparsity of the nonlinear force vector, the efficient factorization of the dynamic stiffness matrix and the use of a gradient-based solution procedure involving analytical gradients. The sparsity of the nonlinear force vector was exploited using an exact condensation procedure. Depending on the extent of this sparsity, this can greatly reduce the resulting problem dimension. This makes the method particularly efficient in the case of localized sources of nonlinearity, such as the contact interfaces of friction-damped systems. The computational benefit achieved by the improvements was evaluated in Section 4.2.4 by analyzing the computation times required for different steps of the iterative solution scheme. Moreover, the joint effect of the three improvements was investigated for the bladed disk case study in Section 7.1.4. The improvements were found to reduce the computation time by one to three orders of magnitude.

Resolution of internal resonances

The detection of internal resonances is important in the present study, since the first bifurcation with respect to increasing kinetic energy bounds the defined regime of interest and represents the natural validity limit of the proposed approach. Using the suggested numerical path continuation was useful for overcoming turning points which are typically accompanied by internal resonances. This strategy clearly revealed the occurring internal resonances in the case of the beam with unilateral contact investigated in Section 6.1. However, more complicated bifurcation behavior may occur as well, including the branching of the solution. The continuation scheme only yields a single solution branch and is therefore not readily capable of finding all periodic motions present in the strongly nonlinear regime. The bladed disk case study showed that bifurcations may be easily overlooked. A closer look on the topological structure of the underlying geometry of the nonlinear mode in the phase space was found to be helpful for the characterization of internal resonances in this case. Thorough bifurcation and stability analyses are in general expected to be ideal supplements to the proposed procedure, but were regarded to be beyond the scope of the present work.

Model reduction

In order to reduce the computational effort required for the vibration prediction of friction-damped systems, a model reduction approach was proposed. The idea of this approach was to bound the system dynamics to only the subspace related to the nonlinear mode, i. e. its two-dimensional invariant manifold. This facilitates a significant reduction of the problem down to only two dimensions to describe the vibration behavior in the dynamic regime of interest.
The required computational cost was compared to reference simulations of the full-order model using the conventional time integration and harmonic balance. The overhead of the model reduction approach is the time required for the preceding modal analysis. For the bladed disk case studies this overhead was found to be in the same order of magnitude as a single frequency-response function computation using the reference method. The subsequent ROM predictions were generally found to be of almost negligible computational cost compared with conventional methods.
It can generally be stated that the overhead required for the model reduction pays off quickly, in particular if the modal characteristics do not have to be re-computed each time when system parameters are varied. Owing to the proposed superposition procedure, it was shown that this expensive re-computation can be completely avoided, if only the parameters associated with the superimposed weak damping or the harmonic forcing are altered.
Furthermore, a scale invariance can be exploited, if the nonlinearity stems solely from unilateral springs and elastic Coulomb friction. In this case, the modal characteristics have to be computed for a particular preload only and can then be determined immediately for a different preload by taking advantage of this scaling property. The scale invariance loses its validity in general, as soon as other sources of nonlinearity are introduced. If, for in-

stance, a geometric nonlinearity is taken into account either in the kinematic description of the contact model or for the global deformations, the scaling property will not hold. It is also important to note that the scale invariance relates to the preload as a whole, and is not applicable, if the distribution of the initial normal pressure is varied. Finally, it has to be remarked that the preload can often not be controlled directly, but it indirectly depends on parameters such as the rotational speed of the bladed disk. These parameters may affect other structural dynamical properties for which the scale invariance generally does not apply.
The proposed ROM was derived for both externally forced and autonomous configurations. The oscillation frequency is equal to the readily known eigenfrequency in the autonomous case, while it corresponds to the excitation frequency in the externally forced case. The special case of simultaneous external and self-excitation was not addressed in the present work.
An averaging formalism has been utilized to derive the ROM to make it capable of predicting unsteady vibrations with slowly varying parameters. The state vector, from which the motion is initiated, must lie on the two-dimensional manifold. It should be noted that this is an important restriction. This restriction is, however, not additional, but it is due to the limited dynamic regime of interest: If the motion is initiated in some distance to the manifold, the flow is *contaminated* and will not necessarily remain arbitrarily close to the invariant manifold. As a consequence, the kinetic energy is not confined to an isolated nonlinear mode anymore. The free decay from a general (off-manifold) starting point, for instance, can thus not be predicted.
It has been shown that the equations governing the steady-state behavior can be obtained as a special case of the general ROM equations. It was further demonstrated, how the method can be adjusted for specific investigations, often involved in the design of friction-damped systems. In particular, the direct analysis of resonances with respect to parameters should be mentioned, which represents an appropriate alternative to the strategies currently employed for this purpose. The versatility and inherent parameter space clearly make the ROM a powerful tool for the prediction of the nonlinear vibration behavior in the regime of interest.

Validation of the ROM

Besides the assumption of an isolated resonance, a cascade of approximations has been introduced in the derivation of the ROM. These approximations are possible sources of inaccuracy. It is useful to recall these approximations at this point:

- superposition of linear, weak damping with matrix $\boldsymbol{C}_{\mathrm{mod}}$
- stretching of the velocity-related subspace of the manifold when the oscillation frequency deviates from the eigenfrequency, $\Omega \neq \omega_0$
- assumption of essentially periodic flow with slowly varying parameters (required for averaging)

- projection of the residual in the reduced subspace only onto fundamental harmonic component of the nonlinear mode
- synthesis of off-resonant modes in their linear form.

For the validation of the proposed approach, several numerical examples were investigated with regard to their modal characteristics and their dynamic behavior under various operating conditions. The ROM prediction quality was evaluated by means of reference results obtained from the full-order model using conventional time integration and harmonic balance.
As long as the linear damping was sufficiently weak, i. e. when it did not induce significant modal coupling, it could be superimposed in the modal space. Throughout the numerical examples, this superposition procedure was employed. To this end, the damping was defined in the linear modal space or simply as proportional damping. The effect of linear damping was particularly relevant for the investigations of the beam with unilateral contact, since the autonomous system is otherwise conservative. The superimposed damping also played an essential role for the self-excited vibrations of the friction-damped beam. Finally, the effect of the amount of hysteretic background damping on the resonance amplitudes of the friction-damped beam was explicitly studied in Section 6.2.3. In all these investigations, no inaccuracy was identified that could be associated with the approximate character of the linear damping superposition. It should be generally noticed that strong linear damping, characterized for instance by significant off-diagonal terms of the modal damping matrix, could also be taken into account with the proposed approach: Instead of the superposition, the modal damping would be treated like the nonlinear forces in this case.
The second approximation mentioned in the above list might cause inaccurate predictions in the externally forced case, namely when the excitation frequency significantly deviates from the eigenfrequency. This has been tested in the numerical examples by investigating the prediction quality of frequency-response curves and resonance passages in the range of at least several percent around the eigenfrequency. Good agreement between ROM predictions and the numerical reference was generally found. Hence, this approximation is justified for the numerical examples in this thesis. In this context, the synthesis of the off-resonant modes in their linearized form should also be mentioned. It has been found that they are not relevant very close to resonance, but that they increase the prediction quality farther away from resonance. This is plausible, since less energy is confined to the considered nonlinear mode in this regime, and the remaining modes become more important. The proposed synthesis is crucial for making the ROM accurate in the linear regime.
It is generally important to assess the prediction quality in the presence of comparatively fast unsteady phenomena: In this case, the oscillation and amplitude modulation take place on very proximate time scales. As a consequence, the averaging procedure leads to inaccurate results. This was particularly the case for the resonance passages of the comparatively simple models of systems with unilateral spring or elastic Coulomb element. The fast amplitude modulation was in these cases caused by the jump phenomenon and

the comparatively fast sweep through resonance, respectively. For slow to moderately fast transient phenomena, it can be stated that the synthesized oscillatory part of the solution was also predicted with reasonable accuracy.
The proposed simplified projection only enforces that the residual is orthogonal to the fundamental harmonic component of the nonlinear mode, but not to its full, multi-harmonic expansion. It is conceivable that this strategy leads to inaccurate predictions regarding the multi-harmonic vibration content. This has been investigated in particular for the bladed disk test case. The predicted relative motion of a contact node was compared to the numerical reference. The contact interface motion featured a significant multi-harmonic character, which was accurately predicted by the ROM.
In summary, it is concluded that the proposed ROM provides high accuracy in the dynamic regime of interest, and therefore the overall approach is regarded as validated.

Applicability to the analysis and the robust design of friction-damped systems involving detailed models

Two state-of-the art structural dynamical models of bladed disks with contact interfaces were considered in Chapter 7. Common modeling assumptions were made. The strongly nonlinear contact interactions were modeled with a considerable level of detail by taking into account stick, slip, and lift-off states in a spatially local manner in the extended friction interfaces.
The investigations were limited to the tuned, i. e. cyclically symmetric assembly. Since the interaction of different modes is a typical phenomenon once the cyclic symmetry is perturbed, the proposed approach is not regarded as useful in the mistuned case. Moreover, if the excitation leads to a response with multiple significant frequencies and/or nodal diameters, the assumption of an isolated resonance is violated, and the method cannot be applied. For the tuned case with an isolated traveling-wave type mode, however, the method allowed the direct assessment of the energy-dependent modal damping ratio, eigenfrequency and deflection shape.
Predictions of the steady-state forced response to traveling-wave type excitation were successfully validated against reference results obtained from high-order harmonic balance. The prediction quality was deemed to be sufficient to perform sensitivity analyses and design optimization based on the proposed ROM procedure. The ROM facilitated the derivation of frequently sought characteristics which are essential for the design of effective friction-damped systems. Thanks to the drastic reduction of the computational cost, sophisticated design strategies can be afforded, such as the probabilistic approach for robust design optimization demonstrated in Section 7.2.

9 Conclusions and future work

Conclusions

The concept of nonlinear modes was applied to friction-damped systems in order to improve the performance of their dynamic analysis and their design process in general. These improvements were accomplished by facilitating (1) the direct assessment of the relevant energy-dependent vibration characteristics and (2) the model reduction down to a very small dimension. Due to the strongly nonlinear character of the contact interactions, friction-damped systems have the potential to exhibit quite complex dynamic behavior. It was generally found that the vibration behavior can be classified into different dynamic regimes. Depending on the operating conditions, friction-damped systems may exhibit linear, weakly nonlinear or strongly nonlinear behavior. The weakly nonlinear regime appeared to be of primary relevance for friction-damped systems, and therefore the present work focused on this regime.
It was demonstrated that the system behaves like a single modal oscillator in the regime of interest. As a consequence of nonlinearity, the properties of this oscillator depend on the kinetic energy. The proposed modal analysis technique can be viewed as a means for identifying these energy-dependent modal properties. In contrast to most existing techniques, the proposed method directly gives rise to a measure of the damping effectiveness. This is obviously a crucial feature for the design assessment of passive vibration reduction mechanisms such as friction damping. The computational method proved to be applicable to detailed models of friction-damped systems, where it exploits the localized nature of the nonlinear contact interactions. The computational cost of the modal analysis was successfully reduced by several orders of magnitude with the aid of several computational improvements. The present work is regarded as a valuable step towards making modal analysis a useful tool for friction-damped systems.
The notion of an equivalent modal oscillator naturally leads to model reduction opportunities. The proposed ROM is based on the modal characteristics obtained by the developed modal analysis technique. It facilitates quantitatively accurate vibration predictions for a wide range of operating conditions. Compared to conventional methods, the prediction effort was reduced by several orders of magnitude. The method is suitable for directly analyzing steady-state vibrations caused by external forcing or negative damping. It also permits the prediction of unsteady phenomena such as the free decay of vibrations and resonance passages. The ROM is equipped with a large parameter space: The parame-

ters associated with background damping, external forcing and the preload of the contact interfaces can be varied without the need for a comparatively expensive re-computation of the modal characteristics. All these parameters are relevant for friction-damped systems and typically have to be varied in the course of the design process. In this context, it was demonstrated how the ROM can be adjusted to directly determine specific, often sought characteristics like performance curves, optimization curves or stability maps.
The overall approach facilitates a significant reduction of the computational cost for the design and the analysis of friction-damped systems. Hence, more accurate models can be afforded considering that the computational resources are limited in practice. Likewise, more sophisticated design strategies can be followed, for instance by taking into account the effect of parameter uncertainties. Hence, the proposed approach facilitates the design of more effective and more reliable friction-damped systems.
A scale invariance was established for models of friction-damped systems where the nonlinearity stems solely from a specific, but widely used contact model. Starting from a computed response for a specific set of parameters, the response does not have to be recomputed to determine the results for other parameter sets, if the preload in the contact interfaces and the external forcing are varied in a certain way. It should be noted that these parameters commonly have to be varied during the design process. The implications of this scaling property extend far beyond the demonstrated application to nonlinear modes and are regarded as quite valuable for the analysis and the design of friction-damped systems in general.

Future work

From a dynamical point of view, it would be interesting to investigate the stability and the bifurcation behavior of nonlinear modes of friction-damped systems more thoroughly. Owing to the conception of nonlinear modes as periodic motions, this task should be feasible with conventional methods.
An extension of the proposed approach beyond its current limit to the regime of an isolated resonance should be attempted. The number of coordinates used for the nonlinear modes would have to be increased depending on the number of interacting modes. This would allow the prediction of the vibration behavior in the presence of internal resonances, and thus extend the ideas of the present into the strongly nonlinear regime.
Due to the generality of most developments, the overall approach should be applicable to problems beyond the class of friction-damped systems. Because of the similarity of the modeling, the application to structures with cracks seems straightforward. The energy-dependent modal characteristics possibly represent useful measures for structural health monitoring.
The approach appears suitable for the modal analysis of structures with generic, nonlinear couplings and attachments. It seems to be well-suited for the design optimization of vibration reduction mechanisms. In particular, applications to vibration damping by means of shape memory alloys, shunted piezoelectric devices or eddy current dampers

are imaginable.
Based on the conception of nonlinear modes proposed in this thesis, a method for the experimental identification of modal characteristics could be developed. In this context, the developed ROM should be useful to interpret and correlate the measured data. The findings suggest that the modal characteristics reflect well the vibration signature of nonlinear systems. These properties probably represent a well-suited base for an experimental identification of model parameters.

A Parseval's theorem

Consider two truncated Fourier series,

$$q(\tau) = \Re\{\sum_{n=0}^{H} \hat{q}_n \mathrm{e}^{\mathrm{i}n\tau}\} \quad \text{and} \quad s(\tau) = \Re\{\sum_{n=0}^{H} \hat{s}_n \mathrm{e}^{\mathrm{i}n\tau}\}\,. \tag{A.1}$$

Parseval's theorem (see e. g. [17]) relates the mean value of the product $q(\tau)s(\tau)$ to the Fourier coefficients $\hat{q}_n$, $\hat{s}_n$ as follows:

$$\frac{1}{2\pi}\int\limits_{(2\pi)} q(\tau)s(\tau)\mathrm{d}\tau = \Re\{\hat{q}_0\hat{s}_0 + \frac{1}{2}\sum_{n=1}^{H}\overline{\hat{q}_n}\hat{s}_n\}\,. \tag{A.2}$$

B Modal properties in accordance with different conceptions

Since the periodic flow conception of nonlinear modes proposed in the present study is different from the damped flow conception proposed by Laxalde and Touverez [94], the modal properties are also defined in a different manner. These differences are demonstrated in this appendix for the special case of a linear, autonomous single-DOF oscillator. Its equation of motion in normalized form reads

$$\ddot{x}(t) + 2D\omega_0\dot{x}(t) + {\omega_0}^2 x(t) = 0\,. \tag{B.1}$$

The modal properties in the nonlinear case must be consistent with the obvious modal properties D, ω_0 in Eq. (B.1). It should be noticed that the following developments can be immediately generalized to linear finite DOF systems if modal decoupling is possible. The derivations also extend to the case of harmonic linearization applied to a single-DOF system, i. e. when the modal properties D, ω_0 are functions of the amplitude $\hat{x}$ assuming the ansatz $x(t) \approx \hat{x}\cos\omega t$.

Damped flow conception
The approach in [94] was inspired by the standard exponential ansatz $x(t) = \Re\{\hat{x}e^{\lambda t}\}$ for damped systems. Substituting this ansatz into Eq. (B.1) leads to the characteristic equation

$$\lambda^2 + 2D\omega_0\lambda + {\omega_0}^2 = 0\,. \tag{B.2}$$

This equation has two solutions

$$\lambda_{1,2} = -D\omega_0 \pm \mathrm{i}\omega_0\sqrt{1-D^2}\,. \tag{B.3}$$

This corresponds to the definition of the complex eigenvalue λ proposed in [94].

Periodic flow conception
The method for the computation of nonlinear modes proposed in this thesis can also be applied to the single-DOF oscillator. Eq. (B.1) takes the form of Eq. (4.4) with $\boldsymbol{M} = 1$, $\boldsymbol{K} = {\omega_0}^2$ and $\boldsymbol{u} = x$, when the dissipative term in Eq. (B.1) is incorporated as $\tilde{\boldsymbol{g}} = 2D\omega_0\dot{x}$. Substituting these expressions into Eq. (4.5) and utilizing $x(t) = \Re\{\hat{x}e^{\mathrm{i}\omega t}\}$ in accordance with the ansatz (4.6), leads to the frequency domain equation of motion

$$\left[-\omega^2 - \xi\mathrm{i}\omega + 2D\omega_0\,\mathrm{i}\omega + {\omega_0}^2\right]\hat{x} = 0\,. \tag{B.4}$$

By choosing

$$\xi = 2D\omega_0\,, \quad \omega = \omega_0\,, \tag{B.5}$$

Eq. (B.5) can be solved, which corresponds to the proposed approach.

C Derivation of the unsteady flow on the invariant manifold

The model reduction idea is select the computed invariant manifold $\boldsymbol{U}$, $\boldsymbol{V}$ defined in Eq. (5.1) as base functions for the generalized coordinates by substituting Eq. (5.1) into Eq. (4.1). This produces a residual $\boldsymbol{R}(t)$,

$$\boldsymbol{R} := \boldsymbol{M}\dot{\boldsymbol{V}} + \boldsymbol{C}_{\mathrm{mod}}\boldsymbol{V} + \boldsymbol{K}\boldsymbol{U} + \tilde{\boldsymbol{g}}\left(\boldsymbol{U},\boldsymbol{V}\right) - \boldsymbol{e} \stackrel{!}{=} \boldsymbol{0}\,. \tag{C.1}$$

In the interest of readability, the dependencies $\boldsymbol{U}\left(a(t),\vartheta(t)\right)$, $\boldsymbol{V}\left(a(t),\vartheta(t)\right)$ and $\boldsymbol{R}(t)$, $\boldsymbol{e}(t)$ are not explicitly denoted in Eq. (C.1) and in the following. The residual is then made orthogonal to the nonlinear mode in a Galerkin sense. This projection involves the integration of the residual over the time scale of the mode, which is carried out by an averaging formalism.

Complexification and slow-fast decomposition

The averaging formalism utilized in this study was inspired by the work of [100] and similar procedures can be found e. g. in [107, 12, 98, 172, 170]. The first step represents a coordinate transform with the intent to decompose the flow into a slowly varying term and a fast oscillation term. In a second step, the fast time scale is averaged out to derive equations governing the flow of the slowly varying term.
Introducing a complex-valued auxiliary function $\boldsymbol{Y}$, the coordinate transform is defined as

$$\boldsymbol{Y} = \boldsymbol{U} + \frac{\boldsymbol{V}}{\mathrm{i}\Omega} =: \underbrace{\boldsymbol{A}}_{\text{slow variation}} \cdot \underbrace{\mathrm{e}^{\mathrm{i}\tau}}_{\text{fast oscillation}} . \tag{C.2}$$

Herein, τ is the fast time scale with $\dot{\tau} = \Omega$. It follows from Eq. (C.2) that

$$\boldsymbol{U} = \frac{\boldsymbol{Y} + \overline{\boldsymbol{Y}}}{2}, \quad \boldsymbol{V} = \mathrm{i}\Omega \frac{\boldsymbol{Y} - \overline{\boldsymbol{Y}}}{2}, \tag{C.3}$$

where $\overline{()}$ denotes the complex conjugate.
Derivation of the second of Eqs. (C.3) with respect to time yields

$$\dot{\boldsymbol{V}} = \mathrm{i}\Omega \left(\dot{\boldsymbol{Y}} - \boldsymbol{V} \right) + \underbrace{\mathrm{i}\dot{\Omega} \left(\boldsymbol{Y} - \boldsymbol{U} \right)}_{\text{neglected}} \approx \mathrm{i}\Omega \left(\dot{\boldsymbol{Y}} - \mathrm{i}\Omega \frac{\boldsymbol{Y} - \overline{\boldsymbol{Y}}}{2} \right) . \tag{C.4}$$

The influence of the term related to the angular acceleration $\dot{\Omega}$ was checked for the numerical studies within this thesis. It was found not to improve the accuracy of the approach significantly, but it certainly increased the computational cost for the prediction. Hence, this term was neglected in the following derivations.
The term $\dot{\boldsymbol{Y}}$ in Eq. (C.4) can be obtained from time derivation of Eq. (C.2) as

$$\dot{\boldsymbol{Y}} = \left(\mathrm{i}\Omega \boldsymbol{A} + \dot{\boldsymbol{A}} \right) \mathrm{e}^{\mathrm{i}\tau} . \tag{C.5}$$

Substitution of invariant manifold

In a conventional averaging procedure, every coordinate would have its independent amplitude and phase. The predicted flow would then in general not lie on the invariant manifold. In order to bound the flow to the invariant manifold, the following expression for $\boldsymbol{A}$ is defined:

$$\boldsymbol{A} \approx a \sum_{n=0}^{H} \hat{\boldsymbol{\psi}}_n (a) \, \mathrm{e}^{\mathrm{i}(n\vartheta - \tau)} . \tag{C.6}$$

By substituting Eq. (C.6) and (C.2) into Eq. (C.3) and comparing the results with Eq. (5.1), it can be verified that this transformation is accurate regarding the generalized coordinates $\boldsymbol{U}$. The velocities $\boldsymbol{V}$, however, only agree with the manifold for the first terms $n = 0, 1$, while there is a phase difference in the higher harmonics $n \geq 2$.

Substituting Eq. (C.2)-(C.6) into Eq. (C.1) transforms the differential equations to the subspace spanned by the invariant manifold. Due to the approximative character of the transformation, the ODEs produce an error, i. e. a nonzero residual $\boldsymbol{R}$. The residual is a function of the modal amplitude a, the phase coordinate of the nonlinear mode ϑ and the phase variable τ. By introducing the phase lag

$$\Delta\vartheta = \vartheta - \tau\,, \tag{C.7}$$

the residual can equivalently be expressed as a function $\boldsymbol{R}(a, \Delta\vartheta, \vartheta)$.

Projection onto nonlinear mode

The residual should not have an influence on the dynamics and should therefore be made orthogonal to the reduced subspace. This is done by a Galerkin-type procedure which enforces that the projection of the residual onto the nonlinear mode is equal to zero,

$$\left\langle \boldsymbol{R}(a, \Delta\vartheta, \vartheta), \sum_{n=0}^{H} \hat{\boldsymbol{\psi}}_n\,(a)\,\mathrm{e}^{\mathrm{i}n\vartheta} \right\rangle := \frac{1}{2\pi} \int\limits_{(2\pi)} \left(\sum_{n=0}^{H} \hat{\boldsymbol{\psi}}_n\,(a)\,\mathrm{e}^{\mathrm{i}n\vartheta} \right)^{\mathrm{H}} \boldsymbol{R}(a, \Delta\vartheta, \vartheta)\mathrm{d}\vartheta = 0\,. \tag{C.8}$$

Note that the inner product in Eq. (C.8) involves the integration over the time scale ϑ of the nonlinear mode. In this study, this procedure has been further simplified by neglecting the projection terms $n \neq 1$ and thus to project only onto the fundamental harmonic $\hat{\boldsymbol{\psi}}_1 \mathrm{e}^{\mathrm{i}\vartheta}$,

$$\left\langle \boldsymbol{R}(a, \Delta\vartheta, \vartheta), \hat{\boldsymbol{\psi}}_1\,(a)\,\mathrm{e}^{\mathrm{i}\vartheta} \right\rangle := \frac{1}{2\pi} \int\limits_{(2\pi)} \left(\hat{\boldsymbol{\psi}}_1\,(a)\,\mathrm{e}^{\mathrm{i}\vartheta} \right)^{\mathrm{H}} \boldsymbol{R}(a, \Delta\vartheta, \vartheta)\mathrm{d}\vartheta = 0\,. \tag{C.9}$$

Hence, it is enforced that the error is not in the subspace spanned by the fundamental harmonic component of the nonlinear mode. This approximation is reasonable, since this component of the flow is, by definition, dominant in the regime of interest.
Now it remains to compute for each term of the residual $\boldsymbol{R}$ in Eq. (C.1) the projection defined in Eq. (C.9). In accordance with the averaging idea, the *slow variables* $a, \Delta\vartheta$ and their dependent quantities $\hat{\boldsymbol{\psi}}_n, \omega_0, D$ are treated as constant on the fast time scale ϑ.

Projection of inertia terms

For the modal inertia forces, the time derivative $\dot{\boldsymbol{A}}$ of the amplitude function in Eq. (C.6) has to be determined from Eq. (C.6),

$$\dot{\boldsymbol{A}} = \sum_{n=0}^{H} \left(\dot{a} + \mathrm{i}a \left[(n-1)\,\Omega + n\Delta\dot{\vartheta} \right] \right) \hat{\boldsymbol{\psi}}_n \mathrm{e}^{\mathrm{i}(n\vartheta - \tau)} + a \frac{\partial \hat{\boldsymbol{\psi}}_n}{\partial a} \dot{a} \mathrm{e}^{\mathrm{i}(n\vartheta - \tau)}\,. \tag{C.10}$$

For a better readability, the dependence on a is not denoted explicitly here and in the following.

The acceleration $\dot{\boldsymbol{V}}$ can then be obtained in terms of the nonlinear mode by substituting Eqs. (C.2), (C.5)-(C.6) and (C.10) into Eq. (C.4).

$$\dot{\boldsymbol{V}} = \mathrm{i}\Omega \left(\left[\mathrm{i}\Omega a + \dot{a} + \mathrm{i}a\Delta\dot{\vartheta} \right] \hat{\boldsymbol{\psi}}_1 + a\frac{\partial \hat{\boldsymbol{\psi}}_1}{\partial a}\dot{a} - \frac{1}{2}\mathrm{i}\Omega a \hat{\boldsymbol{\psi}}_1 \right) \mathrm{e}^{\mathrm{i}\vartheta} + \sum_{n=0, n\neq 1}^{H} \ldots \mathrm{e}^{\mathrm{i}n\vartheta} \,. \tag{C.11}$$

It is convenient to collect the terms associated with $\mathrm{e}^{\mathrm{i}\vartheta}$, since only these terms contribute to the averaged equations. The projection yields

$$\langle \boldsymbol{M}\dot{\boldsymbol{V}}, \hat{\boldsymbol{\psi}}_1 \mathrm{e}^{\mathrm{i}\vartheta} \rangle = -\frac{1}{2}\Omega^2 a - \Omega\Delta\dot{\vartheta}a + \mathrm{i}\Omega\dot{a} + \mathrm{i}\Omega a\dot{a} \underbrace{\hat{\boldsymbol{\psi}}_1^{\mathrm{H}} \boldsymbol{M} \frac{\partial \hat{\boldsymbol{\psi}}_1}{\partial a}}_{=0} \,. \tag{C.12}$$

The last term is identical to zero, which can be easily verified by deriving the mass normalization condition $\hat{\boldsymbol{\psi}}_1^{\mathrm{H}}(a)\, \boldsymbol{M}\hat{\boldsymbol{\psi}}_1(a) = 1$ with respect to a.

Projection of linear elastic and nonlinear terms

This projection is approximated by the modal properties ω_0, D in full accordance with the single modal oscillator assumption:

$$\begin{aligned} \langle \boldsymbol{K}\boldsymbol{U} + \tilde{\boldsymbol{g}}\left(\boldsymbol{U}, \boldsymbol{V}\right), \hat{\boldsymbol{\psi}}_1 \mathrm{e}^{\mathrm{i}\vartheta} \rangle &= \frac{1}{2}\hat{\boldsymbol{\psi}}_1^{\mathrm{H}} \left(\boldsymbol{K}\hat{\boldsymbol{\psi}}_1 a + \hat{\tilde{\boldsymbol{g}}}_1 \right) \\ &= \frac{1}{2}\left({\omega_0}^2 + 2D\omega_0 \mathrm{i}\Omega \right) a \,. \end{aligned} \tag{C.13}$$

The replacement of the vector of nonlinear forces $\boldsymbol{g}$, which is typically expensive to evaluate, by readily available amplitude-dependent modal properties is an important aspect for increasing the efficiency of the ROM.

Projection of superimposed terms

The projection of the linear damping term yields

$$\langle \boldsymbol{C}_{\mathrm{mod}}\boldsymbol{V}, \hat{\boldsymbol{\psi}}_1 \mathrm{e}^{\mathrm{i}\vartheta} \rangle = \frac{1}{2}\hat{\boldsymbol{\psi}}_1^{\mathrm{H}} \boldsymbol{C}_{\mathrm{mod}} \hat{\boldsymbol{\psi}}_1 \mathrm{i}\Omega a \,. \tag{C.14}$$

The essentially mono-harmonic external forcing is first written in amplitude and phase formulation

$$\boldsymbol{e}(t) = \Re\{\hat{\boldsymbol{e}}_1 \mathrm{e}^{\mathrm{i}\tau(t)}\} = \frac{\hat{\boldsymbol{e}}_1 \mathrm{e}^{\mathrm{i}\tau(t)} + \overline{\hat{\boldsymbol{e}}_1} \mathrm{e}^{-\mathrm{i}\tau(t)}}{2} \,, \tag{C.15}$$

using the fast time scale $\tau(t) = \vartheta(t) - \Delta\vartheta(t)$. The projection gives

$$\langle \frac{\hat{\boldsymbol{e}}_1 \mathrm{e}^{\mathrm{i}\tau} + \overline{\hat{\boldsymbol{e}}_1} \mathrm{e}^{-\mathrm{i}\tau}}{2}, \hat{\boldsymbol{\psi}}_1 \mathrm{e}^{\mathrm{i}\vartheta} \rangle = \frac{1}{2}\hat{\boldsymbol{\psi}}_1^{\mathrm{H}} \hat{\boldsymbol{e}}_1 \mathrm{e}^{-\mathrm{i}\Delta\vartheta} \,. \tag{C.16}$$

The projections in Eqs. (C.12)-(C.14) and (C.16) are then collected. By equating real and imaginary parts separately to zero, this finally results in Eq. (5.5).

D Proof of scale invariance of a family of contact laws

Consider the initial value problem formulated in state space for Eq. (4.1),

$$\begin{bmatrix} \dot{\boldsymbol{u}}(t) \\ \ddot{\boldsymbol{u}}(t) \end{bmatrix} + \begin{bmatrix} -\dot{\boldsymbol{u}}(t) \\ \boldsymbol{M}^{-1}\left(\boldsymbol{K}\boldsymbol{u}(t) + \boldsymbol{C}\dot{\boldsymbol{u}}(t) + \boldsymbol{g}\left(\boldsymbol{u}(t), \dot{\boldsymbol{u}}(t), \gamma\right) - \boldsymbol{e}(t)\right) \end{bmatrix} = \boldsymbol{0}\,, \\ \boldsymbol{u}(t=0) = \boldsymbol{u}_0\,,\ \dot{\boldsymbol{u}}(t=0) = \boldsymbol{v}_0\,. \tag{D.1}$$

Herein, γ denotes a scalar parameter of the nonlinear function $\boldsymbol{g}$. The following scale invariance is introduced as theorem:
Theorem (Scale invariance)**.** *If* $\{\boldsymbol{u}(t)\,,\ \dot{\boldsymbol{u}}(t)\}$ *is a solution of Eq. (D.1) for* $\{\boldsymbol{u}_0\,,\ \boldsymbol{u}_0\,,\ \gamma\,,\ \boldsymbol{e}(t)\}$*, then* $\{\kappa\boldsymbol{u}(t)\,,\ \kappa\dot{\boldsymbol{u}}(t)\}$ *with* $\kappa > 0$ *is a solution of Eq. (D.1) for* $\{\kappa\boldsymbol{u}_0\,,\ \kappa\boldsymbol{u}_0\,,\ \kappa\gamma\,,\ \kappa\boldsymbol{e}(t)\}$*.*

Note that the validity is obvious in the linear case with $\boldsymbol{g} \equiv 0$. In the nonlinear case, the validity boils down to the requirement

$$\boldsymbol{g}\left(\kappa\boldsymbol{u}(t), \kappa\dot{\boldsymbol{u}}(t), \kappa\gamma\right) \stackrel{!}{=} \kappa\boldsymbol{g}\left(\boldsymbol{u}(t), \dot{\boldsymbol{u}}(t), \gamma\right)\,. \tag{D.2}$$

The validity of Eq. (D.2) can now be shown element-wise for the vector of nonlinear forces $\boldsymbol{g}$. In this study, the proof is restricted to the unilateral spring nonlinearity and the elastic Coulomb nonlinearity, and it is applied to the preload as parameter $\gamma = p_0$. The contact laws can be written as [182]

$$p_\mathrm{n}(t) = \left(k_\mathrm{n} u_\mathrm{n}(t) + p_0\right)_+ \tag{D.3}$$

$$\boldsymbol{p}_\mathrm{t}(t) = \begin{cases} \boldsymbol{0} & \text{lift-off} \\ k_\mathrm{t}\left(\boldsymbol{u}_\mathrm{t}(t) - \boldsymbol{u}_\mathrm{t}\left(t_\mathrm{stick}\right)\right) + \boldsymbol{p}_\mathrm{t}\left(t_\mathrm{stick}\right) & \text{stick} \\ \mu p_\mathrm{n}(t) \frac{\dot{\boldsymbol{u}}_\mathrm{t}(t)}{\|\dot{\boldsymbol{u}}_\mathrm{t}(t)\|} & \text{slip} \end{cases}\,. \tag{D.4}$$

Herein, $()_+$ is the Heaviside function which returns the argument, if it is positive and zero otherwise. t_stick is the time instant at which the current stick phase began, and $\boldsymbol{u}_\mathrm{t}\left(t_\mathrm{stick}\right), \boldsymbol{p}_\mathrm{t}\left(t_\mathrm{stick}\right)$ are the values just before this transition. The initial normal pressure p_0 can of course be negative to account for initial clearances, see e. g. [128] for details.
For the unilateral spring nonlinearity, the requirement in Eq. (D.2) can be easily verified by substitution:

$$p_\mathrm{n}\left(\kappa u_\mathrm{n}, \kappa p_0\right) = \left(k_\mathrm{n}\kappa u_\mathrm{n} + \kappa p_0\right)_+ = \kappa\left(k_\mathrm{n} u_\mathrm{n} + p_0\right)_+ = \kappa p_\mathrm{n}\left(u_\mathrm{n}, p_0\right)\ \ \forall \kappa > 0\,. \tag{D.5}$$

Note that $\kappa > 0$ is required to factor out κ in this equation.
For each contact node, the tangential friction dynamics depend on the local normal dy-

namics. Since the normal contact law is scalable, also the limiting friction force μp_n is scalable. Thus, for convenience, $\gamma = \mu p_\mathrm{n}$ can be defined as scaling parameter for the friction law, which yields

$$\begin{aligned}
\boldsymbol{p}_\mathrm{t}\left(\kappa\boldsymbol{u}_\mathrm{t}, \kappa\gamma\right) &= \begin{cases} \boldsymbol{0} & \text{lift-off} \\ k_\mathrm{t}\left(\kappa\boldsymbol{u}_\mathrm{t} - \kappa\boldsymbol{u}_\mathrm{t}\left(t_\mathrm{stick}\right)\right) + \kappa\boldsymbol{p}_\mathrm{t}\left(t_\mathrm{stick}\right) & \text{stick} \\ \kappa\gamma\frac{\kappa\dot{\boldsymbol{u}}_\mathrm{t}}{\|\kappa\dot{\boldsymbol{u}}_\mathrm{t}\|} & \text{slip} \end{cases} \\
&= \kappa \begin{cases} \boldsymbol{0} & \text{lift-off} \\ k_\mathrm{t}\left(\boldsymbol{u}_\mathrm{t} - \boldsymbol{u}_\mathrm{t}\left(t_\mathrm{stick}\right)\right) + \boldsymbol{p}_\mathrm{t}\left(t_\mathrm{stick}\right) & \text{stick} \\ \gamma\frac{\dot{\boldsymbol{u}}_\mathrm{t}}{\|\dot{\boldsymbol{u}}_\mathrm{t}\|} & \text{slip} \end{cases} \\
&= \kappa\boldsymbol{p}_\mathrm{t}\left(\boldsymbol{u}_\mathrm{t}, \gamma\right) . \qquad \text{(D.6)}
\end{aligned}$$

The proof needs to be completed by demonstrating the scalability of the transition conditions:

$$\begin{aligned}
&\text{stick-slip transition:} \quad \|\kappa\boldsymbol{p}_\mathrm{t}\| = \kappa\gamma \;\Leftrightarrow\; \|\boldsymbol{p}_\mathrm{t}\| = \gamma\,, \\
&\text{slip-stick transition:} \quad \|k_\mathrm{t}\kappa\dot{\boldsymbol{u}}_\mathrm{t}\| = \kappa\dot{\gamma} \;\Leftrightarrow\; \|k_\mathrm{t}\dot{\boldsymbol{u}}_\mathrm{t}\| = \dot{\gamma}\,. \qquad \text{(D.7)}
\end{aligned}$$

Note that the validity of the scale invariance in the time domain, such as in Eq. (4.1), implies the validity in the frequency domain, as in the nonlinear modal analysis. Hence, the scale invariance can be exploited to obtain the solution of the nonlinear eigenproblem for a parameter value κp_0 from the computed solution for p_0. Thus, the treatment of the preload as an inherent parameter of the ROM, as proposed in Section 5.2, is an exact approach in terms of the considered contact constraints.

E Computational resources for the numerical study in Section 4.2.4

Table E.1: Computational resources for the assessment of the benefits achieved by the proposed numerical improvements of the nonlinear modal analysis technique

property	value
processor	Intel(R) Core(TM)2 Quad Q9550 2.83 GHz
addressable memory	3.62 GB
operating system	Windows 7 (32 Bit)
computational software	Matlab R2012a

List of frequently used symbols

Latin letters

a	modal amplitude
a_{resp}	displacement amplitude of response DOF
a_{tol}	tolerable displacement amplitude
$\boldsymbol{B}$	matrix of shape functions at the contact interface
$\mathcal{C}$	contact interface
$\boldsymbol{C}$	damping matrix
$\boldsymbol{C}_{\mathrm{g}}$	remaining (non-modal-like) part of damping matrix
$\boldsymbol{C}_{\mathrm{mod}}$	modal-like part of damping matrix
D	modal damping ratio
$\tilde{D}$	effective modal damping ratio (including term stemming from $\boldsymbol{C}_{\mathrm{mod}}$)
$\boldsymbol{e}$	excitation force vector
E_{kin}	kinetic energy
f_i	probability density function of parameter i
$\boldsymbol{g}$	nonlinear force vector
H	harmonic order
$\boldsymbol{H}$	dynamic compliance matrix
k_{n}	normal contact stiffness (related to impenetrability condition)
k_{t}	tangential contact stiffness (related to sticking friction)
$\boldsymbol{K}$	stiffness matrix
$\boldsymbol{M}$	mass matrix
$N_{\mathcal{C}}$	number of contact points
N_{d}	number of nodal DOFs of a FE model
N_{dim}	total number of algebraic equations to be solved
N_{dof}	total number of coordinates (either N_{d} or N_{r})
N_{nl}	number of coordinates associated with nonlinear coupling
N_{r}	number of generalized coordinates
N_0	normal preload
N_{p}^*	number of pseudo-periods
$\boldsymbol{N}$	matrix of shape functions within the bodies
p_0	initial normal pressure
$\boldsymbol{p}$	contact pressure vector
Pr	probability

$\boldsymbol{R}$	residual vector
t	time
T	minimal period of oscillation
$\boldsymbol{T}$	matrix with component modes as column vectors
$\boldsymbol{u}$	displacement vector
$\boldsymbol{v}$	velocity vector
$\boldsymbol{U}$	displacement-related subspace of invariant manifold
$\boldsymbol{V}$	velocity-related subspace of invariant manifold
$\boldsymbol{x}$	location vector
Δx_0	initial clearance
$\boldsymbol{X}$	vector of parameters
$\boldsymbol{Z}$	vector of unknowns

Greek letters

δ_{ij}	Kronecker-delta function
ε	excitation level
η	hysteretic damping factor
ϑ	phase coordinate on invariant manifold
λ	complex eigenvalue
μ	friction coefficient
ξ	coefficient of artificial damping term
$\boldsymbol{\varphi}$	eigenvector of linear system
$\hat{\boldsymbol{\psi}}_n$	vector of n-th harmonic coefficients of the nonlinear mode
ω_0	(angular) eigenfrequency
Ω	fundamental (angular) frequency of oscillation
Ω_e	(angular) excitation frequency

Sub-, superscripts, operators

$\dot{()}$	derivative with respect to time
$\hat{()}_n$	n-th harmonic coefficient in a Fourier series
$\overline{()}$	complex conjugate
$()^*$	normalized quantity
$_\mathcal{C}()$	quantity related to the continuous space of the contact interface $\mathcal{C}$
$_\mathcal{D}()$	quantity related to the continuous space within the body $\mathcal{D}$
$_\mathrm{d}()$	quantity related to the discrete space of a FE model
$()^\mathrm{H}$	Hermitian transpose
$\Im\{()\}$	imaginary part
$()^\mathrm{L}$	portion not related to nonlinear coupling (complement to $()^\mathrm{N}$)
$()_\mathrm{n}$	quantity related to the normal contact direction

$()^{\mathrm{N}}$	portion related to nonlinear coupling
$_{\mathrm{r}}()$	quantity related to the reduced space of component modes
$\Re\{()\}$	real part
$()_{\mathrm{t}}$	quantity related to the tangential contact plane
$()^{\mathrm{T}}$	transpose

Abbreviations

CMS	Component Mode Synthesis
DOF	degree of freedom
FE	finite element
FRF	frequency-response function
gFGM	generalized Fourier-Galerkin method
HBM	(high-order) harmonic balance method
NMA	nonlinear modal analysis
ODE	ordinary differential equation
PDF	probability density function
ROM	reduced order model

Glossary

This glossary only comprises a certain amount of technical terms encountered in this thesis, and it is far from being exhaustive. Where possible, these definitions are in line with common textbooks [108, 167] in the field of nonlinear structural dynamics.

attractor Starting from an arbitrary point in the phase space of a non-conservative system, the transient part of the motion decays and the flow tends towards an attractor, excluding the special case of unbounded growth. This attractor can have the form of a point (static), a limit cycle (periodic motion), a torus (quasi-periodic motion) or a fractal structure (chaotic motion).

backbone curve refers to the curve that traces the locus of a maximum of the frequency-response function for a varying control parameter.

background damping refers to a typically small and linear damping of not further specified physical source.

Component Mode Synthesis refers to a dynamic sub-structuring procedure. A larger structure is first decomposed into several smaller sub-structures. The physical coordinates of these sub-structures are then approximated by a set of base vectors, the so-called component modes, and a Galerkin-type projection is carried out. Finally, the reduced sub-structure models are coupled by taking into account displacement compatibility and force equilibrium at the interfaces, or alternatively an appropriate nonlinear contact model.

displacement space refers to the subspace of the state space of a mechanical system that is only related to the generalized coordinates, but not the associated velocities.

dynamic regime It is useful to classify the vibration behavior of a nonlinear system into so-called dynamic regimes, in which certain vibration features remain similar. In the present thesis, three different dynamic regimes are distinguished: (a) the linear regime, in which the modal properties remain constant, (b) the weakly nonlinear regime and (c) the strongly nonlinear regime which begins with the first bifurcation. A particular dynamic regime is linked to bounded ranges of kinetic energy, frequency and system parameters.

essentially (harmonic or periodic) The term 'essentially' is used to embrace not only motions that are exactly harmonic or periodic, but also motions with parameters that vary slowly compared to the underlying base frequency.

external resonance see resonance

flow refers to the temporal evolution of the coordinates of a dynamical system. The flow is commonly represented (a) in the phase space (or projections of it), which is particularly useful to analyze its geometric features, and (b) in the form of time histories to investigate the temporal evolution of individual coordinates.

harmonic either refers to (a) the purely sinusoidal character of a function or (b) a particular term in a Fourier series. In the latter case, the harmonic is a complex-valued quantity. In the present thesis, Fourier series are primarily utilized to describe periodic motions (in time), but they are also used to describe special vibrational deflection shapes that feature a particular order of symmetry (in space) around the circumference of a rotationally periodic structure.

internal resonance refers to a situation in which two or more eigenfrequencies of a dynamical system coincide or are commensurable. This situation can occur in the linear case, in particular if the system features certain symmetries. Otherwise, this situation can be due to nonlinear effects that lead to a dependence of the eigenfrequencies on the vibration level. See also resonance.

invariant manifold Under certain conditions, the entire flow of an autonomous dynamical system takes place only in a smaller subspace of the phase space. In the presence of an isolated resonance, this subspace is two-dimensional. At the equilibrium point, the manifold is tangent to the plane spanned by the corresponding linear modes.

limit cycle If a periodic motion is asymptotically stable, it is referred to as limit cycle, since it forms a closed orbit in phase space. The limit cycle is a special form of an attractor. It should be noticed that limit cycles may occur in autonomous as well as in non-autonomous systems.

modal analysis refers to the process of determining the vibratory properties eigenfrequency, modal damping ratio and vibrational deflection shape of an autonomous dynamical system. If the system is nonlinear, these modal properties are energy-dependent. See also nonlinear mode.

model (order) reduction embraces all approaches to reduce the dimension, i. e. the number of independent coordinates of a set of ordinary differential equations. Two important examples for model reduction addressed in this thesis are Component Mode Synthesis and the proposed reduction to an isolated nonlinear mode. Throughout this thesis, the latter approach is abbreviated as ROM.

nonlinear mode in general refers to a mathematical concept that aims at extending the ideas of linear modal analysis to the nonlinear case. A nonlinear mode should reflect the system's essential vibration behavior in a certain dynamic regime. In the present study, a novel definition is proposed for nonlinear modes of nonconservative autonomous systems: A nonlinear mode is a family of periodic motions of an autonomous nonlinear system. If the system is non-conservative, these periodic

motions are enforced by mass-proportional damping. The mode must coincide with the corresponding linear mode when the kinetic energy tends towards zero. As in the linear case, modal properties like the eigenfrequency (or natural frequency), the modal damping ratio and the vibrational deflection shape can be associated with a mode. In contrast to the linear case, these modal properties are energy-dependent. The functional dependence of a modal property on the energy or the modal amplitude is termed modal characteristic.

operating conditions A system is considered to be under operating conditions, when its (external or internal) loading is taken into account. The vibration behavior under operating conditions is commonly of interest in the design process. In order to obtain a thorough understanding of the underlying vibration mechanisms and to derive certain characteristic quantities, it may be useful to remove (a part of) the load experienced under operating conditions, and thus to consider the nonlinear system in a so-called surrogate configuration. This idea is followed in this study in the derivation of the nonlinear modes: Harmonic forcing and weak linear damping are neglected in the modal analysis step and later superimposed in the ROM to determine the vibration behavior under operating conditions.

periodic motion The motion of a system is denoted periodic, if it repeats precisely after a certain time span, the so-called fundamental period of oscillation. The flow of a periodic motion is located on a closed orbit in phase space.

Poincaré section refers to a section transverse to the flow in the phase space, which generates a stroboscopic image. Poincaré sections are utilized for illustration and stability analysis.

reduced order model see model reduction

resonance refers to a situation in which the flow features only fundamental frequencies that are identical to the system's energy-dependent eigenfrequencies. The resulting motions are either periodic or quasi-periodic, depending on whether the eigenfrequencies are commensurable. If the flow features a dominant fundamental harmonic component, the resonance is termed isolated, otherwise an internal resonance is present. So-called external resonances are caused by external forcing. In a so-called resonance passage, a coincidence occurs of an eigenfrequency and a time-varying external forcing frequency.

state space The dynamic behavior of a mechanical system can be uniquely described in terms of its state vector composed of its generalized coordinates and associated velocities. The corresponding space is termed state space.

weak damping Linear damping is termed weak, if it does not induce significant coupling between the system's modes, neither in the absence or in the presence of nonlinear forces.

Bibliography

[1] A. N. Arkhipov, A. V. Pipopulo, and I. V. Putchkov. Design Tuning of High Aspect Ratio Shrouded Turbine Blades. Proceedings of the ASME Turbo Expo, June 9-13, Berlin, Germany, pp. 1–9, 2008.

[2] R. Arquier, S. Bellizzi, R. Bouc, and B. Cochelin. Two Methods for the Computation of Nonlinear Modes of Vibrating Systems at Large Amplitudes. *Computers and Structures*, 84(24-25):1565–1576, 2006.

[3] E. Balmès. Use of Generalized Interface Degrees of Freedom in Component Mode Synthesis. Proceedings of the 14th International Modal Analysis Conference, February 12-15, Dearborn, MI, USA, pp. 1–7, 1996.

[4] A. Batailly, M. Legrand, P. Cartraud, C. Pierre, and J.-P. Lombard. Study of Component Mode Synthesis Methods in a Rotor-Stator Interaction Case. Proceedings of the ASME International Design Engineering Technical Conferences & Computers and Information in Engineering Conference, September 4-7, Las Vegas, NV, USA, pp. 1–8, 2007.

[5] J. R. Beisheim and G. B. Sinclair. Three-Dimensional Finite Element Analysis of Dovetail Attachments with and without Crowning. Proceedings of the ASME Turbo Expo, June 14-17, Vienna, Austria, pp. 1–12, 2004.

[6] S. Bellizzi and R. Bouc. A New Formulation for the Existence and Calculation of Nonlinear Normal Modes. *Journal of Sound and Vibration*, 287(3):545–569, 2005.

[7] S. Bellizzi and R. Bouc. An amplitude-phase formulation for nonlinear modes and limit cycles through invariant manifolds. *Journal of Sound and Vibration*, 300(3-5):896–915, 2007.

[8] E. J. Berger, D. V. Deshmukh, T. J. Mackin, and H. Inglis. Convergence Behaviors of Reduced-Order Models For Frictional Contacts. *Journal of Vibration and Acoustics*, 127(4):370–381, 2005.

[9] T. Berruti, C. M. Firrone, and M. M. Gola. Modelling Underplatform Dampers in Turbine Blade Vibrations. Proceedings of the XXXII Congresso Nazionale AIAS, September 3-6, Salerno, Italy, pp. 1–12, 2003.

[10] M. Berthillier, C. Dupont, R. Mondal, and J. J. Barrau. Blades Forced Response Analysis with Friction Dampers. *Journal of Vibration and Acoustics*, 120(2):468–474, 1998.

[11] F. Blanc, C. Touzé, J.-F Mercier, K. Ege, and A.-S Bonnet Ben-Dhia. On the Numerical Computation of Nonlinear Normal Modes for Reduced-Order Modelling of Conservative Vibratory Systems. *Mechanical Systems and Signal Processing*, 36(2):520–539, 2013.

[12] N.N Bogolubov and J.A Mitropolsky. *Asymptotic methods in the theory of non-linear oscillations*. Taylor & Francis, 1961.

[13] N. Boivin, C. Pierre, and S. W. Shaw. Non-Linear Normal Modes, Invariance, and Modal Dynamics Approximations of Non-Linear Systems. *Nonlinear Dynamics*, 8(3):315–346, 1995.

[14] M. Bonhage, L. Panning-von Scheidt, and J. Wallaschek. Transient Resonance Passage With Respect to Friction. Proceedings of the ASME Turbo Expo, June 11-15, Copenhagen, Denmark, pp. 1–12, 2012.

[15] J. M. Borrajo, S. Zucca, and M. M. Gola. Analytical Formulation of the Jacobian Matrix for Non-Linear Calculation of the Forced Response of Turbine Blade Assemblies with Wedge Friction dampers. *International Journal of Non-Linear Mechanics*, 41(10):1118–1127, 2006.

[16] C. Bréard, J. S. Green, M. Vahdati, and M. Imregun. A Non-Linear Integrated Aeroelasticity Method for the Prediction of Turbine Forced Response with Friction Dampers. *International Journal of Mechanical Sciences*, 43(12):2715–2736, 2001.

[17] I. N. Bronstein and K. A. Semendjajew. *Taschenbuch der Mathematik*. Teubner, Leipzig, 1987.

[18] T. M. Cameron and J. H. Griffin. An Alternating Frequency/Time Domain Method for Calculating the Steady-State Response of Nonlinear Dynamic Systems. *Journal of Applied Mechanics*, 56(1):149–154, 1989.

[19] T. M. Cameron, J. H. Griffin, R. E. Kielb, and T. M. Hoosac. An Integrated Approach for Friction Damper Design. *Journal of Vibration and Acoustics*, 112(2):175–182, 1990.

[20] A. Cardona, T. Coune, A. Lerusse, and M. Geradin. A Multiharmonic Method for Non-Linear Vibration Analysis. *International Journal for Numerical Methods in Engineering*, 37(9):1593–1608, 1994.

[21] M. P. Castanier and C. Pierre. Modeling and Analysis of Mistuned Bladed Disk Vibration: Current Status and Emerging Directions. *Journal of Propulsion and Power*, 22(2):384–396, 2006.

[22] L. Cesari. Functional Analysis and Periodic Solutions of Nonlinear Differential Equations. *Contributions to differential equations*, 1:149–187, 1963.

[23] D. Cha and D. Sinha. Computation of the Optimal Normal Load of a Friction Damper Under Different Types of Excitation. *Journal of Engineering for Gas Turbines and Power*, 125(4):1042–1049, 2003.

[24] D. Charleux. *Étude des effets de la friction en pied d'aube sur la dynamique des roues aubagées*. PhD thesis, L'École Centrale de Lyon, Lyon, 2006.

[25] D. Charleux, F. Thouverez, and J.P. Lombard. Three-dimensional Multiharmonic Analysis of Contact and Friction in Dovetail Joints. Proceedings of the 22nd International Modal Analysis Conference, January 26-29, Dearborn, MI, USA, pp. 1–9, 2004.

[26] J. J. Chen and C. H. Menq. Periodic Response of Blades Having Three-Dimensional Nonlinear Shroud Constraints. *Journal of Engineering for Gas Turbines and Power*, 123(4):901–909, 2001.

[27] J. J. Chen, B. D. Yang, and C. H. Menq. Periodic Forced Response of Structures Having Three-Dimensional Frictional Constraints. *Journal of Sound and Vibration*, 229(4):775–792, 2000.

[28] B. K. Choi, J. Lentz, A. J. Rivas-Guerra, and M. P. Mignolet. Optimization of Intentional Mistuning Patterns for the Reduction of the Forced Response Effects of Unintentional Mistuning: Formulation and Assessment. *Journal of Engineering for Gas Turbines and Power*, 125(1):131–140, 2003.

[29] Y. H. Chong and M. Imregun. Development and Application of a Nonlinear Modal Analysis Technique for MDOF Systems. *Journal of Vibration and Control*, 7(2):167–179, 2000.

[30] E. Cigeroglu, N. An, and C.-H. Menq. A Microslip Friction Model with Normal Load Variation Induced by Normal Motion. *Nonlinear Dynamics*, 50(3):609–626, 2007.

[31] B. Cochelin and C. Vergez. A High Order Purely Frequency-Based Harmonic Balance Formulation for Continuation of Periodic Solutions. *Journal of Sound and Vibration*, 324(1–2):243–262, 2009.

[32] R. D. Cook. *Concepts and Applications of Finite Element Analysis*. John Wiley & Sons, New York, 4th edition, 2002.

[33] N. Coudeyras, J.-J Sinou, and S. Nacivet. A New Treatment for Predicting the Self-Excited Vibrations of Nonlinear Systems with Frictional Interfaces: The Constrained Harmonic Balance Method, with application to disc brake squeal. *Journal of Sound and Vibration*, 319(3–5):1175–1199, 2009.

[34] R. R. Craig. Coupling of Substructures for Dynamic Analysis: An Overview. Collection of Technical Papers - AIAA/ASME/ASCE/AHS/ASC Structures, Structural Dynamics and Materials Conference, April 3-6, Atlanta, GA, USA, pp. 1–12, 2000.

[35] G. Csaba. Forced Response Analysis in Time and Frequency Domains of a Tuned Bladed Disk with Friction Dampers. *Journal of Sound and Vibration*, 214(3):395–412, 1998.

[36] G. Csaba. *Modelling Microslip Friction Damping and its Influence on Turbine Blade Vibrations*. PhD thesis, Linköping University, Linköping, 1998.

[37] P. R. Dahl. Solid Friction Damping of Mechanical Vibrations. *AIAA Journal*, 14:1675–1682, 1976.

[38] P. J. Davis and P. Rabinowitz. *Numerical integration*. Blaisdell Publishing Company London, 1967.

[39] J. P. Den Hartog. Forced Vibrations with Combined Coulomb and Viscous Friction. *Transactions of ASME*, APM-53-9:107–115, 1931.

[40] E. H. Dowell and H. B. Schwartz. Forced response of a cantilever beam with a dry friction damper attached, part I: Theory. *Journal of Sound and Vibration*, 91(2):255–267, 1983.

[41] R. Elliott, S. Patsias, and P. Doody. Optimisation of Turbine Blade Shroud and Under-Platform Dampers: Part 2 - Numerical Predictions. Proceedings of the 12th International Symposium on Transport Phenomena and Dynamics of Rotating Machinery, February 17-22, Honolulu, HI, USA, pp. 1–9, 2008.

[42] D. J. Ewins. Control of Vibration and Resonance in Aero Engines and Rotating Machinery - An Overview. *International Journal of Pressure Vessels and Piping*, 87(9):504–510, 2010.

[43] C. Farhat and M. Geradin. On a Component Mode Synthesis Method and its Application to Incompatible Substructures. *Computers & Structures*, 51(5):459–473, 1994.

[44] B. Feeny and F. C. Moon. Chaos in a Forced Dry-Friction Oscillator: Experiments and Numerical Modelling. *Journal of Sound and Vibration*, 170(3):303–323, 1994.

[45] A. A. Ferri. Friction Damping and Isolation Systems. *Journal of Vibration and Acoustics und Journal of Mechanical Design / 50th Anniversary of the ASME Design Engineering Division*, 117(B):196–206, 1995.

[46] A. A. Ferri and A. C. Bindemann. Damping and Vibration of Beams with Various Types of Frictional Support Conditions. *Journal of Vibration and Acoustics*, 114(3):289–296, 1992.

[47] A. A. Ferri and E. H. Dowell. Frequency domain solutions to multi-degree-of-freedom, dry friction damped systems. *Journal of Sound and Vibration*, 124(2):207–224, 1988.

[48] A. A. Ferri and B. S. Heck. Vibration Analysis of Dry Friction Damped Turbine Blades Using Singular Perturbation Theory. *Journal of Vibration and Acoustics*, 120(2):588–595, 1998.

[49] S. Filippi, A. Akay, and M. M. Gola. Measurement of Tangential Contact Hysteresis During Microslip. *Journal of Tribology*, 126(3):482–489, 2004.

[50] C. M. Firrone and S. Zucca. Underplatform Dampers for Turbine Blades: The Effect of Damper Static Balance on the Blade Dynamics. *Mechanics Research Communications*, 36(4):515–522, 2009.

[51] C. M. Firrone, S. Zucca, and M. M. Gola. The Effect of Underplatform Dampers on the Forced Response of Bladed Disks by a Coupled Static/Dynamic Harmonic Balance Method. *International Journal of Non-Linear Mechanics*, 46(2):363–375, 2011.

[52] L. Gaul, U. Nackenhorst, K. Willner, and J. Lenz. Nonlinear Damping of Structures with Bolted Joints. Proceedings of the 12th International Modal Analysis Conference, January 31 - February 3, Honolulu, HI, USA, pp. 875–881, 1994.

[53] J. Geisler and K. Willner. Modeling of Jointed Structures Using Zero Thickness Interface Elements. *PAMM*, 7(1):4050009–4050010, 2007.

[54] F. Georgiades, M. Peeters, G. Kerschen, J. C. Golinval, and M. Ruzzene. Nonlinear Modal Analysis and Energy Localization in a Bladed Disk Assembly. Proceedings of the ASME Turbo Expo, June 9-13, Berlin, Germany, pp. 1-8, 2008.

[55] C. Gibert. Fitting Measured Frequency Response Using Non-Linear Modes. *Mechanical Systems and Signal Processing*, 17(1):211–218, 2003.

[56] C. Glocker. *Set-Valued Force Laws: Dynamics of Non-Smooth Systems*. Springer Berlin Heidelberg, 2001.

[57] A. Grace. *Optimization Toolbox: For Use with MATLAB: User's Guide*. The MathWorks Inc, 1990.

[58] J. A. Greenwood and J. B.P. Williamson. Contact of Nominally Flat Surfaces. *Proceedings of the The Royal Society A: Mathematical, Physical & Engineering Sciences*, 295(1442):300–319, 1966.

[59] A. Grolet and F. Thouverez. Free and Forced Vibration Analysis of a Nonlinear System With Cyclic Symmetry: Application to a Simplified Model. *Journal of Sound and Vibration*, 331(12):2911–2928, 2012.

[60] G. v. Groll and D. J. Ewins. The Harmonic Balance Method With Arc-Length Continuation in Rotor/Stator Contact Problems. *Journal of Sound and Vibration*, 241(2):223–233, 2001.

[61] W. Gu, Z. Xu, and S. Wang. Advanced Modelling of Frictional Contact in Three-Dimensional Motion When Analysing the Forced Response of a Shrouded Blade. *Proceedings of the Institution of Mechanical Engineers, Part A: Journal of Power and Energy*, 224(4):573–582, 2010.

[62] J. Guillen. *Studies of the Dynamics of Dry-Friction-Damped Blade Assemblies*. PhD thesis, The University of Michigan, Michigan, 1999.

[63] M. Guskov and F. Thouverez. Harmonic Balance-Based Approach for Quasi-Periodic Motions and Stability Analysis. *Journal of Vibration and Acoustics*, 134(3):031003/1–031003/11, 2012.

[64] G. Haikal and K. D. Hjelmstad. An Enriched Ddiscontinuous Galerkin Formulation for the Coupling of Non-Conforming Meshes. *Finite Elements in Analysis and Design*, 46(6):496–503, 2010.

[65] A. Hohl, C. Siewert, L. Panning, and A. Kayser. Nonlinear Vibration Analysis of Gas Turbine Bladings With Shroud Coupling. Proceedings of ASME Turbo Expo, June 9-13, Berlin, Germany, pp. 1–9, 2008.

[66] L. Huyse, Padula S. L., Lewis R. M., and Li W. Probabilistic approach to free-form airfoil shape optimization under uncertainty. *AIAA Journal*, 40(9):1764–1772, 2002.

[67] H. Irretier and D. B. Balashov. Transient Resonance Oscillations of a Slow-Variant System With Small Non-Linear Damping - Modelling and Prediction. *Journal of Sound and Vibration*, 231(5):1271–1287, 2000.

[68] H. D. Irretier. The Maximum Transient Resonance of Rotating Blades With Regard to Centrifugal Force and Nonlinear Damping Effects. Proceedings of the ASME Turbo Expo, June 2-5, Orlando, FL, USA, pp. 1–7, 1997.

[69] M. H. Jareland. A Parametric Study of a Cottage Roof Damper and Comparison with Experimental Results. Proceedings of the ASME Turbo Expo, June 4-7, New Orleans, LA, USA, pp. 1–9, 2001.

[70] V. Jaumouillé, J. J. Sinou, and B. Petitjean. An Adaptive Harmonic Balance Method for Predicting the Nonlinear Dynamic Responses of Mechanical Systems - Application to Bolted Structures. *Journal of Sound and Vibration*, 329(19):4048–4067, 2010.

[71] L. Jezequel and C. H. Lamarque. Analysis of Non-Linear Dynamical Systems by the Normal Form Theory. *Journal of Sound and Vibration*, 149(3):429–459, 1991.

[72] B. H. Ji, G. H. Zhang, L. T. Wang, Q. Yuan, Q. J. Meng, and D. Y. Liu. Experimental Investigation of the Dynamic Characteristics of the Damped Blade. *Journal of Sound and Vibration*, 213(2):223–234, 1998.

[73] D. Jiang, C. Pierre, and S. W. Shaw. Large-Amplitude Non-Linear Normal Modes of Piecewise Linear Systems. *Journal of Sound and Vibration*, 272(3-5):869–891, 2004.

[74] D. Jiang, C. Pierre, and S. W. Shaw. Nonlinear Normal Modes for Vibratory Systems Under Harmonic Excitation. *Journal of Sound and Vibration*, 288(4-5):791–812, 2005.

[75] H. Jie, S. Yajie, Z. Dayi, and Z. Zigen. Experimental Study of Damping Characteristics of Shrouded Blade. Proceedings of the ASME Turbo Expo, May 14-17, Montreal, Canada, pp. 1–7, 2007.

[76] K. L. Johnson. *Contact Mechanics*. Cambridge University Press, Cambridge, 1989.

[77] Y. Kaneko and H. Ohyama. Analysis and Measurement of Damping Characteristics of Integral Shroud Blade for Steam Turbine. *Journal of System Design and Dynamics*, 2:311–322, 2008.

[78] G. Kerschen, M. Peeters, J. C. Golinval, and A. F. Vakakis. Nonlinear Normal Modes, Part I: A Useful Framework for the Structural Dynamicist: Special Issue: Non-linear Structural Dynamics. *Mechanical Systems and Signal Processing*, 23(1):170–194, 2009.

[79] R. Kielb, J. Barter, O. Chernycheva, and T. Fransson. Flutter of Low Pressure Turbine Blades With Cyclic Symmetric Modes: A Preliminary Design Method. *Journal of Turbomachinery*, 126(2):306–309, 2004.

[80] W.-J Kim and N. C. Perkins. Harmonic Balance/Galerkin Method for Non-Smooth Dynamic Systems. *Journal of Sound and Vibration*, 261(2):213–224, 2003.

[81] Y. B. Kim and S. K Choi. A Multiple Harmonic Balance Method for the Internal Resonant Vibration of a Non-Linear Jeffcott Rotor. *Journal of Sound and Vibration*, 208(5):745–761, 1997.

[82] Y. B. Kim, S. T. Noah, and Y. S. Choi. Periodic Response of Multi-Disk Rotors With Bearing Clearances. *Journal of Sound and Vibration*, 144(3):381–395, 1991.

[83] K. Klamt. *Zur optimalen Schwingungsdämpfung durch trockene Reibung in lokalen und ausgedehnten Fügestellen*. Fortschritt-Berichte VDI, Reihe 11. VDI-Verlag, Düsseldorf, 1990.

[84] D. de Klerk, D. J. Rixen, and S. N. Voormeeren. General Framework for Dynamic Substructuring: History, Review and Classification of Techniques. *AIAA Journal*, 46(5):1169–1181, 2008.

[85] M. Krack, A. Herzog, L. Panning-von Scheidt, J. Wallaschek, C. Siewert, and A. Hartung. Multiharmonic Analysis and Design of Shroud Friction Joints of Bladed Disks Subject to Microslip. Proceedings of the ASME International Design Engineering Technical Conferences & Computers and Information in Engineering Conference, August 12-15, Chicago, IL, USA, pp. 1–10, 2012.

[86] M. Krack, L. Panning-von Scheidt, C. Siewert, A. Hartung, and J. Wallaschek. Analysis and Robust Design of Friction Joints for Vibration Reduction in Bladed Disks. Proceedings of the 10th International Conference on Vibrations in Rotating Machines, February 25-27, Berlin, Germany, pp. 1–11, 2013.

[87] M. Krack, L. Panning-von Scheidt, and J. Wallaschek. A High-Order Harmonic Balance Method for Systems With Distinct States. *Journal of Sound and Vibration*, 332(21):5476–5488, 2013.

[88] M. Krack, L. Panning-von Scheidt, and J. Wallaschek. A Method for Nonlinear Modal Analysis and Synthesis: Application to Harmonically Forced and Self-Excited Mechanical Systems. *Journal of Sound and Vibration*, 332(25):6798–6814, 2013.

[89] M. Krack, L. Panning-von Scheidt, and J. Wallaschek. On the computation of the slow dynamics of nonlinear modes of mechanical systems. *Mechanical Systems and Signal Processing*, 42(1-2):71–87, 2014.

[90] M. Krack, L. Panning-von Scheidt, J. Wallaschek, A. Hartung, and C. Siewert. Reduced Order Modeling Based on Complex Nonlinear Modal Analysis and its Application to Bladed Disks With Shroud Contact. *Journal of Engineering for Gas Turbines and Power*, 135(10):102502/1–102502/8, 2013.

[91] M. Krack, L. Panning-von Scheidt, J. Wallaschek, C. Siewert, and A. Hartung. Robust Design of Friction Interfaces of Bladed Disks With Respect to Parameter Uncertainties. Proceedings of the ASME Turbo Expo, June 11-15, Copenhagen, Denmark, pp. 1–12, 2012.

[92] M. Krack, S. Tatzko, L. Panning-von Scheidt, and J. Wallaschek. Reliability Optimization of Friction-Damped Systems Using Nonlinear Modes. *Journal of Sound and Vibration*, 333:2699–2712, 2014.

[93] P. Kumar and S. Narayanan. Response Statistics and Reliability Analysis of a Mistuned and Frictionally Damped Bladed Disk Assembly Subjected to White Noise Excitation. Proceedings of the ASME Turbo Expo, June 14-18, Glasgow, UK, pp. 1–10, 2010.

[94] D. Laxalde and F. Thouverez. Complex Non-Linear Modal Analysis for Mechanical Systems Application to Turbomachinery Bladings With Friction Interfaces. *Journal of Sound and Vibration*, 322(4-5):1009–1025, 2009.

[95] D. Laxalde, F. Thouverez, and J. P. Lombard. Vibration Control for Integrally Bladed Disks Using Friction Ring Dampers. Proceedings of the ASME Turbo Expo, May 14-17, Montreal, Canada, pp. 1–11, 2007.

[96] D. Laxalde, F. Thouverez, and J.-J Sinou. Dynamics of a Linear Oscillator Connected to a Small Strongly Non-Linear Hysteretic Absorber. *International Journal of Non-Linear Mechanics*, 41(8):969–978, 2006.

[97] B. J. Lazan. *Damping of Materials and Members in Structural Mechanics*. Pergamon Press, Oxford, 1968.

[98] Y. S. Lee, G. Kerschen, A. F. Vakakis, P. Panagopoulos, L. A. Bergman, and D. M. McFarland. Complicated Dynamics of a Linear Oscillator With a Light, Essentially Nonlinear Attachment. *Physica D: Nonlinear Phenomena*, 204(1–2):41–69, 2005.

[99] K. Magnus and K. Popp. *Schwingungen*. Teubner, Stuttgart, 1997.

[100] L. I. Manevitch. The Description of Localized Normal Modes in a Chain of Nonlinear Coupled Oscillators Using Complex Variables. *Nonlinear Dynamics*, 25(1-3):95–109, 2001.

[101] C. Martel and R. Corral. Fluttter Amplitude Saturation by Nonlinear Friction Forces: An Asymptotic Approach. Proceedings of ASME Turbo Expo 2013, June 3-7, San Antonio, TX, USA, pp. 1–9, 2013.

[102] D. N. Mavris, Bandte O., and Delaurentis D. A. Robust design simulation: A probabilistic approach to multidisciplinary design. *Journal of Aircraft*, 36(1):298–307, 1999.

[103] S. Nacivet, C. Pierre, F. Thouverez, and L. Jezequel. A Dynamic Lagrangian Frequency-Time Method for the Vibration of Dry-Friction-Damped Systems. *Journal of Sound and Vibration*, 265(1):201–219, 2003.

[104] G. Nan and X. Ren. Investigation of Dynamical Characteristic of Shrouded Blade of Aero-Engine Subjected to Impact and Friction. Proceedings of the International Conference on Remote Sensing, Environment and Transportation Engineering, June 24-26, Nanjing, China, pp. 8322–8325, 2011.

[105] G. Nan and X. Ren. Nonlinear Dynamic Analysis of Shrouded Turbine Blade of Aero-Engine Subjected to Combination Effect of Impact and Friction. Proceedings of the 13th International Conference on Modeling and Simulation, March 30 - April 1, Cambridge, UK, pp. 212-217, 2011.

[106] A. H. Nayfeh. *Nonlinear Interactions: Analytical, Computational and Experimental Methods*. John Wiley & Sons, New York, 2000.

[107] A. H. Nayfeh. *Introduction to Perturbation Techniques*. John Wiley & Sons, New York, 2011.

[108] A. H. Nayfeh and D. T. Mook. *Nonlinear Oscillations*, volume 1979. John Wiley & Sons, New York.

[109] D. Noreland, S. Bellizzi, C. Vergez, and R. Bouc. Nonlinear Modes of Clarinet-Like Musical Instruments. *Journal of Sound and Vibration*, 324(3-5):983–1002, 2009.

[110] D. Ottl. Modelle und mathematische Beschreibung, Versuchstechniken zur Messung von Dämpfungskenngrößen. In *VDI-Richtlinie 3830: Werkstoff- und Bauteildämpfung*, pages 1–16. 2007.

[111] L. Panning. *Auslegung von Reibelementen zur Schwingungsdämpfung von Turbinenschaufeln*. PhD thesis, Universität Hannover, Hannover, 2005.

[112] L. Panning, W. Sextro, and K. Popp. Optimization of Interblade Friction Damper Design. Paper 2000-GT-0541, Proc. of ASME Turbo Expo 2000, Power for Land, Sea and Air, May 8-11, Munich, Germany, 2000.

[113] L. Panning, W. Sextro, and K. Popp. Spatial Dynamics of Tuned and Mistuned Bladed Disks with Cylindrical and Wedge-Shaped Friction Dampers. *International Journal of Rotating Machinery*, 9(3):219–228, 2003.

[114] M. Peeters, R. Viguié, G. Sérandour, G. Kerschen, and J. C Golinval. Nonlinear Normal Mdes, Part II: Toward a Pactical Computation Using Numerical continuation Techniques: Special Issue: Non-linear Structural Dynamics. *Mechanical Systems and Signal Processing*, 23(1):195–216, 2009.

[115] L. Peletan, S. Baguet, M. Torkhani, and G. Jacquet-Richardet. A Comparison of Stability Computational Methods for Periodic Solution of Nonlinear Problems With Application to Rotordynamics. *Nonlinear Dynamics*, 72(3):671–682, 2013.

[116] P. Pennacchi, S. Chatterton, N. Bachschmid, E. Pesatori, and G. Turozzi. A Model to Study the Reduction of Turbine Blade Vibration Using the Snubbing Mechanism. *Mechanical Systems and Signal Processing*, 25(4):1260–1275, 2011.

[117] E. Pesheck and C. Pierre. A Global Methodology for the Modal Reduction of Large Nonlinear Systems Containing Quadratic and Cubic Nonlinearities. Proceedings of the ASME Design Engineering Technical Conferences, September 14-17, Sacramento, CA, USA, pp. 1–11, 1997.

[118] E. Pesheck and C. Pierre. An Analysis of a Friction Damped System Using two Component Mode Methods. Proceedings of the ASME Design Engineering Technical Conferences, September 14-17, Sacramento, CA, USA, pp. 1–11, 1997.

[119] E. Pesheck, C. Pierre, and S. W. Shaw. Accurate Rreduced-Order Models for a Simple Rotor Blade Model Using Nonlinear Normal Modes. *Mathematical and Computer Modelling*, 33(10–11):1085–1097, 2001.

[120] E. Pesheck, C. Pierre, and S. W. Shaw. A New Galerkin-Based Approach for Accurate Non-Linear Normal Modes Through Invariant Manifolds. *Journal of Sound and Vibration*, 249(5):971–993, 2002.

[121] E. P. Petrov. Method for Direct Parametric Analysis of Nonlinear Forced Response of Bladed Discs with Friction Contact Interfaces. *Journal of Turbomachinery*, 126(4):654–662, 2004.

[122] E. P. Petrov. Direct Parametric Analysis of Resonance Regimes for Nonlinear Vibrations of Bladed Discs. *Journal of Turbomachinery*, 129(3):495–502, 2006.

[123] E. P. Petrov. Analysis of Robustness for Forced Response of Nonlinear Structures With Uncertainties in Parameters of Joints. Proceedings of the 36th International Congress and Exposition on Noise Control Engineering, August 28-31, Istanbul, Turkey, 2007.

[124] E. P. Petrov. A Sensitivity-Based Method for Direct Stochastic Analysis of Nonlinear Forced Response for Bladed Discs With Friction Interfaces. *Journal of Engineering for Gas Turbines and Power*, 130(2):022503/1–022503/9, 2008.

[125] E. P. Petrov. Analysis of Sensitivity and Robustness of Forced Response for Nonlinear Dynamic Structures. *Mechanical Systems and Signal Processing*, 23(1):68–86, 2009.

[126] E. P. Petrov. A High-Accuracy Model Reduction for Analysis of Nonlinear Vibrations in Structures With Contact Interfaces. *Journal of Engineering for Gas Turbines and Power*, 133(10):102503/1–102503/10, 2010.

[127] E. P. Petrov. Analysis of Flutter-Induced Limit Cycle Oscillations in Gas-Turbine Structures With Friction, Gap, and Other Nonlinear Contact Interfaces. *Journal of Turbomachinery*, 134(6):061018/1—061018/13, 2012.

[128] E. P. Petrov and D. J. Ewins. Analytical Formulation of Friction Interface Elements for Analysis of Nonlinear Multi-Harmonic Vibrations of Bladed Disks. *Journal of Turbomachinery*, 125(2):364–371, 2003.

[129] E. P. Petrov and D. J. Ewins. Generic Friction Models for Time-Domain Vibration Analysis of Bladed Disks. *Journal of Turbomachinery*, 126(1):184–192, 2004.

[130] E. P. Petrov and D. J. Ewins. Effects of Damping and Varying Contact Area at Blade-Disk Joints in Forced Response Analysis of Bladed Disk Assemblies. *Journal of Turbomachinery*, 128(2):403–410, 2006.

[131] E. P. Petrov, Z.-I Zachariadis, A. Beretta, and R. Elliott. A Study of Nonlinear Vibrations in a Frictionally-Damped Turbine Bladed Disc With Comprehensive Modelling of Aerodynamic Effects. Proceedings of the ASME Turbo Expo, June 11-15, Copenhagen, Denmark, pp. 1–13, 2012.

[132] F. Pfeiffer and M. Hajek. Stick-Slip Motion of Turbine Blade Dampers. *Philosophical Transactions of the Royal Society A: Mathematical, Physical & Engineering Sciences*, 338(1651):503–517, 1992.

[133] C. Pierre, D. Jiang, and S. W. Shaw. Nonlinear Normal Modes and Their Application in Structural Dynamics. *Mathematical Problems in Engineering*, 2006(10847), 2006.

[134] K. Popp, L. Panning, and W. Sextro. Vibration Damping by Friction Forces: Theory and Applications. *Journal of Vibration and Control*, 9(3-4):419–448, 2003.

[135] O. Poudou, C. Pierre, and B. Reisser. A New Hybrid Frequency-Time Domain Method for the Forced Vibration of Elastic Structures With Friction and Intermittent Contact. Proceedings of the 10th International Symposium on Transport Phenomena and Dynamics of Rotating Machinery, March 7-11, Honolulu, HI, USA, pp. 1–14, 2004.

[136] R. H. Rand. A Direct Method for Non-Linear Normal Modes. *International Journal of Non-Linear Mechanics*, 9(5):363–368, 1974.

[137] L. Renson, G. Deliége, and G. Kerschen. An Effective Finite-Element-Based Method for the Computation of Nonlinear Normal Modes of Nonconservative Systems. *Meccanica*, pages 1–16, 2014.

[138] P. Ribeiro and M. Petyt. Nonlinear Vibration of Plates by the Hierarchical Finite Element and Continuation Methods. *International Journal of Mechanical Sciences*, 41(4-5):437–459, 1999.

[139] P. Ribeiro and M. Petyt. Non-Linear Free Vibration of Isotropic Plates With Internal Resonance. *International Journal of Non-Linear Mechanics*, 35(2):263–278, 2000.

[140] R. M. Rosenberg. Normal Modes of Nonlinear Dual-Mode Systems. *Journal of Applied Mechanics*, 27:263–268, 1960.

[141] L. Salles, C. Schwingshackl, and Green J. Modelling Friction Contacts in Nonlinear Vibration of Bladed Disks. Proceedings of the World Tribology Congress, September 8-13, Torino, Italy, pp. 1–1, 2013.

[142] K. Y. Sanliturk and D. J. Ewins. Modelling Two-Dimensional Friction Contact and Its Application Using Harmonic Balance Method. *Journal of Sound and Vibration*, 193(2):511–523, 1996.

[143] K. Y. Sanliturk, D. J. Ewins, and A. B. Stanbridge. Underplatform Dampers for Turbine Blades: Theoretical Modeling, Analysis, and Comparison With Experimental Data. *Journal of Engineering for Gas Turbines and Power*, 123(4):919–929, 2001.

[144] F. Schilder, W. Vogt, S. Schreiber, and H. M. Osinga. Fourier Methods for Quasi-Periodic Oscillations. *International Journal for Numerical Methods in Engineering*, 67(5):629–671, 2006.

[145] C. W. Schwingshackl, D. Di Maio, and J. S. Green. Modelling and Validation of the Nonlinear Dynamic Behavior of Bolted Flange Joints. *Journal of Engineering for Gas Turbines and Power*, 135(12):122504/1–122504/8, 2013.

[146] D. J. Segalman. Model Reduction of Systems With Localized Nonlinearities. *Journal of Computational and Nonlinear Dynamics*, 2(3):249–266, 2007.

[147] W. Sextro. The Calculation of the Forced Response of Shrouded Blades with Friction Contacts and Its Experimental Verification. Proceedings of the ASME Turbo Expo, May 8-11, Munich, Germany, pp. 1–8, 2000.

[148] R. Seydel. *Practical Bifurcation and Atability Analysis: from Equilibrium to Chaos*. Springer New York, 1994.

[149] S. W. Shaw and C. Pierre. Non-Linear Normal Modes and Invariant Manifolds. *Journal of Sound and Vibration*, 150(1):170–173, 1991.

[150] S. W. Shaw and C. Pierre. Normal Modes for Non-Linear Vibratory Systems. *Journal of Sound and Vibration*, 164(1):85–124, 1993.

[151] S. W. Shaw and C. Pierre. Normal Modes of Vibration for Non-Linear Continuous Systems. *Journal of Sound and Vibration*, 169(3):319–347, 1994.

[152] C. Siewert, M. Krack, L. Panning, and J. Wallaschek. The Nonlinear Analysis of the Multiharmonic Forced Response of Coupled Turbine Blading. Proceedings of the 12th International Symposium on Transport Phenomena and Dynamics of Rotating Machinery, March 17-22, Honolulu, Hawaii, USA, pp. 1–11, 2008.

[153] C. Siewert, L. Panning, C. Gerber, and P. A. Masserey. Numerical and Experimental Damping Prediction of a Nonlinearly Coupled Low Pressure Steam Turbine Blading. Proceedings of the ASME Turbo Expo 2008, June 9-13, Berlin, Germany, pp. 1–12, 2008.

[154] C. Siewert, L. Panning, A. Schmidt-Fellner, and A. Kayser. The Estimation of the Contact Stiffness for Directly and Indirectly Coupled Turbine Blading. Proceedings of the ASME Turbo Expo, May 8-11, Barcelona, Spain, pp. 1–13, 2006.

[155] C. Siewert, L. Panning, J. Wallaschek, and C. Richter. Multiharmonic Forced Response Analysis of a Turbine Blading Coupled by Nonlinear Contact Forces. *Journal of Engineering for Gas Turbines and Power*, 132(8):082501/1–082501/9, 2010.

[156] A. Sinha and J. H. Griffin. Friction Damping of Flutter in Gas Turbine Engine Airfoils. *AIAA Journal of Aircraft*, 20(4):372–376, 1983.

[157] A. Sinha, J. H. Griffin, and R. E. Kielb. Influence of Friction Dampers on Torsional Blade Flutter. *Journal of Engineering for Gas Turbines and Power*, 108(2):313–318, 1986.

[158] A. V. Srinivasan. Flutter and Resonant Vibration Characteristics of Engine Blades. *Journal of Engineering for Gas Turbines and Power*, 119(4):742–775, 1997.

[159] P. Sundararajan and S. T. Noah. Dynamics of Forced Nonlinear Systems Using Shooting/Arc-Length Continuation Method—Application to Rotor Systems. *Journal of Vibration and Acoustics*, 119(1):9–20, 1997.

[160] W. Szemplinska-Stupnicka. The Modified Single Mode Method in the Investigations of the Resonant Vibrations of Non-Linear Systems. *Journal of Sound and Vibration*, 63(4):475–489, 1979.

[161] W. Szemplinska-Stupnicka. "Non-Linear Normal Modes" and the Generalized Ritz Method in the problems of vibrations of non-linear Elastic Continuous Systems. *International Journal of Non-Linear Mechanics*, 18(2):149–165, 1983.

[162] J. Szwedowicz, M. Kissel, B. Ravindra, and R. Kellerer. Estimation of Contact Stiffness and Its Role in the Design of a Friction Damper. Proceedings of the ASME Turbo Expo, June 4-7, New Orleans, LA, USA, pp. 1–8, 2001.

[163] J. Szwedowicz, T. Secall-Wimmel, and P. Dünck-Kerst. Damping Performance of Axial Turbine Stages With Loosely Assembled Friction Bolts: The Non-Linear Dynamic Assessment – Part II. Proceedings of the ASME Turbo Expo, May 14-17, Montreal, Canada, pp. 1–14, 2007.

[164] J. Szwedowicz, W. Sextro, R. Visser, and P. A. Masserey. On Forced Vibration of Shrouded Turbine Blades. Proceedings of ASME Turbo Expo, June 16-19, Atlanta, GA, USA, pp. 1–10, 2003.

[165] D. M. Tang, E. H. Dowell, and J. E. Albright. Damping in Beams with Multiple Dry Friction Supports. *AIAA Journal of Aircraft*, 24(11):820–832, 1987.

[166] D. L. Thomas. Dynamics of Rotationally Periodic Structures. *International Journal for Numerical Methods in Engineering*, 14(1):81–102, 1979.

[167] J. M. T. Thompson and H. B. Stewart. *Nonlinear dynamics and chaos*. John Wiley & Sons, New York, 2002.

[168] C. Touzé and M. Amabili. Nonlinear Normal Modes for Damped Geometrically Nonlinear Systems: Application to Reduced-Order Modelling of Harmonically Forced Structures. *Journal of Sound and Vibration*, 298(4–5):958–981, 2006.

[169] M. Urabe. Galerkin's Procedure for Nonlinear Periodic Systems. *Archive for Rational Mechanics and Analysis*, 20(2):120–152, 1965.

[170] A. F. Vakakis, O. V. Gendelman, G. Kerschen, L. A. Bergman, D. M. McFarland, and Y. S. Lee. *Nonlinear Targeted Energy Transfer in Mechanical and Structural Systems*. Springer Berlin Heidelberg, 2008.

[171] A. F. Vakakis, T. Nayfeh, and M. King. A Multiple-Scales Analysis of Nonlinear, Localized Modes in a Cyclic Periodic System. *Journal of Applied Mechanics*, 60(2):388–397, 1993.

[172] A.F Vakakis, L.I Manevitch, Y.V Mikhlin, V.N Pilipchuk, and A.A Zevin. *Normal Modes and Localization in Nonlinear Systems*. John Wiley & Sons, New York, 2008.

[173] A. Visintin. *Differential Models of Hysteresis*. Springer Berlin, 1994.

[174] A. Weinstein. Normal Modes for Nonlinear Hamiltonian Systems. *Inventiones Mathematicae*, 20(1):47–57, 1973.

[175] Y. K. Wen. Method for Random Vibration of Hysteretic Systems. *Journal of the Engineering Mechanics Division*, 102(2):249–263, 1976.

[176] W. E. Whiteman and A. A. Ferri. Displacement-Dependent Dry Friction Damping of a Beam-Like Structure. *Journal of Sound and Vibration*, 198(3):313–329, 1996.

[177] W. E. Whiteman and A. A. Ferri. Multi-Mode Analysis of Beam-Like Structures Subjected to Displacement-Dependent Dry Friction Damping. *Journal of Sound and Vibration*, 207(3):403–418, 1997.

[178] W. E. Whiteman and A. A. Ferri. Suppression of Bending-Torsion Flutter through Displacement-Dependent Dry Friction Damping. *AIAA Journal*, 37(1):79–83, 1999.

[179] W. Wickord. Front Load Design: Ein integrales Konzept zur Bewertung von Chancen und Risiken beim Entwurf mechatronischer Systeme. In *VDI-Berichte*. VDI Verlag, Paderborn, 2000.

[180] K. Willner. *Kontinuums-und Kontaktmechanik: Synthetische und Analytische Darstellung*. Springer Berlin Heidelberg, 2003.

[181] C. Canudas de Wit, H. Olsson, K. J. Astrom, and P. Lischinsky. New Model for Control of Systems With Friction. *IEEE Transactions on Automatic Control*, 40(3):419–425, 1995.

[182] P. Wriggers. *Computational Contact Mechanics*. Springer Berlin Heidelberg, 2006.

[183] W. Wurpts and J. Twiefel. Analysis of Ultrasonic Vibro-Impact Systems With Equivalent Circuits and the Harmonic Balance Method. *Sensors and Actuators, A: Physical*, 200:114–122, 2013.

[184] B. D. Yang, M. L. Chu, and C. H. Menq. Stick-Slip-Separation Analysis and Nonlinear Stiffness and Damping Characterization of Friction Contacts Having Variable Normal Load. *Journal of Sound and Vibration*, 210(4):461–481, 1998.

[185] B. D. Yang and C. H. Menq. Modeling of Friction Contact and Its Application to the Design of Shroud Contact. *Journal of Engineering for Gas Turbines and Power*, 119(4):958–963, 1997.

[186] B. D. Yang and C. H. Menq. Characterization of 3D Contact Kinematics and Prediction of Resonant Response of Structures Having 3D Frictional Constraint. *Journal of Sound and Vibration*, 217(5):909–925, 1998.

[187] Y. P. Zaspa. Nonlinear Shapes of Steady-State Vibrational Oscillations of Mechanical Contact. Symmetrical Tangential Oscillations. *Journal of Friction and Wear*, 28(1):87–104, 2007.

[188] S. Zucca, C. M. Firrone, and M. M. Gola. Modeling Underplatform Dampers for Turbine Blades: A Refined Approach in the Frequency Domain. *Journal of Vibration and Control*, 19(7):1087–1102, 2013.